UNIVERSITÄT
BERN

Graduate School for Cellular and Biomedical Sciences

University of Bern

Characterization of the Deformation Behavior and Mechanical Response of the Femoro-popliteal Arterial Tract after Stent Placement

PhD Thesis submitted by

Can Gökgöl

from **Turkey**

for the degree of

PhD in Biomedical Engineering

Supervisor
Prof. Dr. Philippe Büchler
Institute for Surgical Technology and Biomechanics
Faculty of Medicine of the University of Bern

Co-advisor
Prof. Dr. Dominik Obrist
ARTORG Center for Biomedical Engineering Research
Faculty of Medicine of the University of Bern

UNIVERSITÄT
BERN

Accepted by the Faculty of Medicine, the Faculty of Science and the Vetsuisse Faculty of the University of Bern at the request of the Graduate School for Cellular and Biomedical Sciences

Bern, Dean of the Faculty of Medicine

Bern, Dean of the Faculty of Science

Bern, Dean of the Vetsuisse Faculty Bern

Acknowledgments

First of all, I'd like thank my supervisor Prof. Dr. Philippe Büchler for his guidance and friendship. Without his continuous support, this thesis would not have been as successful as it is now. Massive thanks, in equal measure, to Prof. Dr. med. Nicolas Diehm, whose efforts in obtaining clinical data and funding have to be acknowledged. I am deeply grateful for the opportunity to have worked in such a fruitful collaboration.

Special thanks to Prof. Dr. Guoyan Zheng and Dr. Steffen Schumann for their outstanding work on the 3D reconstruction algorithm. I'd also like to thank Dr. Farhad Rikhtegar Nezami for his contributions to the numerical framework through his expertise on the CFD analyses.

Many thanks go to my mentor Prof. Dr. Philippe Zysset and to my co-advisor Prof. Dr. Dominik Obrist for carefully evaluating my progress. Thanks to Prof. Dr. Justyna Czerwinska for providing an early feedback on my work.

Over the years, my project has been funded by various different institutions. Among them, I'd firstly like to thank Biotronik AG (Bülach, Switzerland). Special thanks to Dr. Aldo Jakob, Raimund Möhl, Frank Bakczewitz and Markus Wolfer for the monthly teleconferences during the first year of my project. Our discussions helped me understand the different aspects of Nitinol stents much faster than I would on my own. I'd also like to express my gratitude to the National Center for Competence in Research on Co-Me, the Research Council of the Kantonsspital Aarau, the Swiss Heart Foundation and the Gotthard Schettler Foundation for their financial support.

Special thanks to the past and current members of the Computational Biomechanics Group, specifically to Steve Berger, Tobia Brusa, Dr. Elham Tagzizadeh, Thomas Wyss, Dr. Daniel Abler and Dr. Christoph Reutlinger. Our discussions and team dynamic helped me overcome many challenges in my work and turned many an unbearable workdays into enjoyable occasions.

Many thanks to the administrative staff of the ISTB, in special to Denise Schär, but also to Annelies Neuenschwander, Barbara Schmitter and Karin Fahremann-Nolte, for their help with making my stay in Switzerland a smooth one. I’d like to thank Dr. Waldo Valenzuela and Vimal Chandran for all their help with my server problems. I’d also like to thank all my colleagues in ISTB for making it a wonderful place to work.

Special thanks to Alp Evren and Kerem Özaçmak for being great friends, and to Batuhan Bal and Gülseda & Onur Güngör for providing me with a second home whenever I was in Turkey.

I’d like to thank my parents, who have stood beside me with unwavering support since the beginning. I hope that I can continue to make them both proud. This thesis is partly dedicated to them.

Finally, I’d like to thank my wife, Ezgi Köker Gökgöl, who has taken all the hardships and struggles I had during my studies and turned them into an ever increasing love. Without her support, none of this would have been possible. This is for her.

Abstract

The femoro-popliteal (FP) segment is the most commonly diseased artery of the peripheral circulation. Obstructions of these lower-limb arteries are frequent and even with the new generation Nitinol stents (drug-eluting or otherwise), long-term restenosis rates following endovascular procedures range from 15 to 40% and are much higher compared with the long-term outcomes after coronary artery interventions.

The major difference between peripheral and coronary arteries concerns their mechanical environments, with the FP arterial segments being subjected to repeated external deformations during leg flexion. It has been widely hypothesized that the high distortion of the tissues due to the un-physiological deformations of the arteries following stent implantation is the main cause for restenosis. However, there is very limited information on the FP artery deformations of patients with Peripheral Arterial Disease (PAD). Furthermore, the effects of endovascular therapy on the deformation behavior of the PAD-afflicted FP arteries are currently unknown. As such, further research on the deformations of the FP arteries is warranted to not only improve existing stent designs, but to also determine the correct interventional procedure.

The main objectives of this thesis were to characterize the deformation behavior and mechanical response of the FP arterial tract through clinical and numerical investigations. The former was achieved by, first, investigating the pre-angioplasty deformations of the FP arteries during leg flexion in a pilot study of five patients with PAD and utilizing 3D rotational angiography. The methodology was then adapted to perform a clinical study of 35 patients with PAD, in which X-ray angiography was used to image the FP arteries in straight and flexed positions prior to endovascular therapy and following either Percutaneous Transluminal Angioplasty (PTA) or primary Nitinol stent implantation. The 3D models of the FP arteries were reconstructed from the 2D X-ray angiograms and the deformations of axial deformation and

curvature were quantified. Both studies showed that the PAD-afflicted FP arterial segment undergoes significant shortening and an increase in curvature with leg flexion. Comparisons between the pre- and post-treatment deformations, as well as between the different treatment methods, suggested that the choice of the treatment method significantly affects the post-interventional axial deformations of the FP arteries (post-balloon: 7.6% ± 4.9%; post-stent: 3.2% ± 2.9%; *P*: 0.004). As such, while PTA results in a more flexible artery, stents restrict the arteries' shortening capabilities. Depending on the anatomical position of the stents, this axial stiffening of the arteries may lead to chronic kinking, which may cause occlusions and, consequently, impact the long-term success of the procedure. As current stent designs were found to conform to the curvature behavior of the FP arterial tract, improvements should be focused on reproducing the native axial stiffness of the artery to reduce the risk of restenosis for patients that will have to undergo stent implantation.

The complexities caused by leg flexion are further exacerbated by controversial clinical practices, such as Nitinol stent oversizing. The procedure is frequently performed in peripheral arteries to ensure a desirable acute lumen gain and strong wall apposition, and to prevent stent migration. However, the increased radial force exerted onto the arterial walls by the oversized stents could lead to significant arterial damage and, in turn, restenosis. The contradictory findings between animal and clinical studies, in conjunction with the majority of the numerical studies focusing on balloon-expandable stents, suggests that the efficacy of the procedure remains as an issue to be answered.

The mechanical behavior of the FP artery under Nitinol stent oversizing was investigated by creating a validated finite element (FE) framework, which included numerical models of healthy FP arteries with patient-specific geometries and idealized arteries with clinically relevant levels of PAD. Based on the artery model, either only stent implantation or the complete endovascular therapy (PTA + stent implantation) was simulated. Four different stent-to-artery ratios ranging from 1.0 to 1.8 were used in the simulations. For the healthy arteries, additional analyses, in the form of computational fluid dynamics (CFD) analyses and fatigue behavior of the stents, were performed to observe the hemodynamic behavior of the arteries with respect to increased oversizing ratios. For the calcified arteries, three different plaque types were modeled to report the influence of the plaque behaviors on the outcomes of endovascular therapy and stent oversizing. Regardless of the presence of a plaque tissue, results showed that Nitinol stent oversizing was found to produce a marginal lumen gain in contrast to a significant increase in arterial stresses. For the lightly and moderately calcified arteries, oversizing was found to be non-critical; whereas for healthy and heavily calcified arteries, the procedure should be avoided due to a risk of tissue failure. These adverse effects to both the artery walls and stents may create circumstances for restenosis. Although the ideal oversizing ratio is stent-specific, the studies showed that Nitinol stent oversizing has a very small impact on the immediate lumen gain, which contradicts the clinical motivations of the procedure.

In order to predict the possibility of restenosis through mechanical markers that are associated with the effects of leg movement following stent implantation, clinical investigations should be complimented with patient-specific numerical analyses. Combining intra-arterial imaging methodologies with in-vivo arterial deformations, which can be translated to FE simulations as boundary conditions, and building upon the numerical framework that is introduced in the 2nd part of this thesis, it’s possible to generate accurate patient-specific models. These models, evaluated in conjunction with clinical follow-ups, are expected to provide a deeper understanding of the mechanical background of restenosis in peripheral arteries.

Contents

1. Introduction 1

1.1 Clinical Background 1

1.2 Causes for Restenosis 2

1.2.1 Stent Fractures 2

1.2.2 Arterial Deformations 3

1.2.3 Nitinol Stent Oversizing 9

1.3 Thesis Objectives 14

2. In-vivo Deformations of the Popliteal Artery during Leg Flexion in Subjects with Peripheral Arterial Disease 17

2.1. Introduction 17

2.2. Materials and Methods 18

2.2.1. Patient Selection 18

2.2.2. Image Acquisition 19

2.2.3. Quantification of Arterial Deformations 21

2.3. Results 23

2.4. Discussion 25

2.5. Conclusion 27

3. In-vivo Quantification of Femoro-popliteal Artery Deformations: Percutaneous Transluminal Angioplasty vs. Nitinol Stent Placement 29

3.1. Introduction 29

3.2. Materials and Methods 31
3.2.1. Data Acquisiton 31
3.2.2. 3D Reconstruction of the Arterial Centerline 33
3.2.3 Arterial Deformations 35
3.3. Results 36
3.4. Discussion 40
3.5. Conclusion 44
4. Nitinol Stent Oversizing in Patients Undergoing Popliteal Artery Revascularization: A Finite Element Study 45
4.1. Introduction 45
4.2. Materials and Methods 46
4.3. Results 55
4.4. Discussion 61
4.5. Conclusion 65
5. Numerical Modeling of Nitinol Stent Oversizing in Arteries with Peripheral Arterial Disease: The Influence of Plaque Type 67
5.1. Introduction 67
5.2. Materials and Methods 69
5.3. Results 76
5.4. Discussion 83
5.5. Conclusion 87
6. Conclusion & Outlook 89
Bibliography 95

List of Figures

1.1. Following the implantation of a single, long Nitinol stent along the FP artery, the bending of the leg results in an extreme deformation (i.e. kinking) at the non-stented popliteal artery adjacent to the distal end of the stent (Image taken from Arena[3])………………………………………… 5

1.2. The angiographic (**l1**, **m1** & **h1**) and histology images (**l2**, **m2**, **h2** & **l3**, **m3**, **h3**) of the iliofemoral arteries of Yucatan swine stented with different oversizing ratios show that increased oversizing (> 1.6) leads to extensive damage to the artery walls, increased neointimal hyperplaisia and, consequently, restenosis (Image taken from Zhao et al.[137])……… 11

2.1. Positioning of the leg during 3D rotational angiography: Straight (left) and flexed (right) with the help of a cast designed to simulate the walking condition……………………………………… 20

2.2. Threshold-based segmentation of the bone and artery for patient #1 with the leg in a straight position (left) and after flexion (right)……………………………………………………………… 21

2.3. Quantification of deformations on the artery: For axial elongation (left), the difference in length of the centerline between the identified landmarks was measured; for torsion (middle), the change in orientation of arterial branches was calculated; and for curvature (right), the inverse of the radius of the circle, defined by three points on the centerline, was calculated……… 22

2.4. Deformation behaviors of the popliteal arterial segments of five patients with respect to different calcification levels for the maximum curvatures (cm^{-1}) in straight (black) and flexed (gray) legs. Vascular calcification was assessed using a semi-quantitative scoring system: no (0), moderate (1) and heavy (2) calcification……………………………………………………… 24

3.1. The phantom that is attached to the patients' legs during image acquisition is used to calibrate the 2D angiographic images using the fiducials embedded into its surface……………… 34

3.2. Pair of angiographic images with the semi-automatically extracted arterial tree (a) (b); reconstructed 3D arterial tree on top of a radiograph (c); the reconstructed 3D arterial tree (d)……… 35

3.3. Angiographic images of the FP arteries of 4 patients acquired prior to PTA (a, c, e) and following primary Nitinol stent implantation (b, d, f) and with a hip/knee flexion of 20°/70°. For all cases, the placement of the stents in the higher deformational segments of the FP artery increased the arterial curvatures compared to the pre-treatment phase, leading to extreme deformations, such as arterial kinking, with leg flexion………………………………………… 39

3.4. Angiographic images of the FP artery of one patient acquired prior to (a) and following (b) PTA and with a hip/knee flexion of 20°/70°. Performing PTA resolved the arterial kinking observed in the pre-treatment phase and returned the artery to a more natural deformation behavior…… 42

4.1. The production geometries of the Astron-Pulsar and the Astron stents showed that the Astron had a larger strut width, thickness and outer diameter than the Astron stent. Despite the geometrical differences, both stents had the same patterns………………………………………… 49

4.2. The preconditioning and deployment of a Nitinol stent into a patient-specific popliteal artery. By radially displacing the nodes of the expansion tool (not shown), the Astron-Pulsar stent is expanded to its unconstrained diameter of 7mm (left). After annealing, the stent is crimped to its deployment diameter of 1.2 mm by radial displacement of the nodes of the crimp tool (middle-left). The insertion to the patient’s artery is achieved by a displacement-controlled deformation of the crimp tool into the shape of the arterial midline (middle-right). The crimp-tool is then expanded to its initial diameter, which corresponds to the deployment of the stent as it is detached from the tool to contact the arterial walls (right)……… 52

4.3. Uniaxial extension tests of the adventitial layer excised in circumferential (top left) and axial (top right) directions are numerically modeled and the resultant stress-strain relationships (red) are found to be in range of the diverse mechanical behaviors obtained via experiments (blue). The numerically obtained radial forces (green) of the Astron-Pulsar stent correspond to the experimental measurements (black) (bottom left). Additionally, the comparison of the radial forces of Astron-Pulsar (black) and Astron (green) stents highlights the stiffer nature of the Astron stent (bottom right)……………………………………………………………… 56

4.4. Following deployment, strains are concentrated at the outer sides of the struts (left) and stress distribution in different layers of the artery demonstrates the load-carrying behavior of the adventitia (bottom-right)………………………………………………………………………………………… 57

4.5. The average maximum arterial circumferential stresses of the patient-specific arteries (red) exceed the stress levels observed in a straight artery (black) and show a less emphasized non-linear behavior for all blood pressure values (range: 80 mmHg – 160 mmHg) (left). Regardless of the arterial geometries, a very small lumen gain is achieved by oversizing the stents (right)………………………………………………………………………………………………… 57

4.6. The stent with a higher radial force, Astron (green), was found to create significantly higher stress levels than the Astron-Pulsar stent (red) (left). In comparison, a very limited increase in lumen gain is observed to create a mismatch in arterial stress-lumen relationship (right). Regardless of the stent designs, a very small lumen gain is achieved by oversizing the stents (right)……………………………………………………………………………………………………. 58

4.7. The fatigue behavior of the Pulsar stent when deployed into a geometrically accurate artery with unconstrained stent diameters of 5 mm (top left), 6 mm (top right), 7 mm (bottom left) and 9 mm (bottom right): As the oversizing ratio is increased, the strain amplitude of more points are found to migrate towards the Nitinol safety limit of 0.4; thereby decreasing the safety factor of the stent……………………………………………………….. 59

4.8. Instantaneous pattern of WSS distribution on stented popliteal artery at different instants of a cardiac cycle marked by solid red line on a flow rate profile inset. WSS is shown at: (A) t = 0.13 second (B) t = 0.44 second and (C) t = 0.64 second. Panel (D) shows how the symmetric velocity profile is distorted toward the outer wall owing to arterial curvature. This affects the WSS distribution considerably………………………………………………………………….. 60

4.9. Normalized surface area exposed to TAWSS of less than 0.5 Pa (left) and OSI of more than 0.1 (right). Oversizing leads to larger areas being exposed to low TAWSS and more prominent atheroprone conditions at the arterial wall, which is more noticeable for the cases with the stiffer Astron stent. On the other hand, while the local mechanical environment induced by oscillatory characteristics of blood flow significantly increase with the deployment of Astron, they are not directly affected by stent oversizing……………………… 61

5.1. The complete procedure of an endovascular therapy in an artery with a clinically relevant level of PAD (70% stenosis): The pressurization of the artery with the physiological blood pressure of 120 mmHg and the positioning of the angioplasty balloon (a), unfolding of the angioplasty balloon with a pressure of 7 atm to simulate plaque failure (b), folding of the angioplasty balloon and evaluation of the expanded lumen diameter (c), representation of the Nitinol stent and the crimp tool in their unconstrained diameters prior to crimping of the stent (d), crimping of the Nitinol stent to a crimp diameter of 1.2 mm to simulate insertion into the artery (e), and the deployment of the stent into the artery (f)………………………………… 70

5.2. The average stress-strain behaviors of the lightly (n=3), moderately (n=5) and heavily (n=12) calcified femoral plaque types under uniaxial tensile tests show that the moderately calcified plaque have the highest stiffness; while the lightly and heavily calcified plaque types have similar mechanical behaviors prior to tissue failure.[25] The tissue damage was modeled using perfect plasticity with the heavily calcified plaque reaching its constant stress threshold the earliest (160 kPa at a nominal strain of 0.55) and the lightly calcified plaque reaching it the latest (300 kPa at a nominal strain of 1.15) (Table 5.1)………………………………… 73

5.3. The radial force profiles of the Nitinol stent for each of the unconstrained stent diameters showed that increasing the oversizing ratio led to an increase in the radial force of the stent during crimping and deployment into the artery. As a result, the 9 mm stent exerted the highest radial force onto the artery, whereas the 5 mm stent exerted the lowest. On the other hand, the difference between the radial forces of the 6 and 7 mm stents during deployment was found to be marginal. For visualization purposes, the full radial force profile during the crimping and deployment of stent is only shown for the 9 mm stent…………………… 76

5.4. The PEEQ distributions in the atherosclerotic tissues following the 1st PTA showed that the heavily calcified plaque had the largest plastic strain and, as such, the largest plastic deformation (c). The extent of plastic deformation was followed by the moderately calcified plaque (b) and, finally, the lightly calcified plaque (a). Performing a 2nd PTA resulted in a significant increase in the plastic strain level of the moderately calcified plaque (e). On the other hand, while the 2nd PTA also increased the extent of plastic deformation experienced by the lightly calcified plaque; the overall plastic strain was still lower than the other plaque types (d)…… 79

5.5. The stress distribution in the artery with moderately calcified plaque following stent implantation showed that, regardless of the oversizing ratio, the most failure-prone layer was the healthy adventitia over the diseased region. Increasing the oversizing ratio led to an increase in the circumferential stresses of the artery, with the 9 mm stent (d) producing the highest stress, followed by the 7 mm stent (c), the 6 mm stent (b) and, finally, the 5 mm stent (a)…… 81

5.6. The stress distribution in the healthy adventitia has been reported for the different plaque types and oversizing ratios. Similar to the 95th percentile, the average stresses were lower for the artery with the lightly calcified plaque, followed by the arteries with moderately and heavily calcified plaques. The stress values in the adventitia showed a larger scattering for the artery with the moderately calcified plaque than for the other types of calcification. The wider distribution can be attributed to the plaque stiffness. Despite these differences, there was a linear relationship between the unconstrained stent diameters and the circumferential stresses (the 95th percentile, the 75th percentile, as well as the median values) for all the artery models…………………………………………………………………………………… 82

5.6. Regardless of the plaque type, Nitinol stent oversizing resulted in a linear increase in both the arterial circumferential stresses (left) and the lumen gains (right). For each oversizing ratio, the highest circumferential stresses were found to be in the artery with heavily calcified plaque, while the lowest were in the artery with lightly calcified plaque. On the other hand, the highest lumen gain was reported to be in the artery with lightly calcified plaque, followed by the arteries with heavily and moderately calcified plaques. In comparison, oversizing in a non-calcified artery resulted in a non-linear increase in arterial stresses, as well as in the lumen gain. Furthermore, diseased arteries were found to be less sensitive to oversizing than healthy arteries due to a smaller increase in the arterial stresses between each oversizing ratio………………………………………………………………………………………… 83

List of Tables

2.1. Patient demographics, clinical presentation, cardiovascular risk factor profile and level of calcification…… 19

2.2. Three-dimensional arterial deformations of the popliteal arterial segment during knee flexion in five patients undergoing endovascular therapy; axial compression, twist rate and curvature…….. 23

3.1. Patient demographics, level of calcification, as well as the description of the lesions and implanted stents in the stent group……………………………………………………………………………………… 32

3.2. Patient demographics, level of calcification, as well as the description of the lesions and PTA-balloons in the PTA group……………………………………………………………………………………… 33

3.3. The axial deformation and the mean and maximal curvatures of the FP arteries due to a hip/knee flexion of 20°/70° within the lesions and regions that are proximal or distal to the lesions. The measurements correspond to the average deformations performed prior to PTA, divided into their respective groups of only ballooned (Pre-PTA) and stented (Pre-Stent) after PTA only (post-PTA); and following primary stent implantation (post-stent). The *P* values show the effect of leg flexion on the mean and maximal curvatures of the arteries obtained from paired t-tests... 38

4.1. Material parameters for the individual layers of the artery; intima, media and adventitia. 48

4.2. Material parameters for the Nitinol model obtained from the laser-cut stent……………….. 49

5.1. Material parameters (C10, C20 and C30) of the Yeoh SEF model for the lightly, moderately and heavily calcified arteries represent the average mechanical behavior of the plaque tissue under uniaxial extension tests[25,26]. The plasticity threshold corresponds to the failure stress of the tissues……………………………………………………………………………………………… 72

5.2. The circumferential stresses (95th percentile) in the adventitial layer following the pressurization of the artery with a physiological blood pressure of 120 mmHg (Pre-Angio), balloon angioplasty and stent implantation for the arteries with lightly, moderately and heavily calcified plaques.. 78

5.3. The minimum lumen diameter following the pressurization of the artery with a physiological blood pressure of 120 mmHg (Pre-Angio), balloon angioplasty and stent implantation for the arteries with lightly, moderately and heavily calcified plaques.. 78

Chapter 1

Introduction

1.1 Clinical Background

Obstructions of the femoro-popliteal arteries in the lower limbs of the body – clinically commonly manifested as peripheral arterial disease (PAD) – is mainly caused by atherosclerosis.[47] The disease is estimated to be present in 3% of people in the age range of 40 - 59 years and in 20% of people over 70 years of age.[89] In addition, between the years 2000 and 2010, a 23.5% increase in worldwide PAD incidence has been reported.[39] The introduction of balloon angioplasty, a mechanical widening of an obstructed artery through a small arterial puncture hole, has made this method the foremost in the treatment of PAD ever since its introduction over three decades ago.[89] Its major advantages over surgical revascularization are related to its minimal-invasiveness. However, endovascular therapy for femoro-popliteal (FP) arterial obstructions may be associated with a very high frequency of disease recurrence due to restenosis. Restenosis, a re-narrowing of the artery post angioplasty, may be caused by arterial elastic recoil[79], negative arterial remodeling[113] and neointimal hyperplasia[102] and remains the Achilles' heel of this minimally-invasive treatment approach.

The placement of stents into widened arteries to relieve blockages and act as mechanical scaffoldings has been an effective treatment method since its inception.[47,89] While stent implantation has largely insured high success rates for coronary arteries[59,80,84,134], it could not overcome the issue of restenosis in peripheral arteries. With the implantation of balloon-expendable stents, patency rates dropped to levels obtained with performing only percutaneous transluminal angioplasty (PTA) after only six months or one year.[7,10,48] Therefore, more flexible stents have been developed for the peripheral arteries. These selfexpendable Nitinol stents improved the clinical outcomes and showed an increase in the rates of primary patency and freedom from target lesion revascularization (TLR) compared to previous approaches.[30,68,74,115] However, restenosis still remains a significant problem in the peripheral arteries with clinically significant restenosis occurring in about one third of the patients undergoing placement of bare metal Nitinol stents.[106] While the introduction of drug-eluting Nitinol stents helped further solve the issues caused by non-coated stents, the long-term restenosis rates of 17% (from controlled clinical trials) and an even worse real-world outcome of 37% suggest that the problems caused directly by this mechanically challenging anatomical region continue to persist.[27,28,33,58,103,115] Recently, drug-coated balloons have been proposed as an alternative to stent implantation altogether.[103] The long-term outcomes of the initial reports seem to favor this “leave-nothing-behind” approach with restenosis rates of 17%[125] and 19%[132] comparing favorably with the outcomes from drug-eluting stents. However, limited number of clinical trials and contradictory outcomes among different devices[99,125,132] suggest that the technology needs further advancements before it can be considered the gold standard among the available endovascular treatments. Furthermore, bail-out stenting will continue to be utilized for cases, in which the PTA results in suboptimal revascularization. Therefore, there is a need to improve the long-term outcomes of stent implantation in FP arteries.

1.2 Causes for Restenosis

A number of clinical and numerical studies analyzed the causes for in-stent restenosis in FP arteries[31,35–37,65,82,105,109,118]. Due to the flexion of the knee, the FP artery is constantly subjected to mechanical deformations caused by the physiological activities of the patients. As a consequence, the Superficial Femoral Artery (SFA) and the popliteal artery are submitted to significant shortening, elongation, torsion, flexion, and vulnerability to external compression.

1.2.1 Stent Fractures

It has been proposed that stent fractures are caused by this complex biomechanical environment of the arterial tract. These deformations were reported to reduce the fatigue life of the stents implanted in these lower-limb arteries.[4,6,37,41,57,65,86,88,92,118] Iida et al. analyzed the effect of exercise on stent fractures by performing follow-up studies on 40 patients, who underwent Nitinol stent placement.[57] While the lesion length, region and level of calcification and the number of implanted stents all influenced the fracture rates, the amount of exercise was found to be the main motivator for stent fractures. Babalik and colleagues reported the results of a case report, in which a patient with high grade stenosis in the left popliteal artery was implanted with 2 overlapping self-expandable stents.[6] Stent fractures were found to have occurred 6 months after implantation due to flexion of the knee joint. Via single-case studies, Kröger et al. investigated the effect of leg movement on both balloon and self-expandable stents and linked the stent failures with leg flexions.[65] Solis et al. presented a single case study, in which a patient, who had a severe background of Peripheral Vascular Disease (PVD), was implanted with a self-expandable stent around a high flexion point.[118] After only 4 months, a resultant stent fracture had led to the formation of a pseudo aneurysm. Based on these observations, these single-case studies[6,65,118], as well as some major multi-center trials[105,109], suggested a link between stent fractures and in-stent restenosis or reduced patency of the stented segment.

Despite the studies that suggested a correlation between stent fractures and restenosis, this hypothesis was in question from the start.[9,33,127] Analyzing the 1-year outcome of the DURABILITY I trial, in which 151 patients with varying levels of PAD were implanted with PROTÉGÉ Everflex stents, Bosiers and co-workers reported a fracture rate of 8.1%.[9] 70% of these cases, which included 40% of the severe fracture category, showed no restenosis. The results of the SIROCCO trial, in which 93 patients were implanted with either drug-eluting or bare SMART stents, displayed a fracture rate of 22% at a 2-year follow-up.[33] The relation between the stent fractures and in-stent restenosis was not clearly reported; however, it was noted that all but one of the fracture cases were clinically asymptomatic. The theory that stent fractures lead to in-stent restenosis has also been refuted by recent clinical studies performed with new generation of stents. These studies report that stent fracture rates have decreased to only a few percent[133], while long-term clinical outcomes continue to remain poor.[27,28,72,104,133]

1.2.2 Arterial Deformations

Another possible cause for in-stent restenosis is the trauma to the inner or outer layers of the artery induced by its interaction with the rigid Nitinol stent. The combined effect of the arterial deformations during motion of the leg and the difference in mechanical stiffness between the stent and the arterial wall is reported to produce harsh contact conditions between stents and tissues. In turn, these repeated mechanical interactions could lead to acute and chronic irritation of arterial walls, which may trigger restenosis.[36,86,96] Furthermore, changes in the mechanical environment following stent implantation might lead to kinking of the native FP arterial segment, either distal or proximal to the stented regions.[4,86]

Clinical Investigations

Arena reported severe edge dissections at the proximal and distal ends of the Nitinol stents implanted in 2 patients with different clinical backgrounds.[3,4] In both cases, the motion of the SFA and the popliteal arteries led to unnatural, even flow-limiting kinking in the immediate unstented segments, which became worse with recurrent leg flexions (Fig. 1.1). This extreme deformation behavior may lead to further arterial re-obstructions, including complete occlusions of the FP segment, and to repeat revascularizations shortly after the primary endovascular operation. Consequently, it is reasonable to assume that the complex biomechanical properties of the femoro-popliteal arterial tract play a crucial role in the re-obstruction of the arteries subsequent to endovascular therapy.

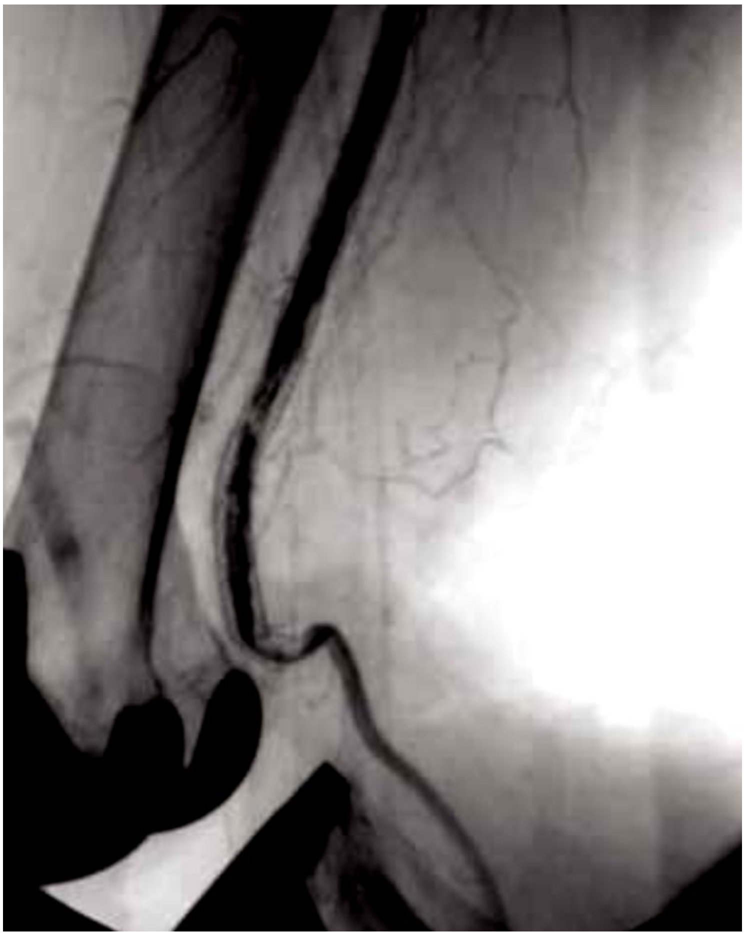

Figure 1.1. Following the implantation of a single, long Nitinol stent along the FP artery, the bending of the leg results in an extreme deformation (i.e. kinking) at the non-stented popliteal artery adjacent to the distal end of the stent (Image taken from Arena[3]).

To date, the flexion behavior of the FP arterial tract is only very poorly understood. While it is clear that the FP arterial segment is exposed to a variety of biomechanical strains during knee flexion, the behavior of this segment post placement of Nitinol stents is complex. Several in-vivo studies have been conducted to evaluate the arterial deformations due to the motion of the leg.[16,17,31,40,44,46,63,87] Cheng et al. performed contrast medium-enhanced magnetic resonance (MR) imaging on both legs of 8 human subjects (mean age ± SD: 27 ± 5 y) with no PAD.[17] The SFAs were imaged with patients in supine and fetal positions and the analyzed segments were isolated to the iliofemoral arteries between the profunda femoris and descending genicular arteries. For both legs, significant shortening and twisting of the SFAs were observed as the patients moved to fetal positions. In an effort to investigate the effect of age on arterial deformations, Cheng and colleagues redid the same study on 7 older, healthy human subjects (mean age ± SD: 56 ± 5 y).[16] While the imaging protocol and the investigated arterial segments correlated with the previous study, the condition for the leg motion was changed to a slightly lesser knee/hip flexion of 90º/40º to better conform to the patients' ages. As with the previous study, the arteries shortened in length and twisted due to the flexion; however, the values for these deformation metrics were lower in older patients, suggesting a less-compliant artery with increased age. Furthermore there was significant bending observed in the arteries of older patients, which was associated with the reduced slack towards axial shortening. Nikanorov et al. estimated the arterial deformations prior to and following stent implantation into the SFAs of 8 cadavers, which underwent lateral radiograph imaging in straight, walking and sitting positions.[88] Klein and coworkers constructed 3D models of the FP arteries of 10 patients (mean age ± SD: 57 ± 10.2 y), who underwent angiographic imaging in straight and crossed leg positions.[63] The patients were diagnosed with PAD, but the study group was limited in the sense that they either had mild or no calcifications. The measured arterial deformations compared well with other studies, as the results showed significant arterial shortening, twisting and bending as the leg moved from straight to crossed leg position. While the above-mentioned studies made important contributions to the small, but ever-expanding field of in-vivo estimation of peripheral arterial deformations, the investigated subjects did not represent the patient population that undergoes endovascular therapy of the lower-limbs.

Recent studies tried to overcome these limitations by performing these measurements in patients with clinically relevant PAD and with patients implanted with stents. Nikanorov and colleagues performed lateral radiographs on 17 patients, none of whom had severe calcifications.[87] The patients were implanted with 23 Absolute (Abbott Vascular, Santa Clara, CA, USA) self-expandable Nitinol stents and the images were taken in leg positions used in their cadaver study.[88] The measurements, estimated from the 2D images, showed that the amount of bending and shortening in the popliteal artery was more critical than the SFA and that the chronic leg movement had limited impact on the arterial deformations in the long-term. The major limitation of this work was in the methodology. By performing the measurements on single 2D radiographs, the authors have overlooked the three-dimensional nature of the arterial deformations, which may introduce inaccuracies to their findings. Finally, Ganguly et al. utilized a C-arm computed tomography system to acquire the images of the lower-limbs of 13 human subjects that had stents.[40] The images were taken with the legs in straight and flexed positions. They used an in-house semi-automatic image analysis software to measure the compression, twisting and bending of the investigated segments and, similar to the previous studies, reported a shortening in the lengths and an increase in the curvatures of the stents. However, the limited information concerning the flexion angle, stent types and lesion locations makes it difficult to accurately interpret their results.

Following implantation, stents are expected to locally modify the stiffness of the artery, which will lead to a concentration of deformations in the unstented arterial sections.[4] The deformations of these bare arteries in the close vicinity of the stented segments are currently unknown. Repetition of these non-physiological large deformations could increase the risk of restenosis through chronic arterial damage and abnormal blood flow conditions. This observation raises another research question concerning the appropriate stenting procedure in the regions subjected to large deformations. A couple of clinical studies suggested that stents that are implanted in the close proximity of the high curvature areas lead to the aforementioned kinking phenomena[4,112]. These clinical observations question current paradigm of spot stenting (i.e. covering only the atherosclerotically diseased part of the artery) for the obstructions in the high curvature areas of the FP intersection. An alternative approach would be to use longer stents that cover the majority of these high-risk areas, which is expected to produce a smoother deformation of the artery and avoid kinking. Currently, no study has investigated the deformation behavior of the high curvature areas when implanted with long stents. A comparison between spot-stenting vs. long stenting may give further insight into the ideal stenting approach to decrease restenosis rates.

Numerical Studies

In addition to the local deformations of the lower extremities, the loads acting on the arteries will induce additional damage to the arterial walls. During flexion of the leg, increased compression and shear forces will be exerted onto the stent, leading to increased stresses in the arteries and higher shear stresses at the stent/artery interface. These increased loads have been proposed to increase the damage to the arterial walls.[36,86,129] However, information on the mechanical environment at the level of the stent/artery interface cannot be accessed clinically. Therefore, numerical models that enable the analyses of local stent-artery interactions are needed.

Numerical tools, finite element (FE) and computational fluid dynamics (CFD) analyses have been widely used to analyze stent design[34,77,124], stent-artery[5,66,76,123], stent-balloon[81,131] and stent-graft interactions[64], as well as structural stress distributions in different layers of the artery, hemodynamical properties along the lumen surface and fatigue performance of stents under different loading conditions.[32,75,76,91,131,135] However, the majority of the existing studies were focused on the coronary arteries and only a handful of studies were concerned with peripheral artery deformations.

Early et al. performed various numerical analyses concerning the deformations of stented peripheral arteries.[35–37] They proposed FE analyses on the deployment of balloon-expandable and Nitinol stents in peripheral arteries and calculated the stress distribution in the tissue walls following the application of a bending boundary condition onto the artery.[37] Their results suggested that arterial bending could be the primary cause of high restenosis rates observed in the FP arterial tract. In a following study, they used FE modeling to investigate the effects of the mechanical environment of peripheral arteries on Nitinol stents through bending and compression simulations.[36] Their results implied that the different arterial segments (SFA and popliteal artery) along the complete FP arterial tract behave differently towards bending and compression and location specific stents should be used in FP arteries to avoid restenosis. However, both studies were limited as they used idealized artery models with a simple mechanical behavior and the boundary conditions they applied were not an accurate representation of the biomechanical environment of the FP arteries.

Diehm et al. developed patient-specific FE models from magnetic resonance angiography (MRA) images of the lower limbs, in both extended and flexed positions, to simulate the bending of the knee.[31] Their aim was to observe the mechanical environment of the FP artery during this flexion. Although their FE model is interesting, no implants were considered in this work. In addition, this study only focused on healthy patients and the amount of bending considered was relatively small when compared to other studies. In two very recent studies, Ghriallais and Bruzzi proposed a FE framework, which includes models of arteries, muscles and bones, to model leg flexion and investigate the deformations and stress/strain characteristics of both healthy and pseudo-stented arteries.[85,86] Their results showed that the mechanical environment of the stented arteries change drastically compared to the healthy arteries and allude to arterial buckling around the ends of the stented region based on stress concentrations. The study, however, is limited by the lack of an actual stent model as the stented regions were created by solely changing the stiffness of the arteries. As a result, the deployment procedure and the complex contact interactions between the stent and the artery walls were completely overlooked. Furthermore, the proposed approach has not been validated.

A few other teams also studied the effect of the mechanical loading following stent implantation in peripheral arteries.[32,49,75,82,91,96] Müller-Hülsbeck et al. used FE analysis to investigate the strain distribution and, consequently, the fatigue failure of different Nitinol stents under bending, compression and torsion in the SFA. While the work provided interesting findings concerning the strain characteristics for different stent types, the loading conditions used in this work were based on an ex-vivo setting and only included the stent itself without an artery model.[82] Similarly, Harvey compared two stent designs submitted to basic loading conditions and pulsatile blood pressure.[49] In a numerical study, Rebelo et al. [96] studied the effect of blood flow on the fatigue behavior of the stent, but neglected the mechanical effects of the arterial deformations. Dordoni et al. have used FE models to analyze the effects of arterial deformations following PTA and primary stent implantation of arteries with different plaque geometries.[32] Petrini et al. have developed a tool to apply patient-specific arterial shortening during leg flexion to an idealized arterial model with the intention to detect possible stent fractures.[91] However, these models only focused on the deformation of the stent and its fatigue behavior. Furthermore, the process of balloon angioplasty, which is a mandatory step prior to Nitinol stent deployment, have been completely overlooked by most of these studies[35–37,49,96]. On the other hand, when the procedure was included in the analyses, the resultant lesion configuration following balloon expansion have not been verified as there is a lack of information on the mechanical behavior of the plaque under the loads inflicted during endovascular therapy. As such, the simplifications adopted towards the plaque behavior, such as using a perfect plasticity or stress softening model for plaque failure, possibly limit the accuracy of the results.

1.2.3 Nitinol Stent Oversizing

The desired outcome of any endovascular procedure is to have a satisfactory lumen gain and sustain it in the long-term. For cases where clinicians suspect a possibility of lumen narrowing following PTA, stents are deployed to act as an internal scaffold. However, the decision to implant a stent, as well as the stent's size, is not defined by any objective criteria and mostly relies on the expertise of the clinicians. The necessity to implant a stent can be determined based on the severity of the calcification and the amount of elastic recoil following PTA. On the other hand, stent sizing remains a delicate matter; its consequences not only showing differences between different anatomical regions[93,101,137], but also within the same arteries.[11,61]

Clinical Investigations

Stent sizing is defined as the ratio of unconstrained stent diameter to non-calcified lumen diameter. For the cases, in which this ratio is below 1.0, the stent is deemed to be undersized. On the other, if this ratio above 1.0, the stent is considered to be oversized.

In clinical practice, choosing a nominal stent diameter that is 1 mm larger than the artery diameter has been suggested.[101] However, this limit is frequently exceeded in order to establish an optimal wall contact with the artery[61], avoid stent mallapposition[93] and prevent stent migration.[121] Despite these seeming advantages, excessive radial forces exerted by the oversized stents and an overstretching of the artery walls can create the circumstances for arterial damage, neointimal/adventitial hyperplasia and, ultimately, restenosis.

Both clinical and numerical studies on Nitinol stent oversizing in peripheral arteries are scarce.[20,43,45,101,130,136,137] Therefore, in order to have a better understanding of the subject matter and show the conflicting results of the clinical studies, this review also includes some notable works on self-expandable stent oversizing in carotid arteries.[11,61,93]

Regardless of the anatomical location, the majority of the studies have been performed on healthy animals. Zhao et al. implanted 28 Nitinol stents into 14 Yucatan swine.[137] Stents were implanted in pairs into the left or right iliofemoral arteries and overlapped each other. The oversizing ratio ranged from 1.2-1.9 and a threshold from normal-sizing to oversizing was set as 1.4. Based on this limit, 8 of the swine were normal-sized and 6 were oversized. At a 6 month follow-up, it was found the luminal area stenosis increased linearly with increased oversizing. Furthermore, exceeding the aforementioned threshold resulted in the overstretching of the artery walls that led to arterial damage, neointimal proliferation (NIP) and luminal area stenosis (Fig. 1.2). The study concluded with a recommended oversizing ratio between 1.1 and 1.4. Saguner and coworkers deployed 10 uncoated and 6 Tinox-coated Nitinol stents in 6 mini-pigs.[101] 4 pigs got 3 stents (left and right external iliac artery; and either left or right SFA); while 2 pigs got 2 stents (left and right external iliac artery). Based on Zhao’s work, the normal-to-oversized stent threshold was taken as 1.4. The follow-up study was 5 months later. Out of 16 stents, 21 segments were recovered; among these, 12 were normal-sized and 9 were oversized. The clinical outcome was similar to the previous study, with increased NIP and in-stent restenosis being observed with increased oversizing and above the threshold of 1.4. Tinox-coating did not yield a better outcome.

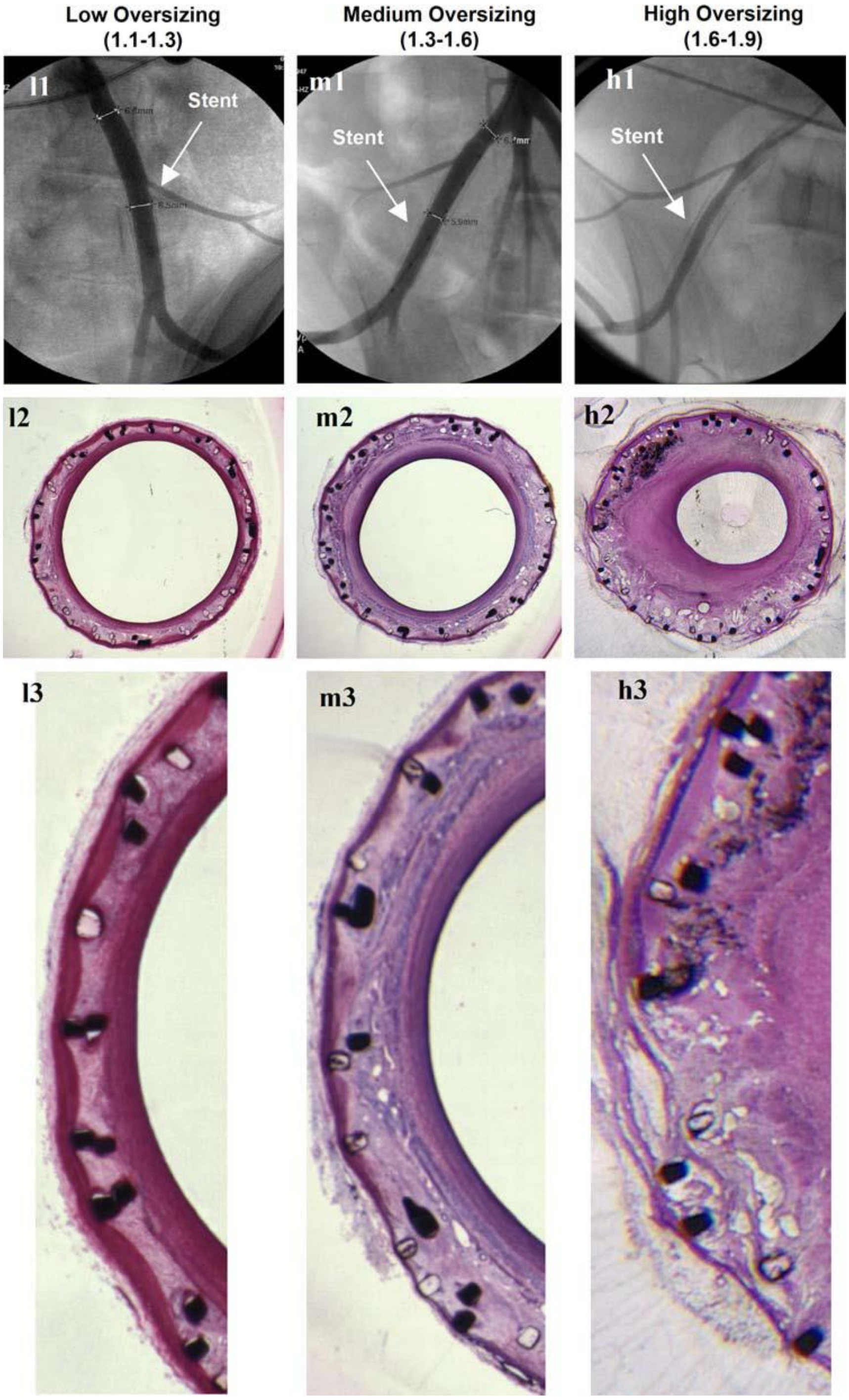
Low Oversizing
(1.1-1.3)
Medium Oversizing
(1.3-1.6)
High Oversizing
(1.6-1.9)
l1
Stent
m1
Stent
h1
Stent
l2
m2
h2
l3
m3
h3

Figure 1.2. The angiographic (**l1**, **m1** & **h1**) and histology images (**l2**, **m2**, **h2** & **l3**, **m3**, **h3**) of the iliofemoral arteries of Yucatan swine stented with different oversizing ratios show that increased oversizing (> 1.6) leads to extensive damage to the artery walls, increased neointimal hyperplaisia and, consequently, restenosis (Image taken from Zhao et al.[137]).

Cho et al. implanted a total of 6 Nitinol stents into 6 beagles.[20] In each case, the stents covered the abdominal aorta and the right external iliac artery. This resulted in a varying oversizing ratio along the length of the stented segment with the average values being 1.2 and 2.0 for the aortas and iliac arteries, respectively. At a 3 month follow-up, the amount of NIP was significantly higher in the oversized iliac arteries compared to the aortas. Zamora and colleagues deployed a total of 12 self-expanding stents (Wallstent) in common iliac veins of 6 mini-pigs and divided the subjects into 3 oversizing groups of 119% to 152%; 153% to 186%; and 187% to 220%.[136] At a 3 month follow-up, all subjects showed neointimal hyperplasia and lumen loss; however, a statistically significant increase in in-stent restenosis due to stent oversizing was only observed for the cases with the oversizing ratio above 153%. Finally, a very early study by Vorwerk et al. approaches the subject not through stent oversizing, but by implanting two different types of Wallstents with different radial forces into the femoral arteries of 15 FP arteries of 10 dogs.[130] In contrast to the previously reported studies, it was found that the amount of NIP at 6 months was the same for both stents and that a lower radial force did not mean lower tissue formation.

In order to make a comparison between 4 different stent types, Cha et al. implanted a total of 22 self-expandable stents in both common carotid arteries of 9 canines.[11] The resultant oversizing ratios ranged from 1.2 to 1.5. A follow-up at 6 months showed that there was a significant average late lumen loss in 3 of the stent groups, with complete occlusion being observed in the remaining group. Furthermore, stents that resulted in higher initial lumen gains led to higher amounts of neointimal hyperplasia. Kirsch et al. deployed a total of 24 Nitinol stents, which included 3 different stent types, in 6 greyhound dogs.[61] Each dog were implanted with 4 stents; 2 in the right and 2 in the left common carotid arteries. While the distally implanted stents were normal-sized with oversizing ratios that ranged from 1.2-1.4; the proximally implanted stents were over-sized with ratios of 2.0-2.5. Contrary to the previous work, the amount of neointimal hyperplasia was found to be the same for both oversized and normal-sized stents. Moreover, all stents had low neointimal response. Finally, Piamsomboon and colleagues have implanted 63 self-expanding stents (Wallstent) in 59 human patients, who had more than 60% stenoses in their internal carotid arteries.[93] The oversizing ratio for all stents were between 1.4 to more than 2.0. The calcifications were cracked and stents were post-dilated. At a follow-up of 6 months, it was found that oversizing did not lead to late restenosis; moreover, late lumen loss was lower with increased oversizing.

This last study is especially relevant considering it’s the only one that is performed on human patients and with clinically relevant stenosis levels.

Numerical Studies

The small number of clinical studies, the inter-variability between stents, species and the arterial segments within said studies and a lack of clinical investigations performed on human subjects warrant further research into this controversial clinical phenomenon. Numerical models can easily be implemented in order to have a better description of the biomechanical implications of oversizing on arterial tissues. However, not only the number of studies that were concerned with stent oversizing are limited, but they focused on the deployment of balloon-expandable stents in idealized models of healthy[13,15,66] and calcified[14,128] coronary arteries.

The most notable work on the subject was conducted by Chen and colleagues.[13–15] By utilizing CFD and structural FE analyses, they have performed simulations of balloon-expandable stent implantation in idealized, non-calcified coronary arteries and investigated the effects of both stent undersizing and oversizing.[13] They found that while a small amount of undersizing (5%) resulted in worse outcomes concerning Wall Shear Stress (WSS), Wall Shear Stress Gradient (WSSG) and Oscillatory Shear Index (OSI), 20% undersizing produced results similar to 0% undersizing. On the other hand, increased oversizing was reported to lead to increased circumferential wall stresses. They followed this work by performing an animal study (in conjunction with additional CFD and FE simulations), in which they implanted the coronary arteries of 10 swine with both undersized (10%) and oversized (10%, 20% and 30%) balloon-expandable stents.[15] Comparing the results from numerical analyses with the extent of damage and neointimal hyperplaisia observed 4 weeks after implantation, they reported findings similar to their previous work and concluded that stent missizing may lead to restenosis through adverse effects on the hemodynamical behavior of the arteries and increased wall stresses. However, the experiments were not used to model the arteries and, as such, they cannot be seen as a direct validation of the numerical models. Additionally, neither of the studies included the plaque tissue, which is necessary to represent the target demographic that undergoes stent implantation. In order to overcome this limitation, the same group introduced a simplified calcification to their numerical models to investigate the effects of balloon-expandable stent missizing on diseased arteries.[14] The results were similar to their previous works, as they reported a decrease in low WSS and increases in WSSG, OSI and wall stresses with increased oversizing. However, their results were limited as they neither simulated balloon angioplasty nor any kind of failure mechanism for the plaque, which is a crucial and necessary step performed during a routine endovascular therapy.

Although not directly investigating the concept of stent oversizing, there are additional studies which have suggested that an increased circumferential deformation of the artery leads to a decrease in the WSS and higher circumferential wall stresses, both of which have been linked with restenosis.[66,128] However, none of these studies are directly adaptable to the endovascular procedures performed in lower-limbs due to the differences in stent types, deployment techniques (i.e. balloon-expandable vs. self-expandable) and artery, as well as atherosclerotic plaque, models. Furthermore, they do not represent the common clinical practice due to the use of healthy arterial models and the exclusion of PTA.

1.3 Thesis Objectives

Within the last two decades, the number, as well as the scope, of both clinical and numerical studies concerning FP artery deformations and FP artery stenting has substantially increased. The primary aims of these studies were to improve current stent designs, establish ideal stent implantation methods and reduce restenosis rates that have been negatively affecting the long-term outcomes of endovascular procedures performed on the FP arteries. However, with the majority of the works being conducted on subjects that do not represent the population targeted for endovascular therapy of the FP arteries, the results can only give limited information on the FP artery deformations. Currently, the deformation behavior of the FP arteries with PAD and the effects of Nitinol stent implantation on the deformations of said arteries are only partially understood. Furthermore, there is no reported data regarding the influence of plain old balloon angioplasty (POBA) on the deformations of the FP arteries diagnosed with PAD. Therefore, the first objective of this thesis was to:

To quantify the in-vivo deformations of the popliteal arterial segment during leg flexion in subjects with clinically relevant (Fontaine Stage IIb) PAD.

Five patients with varying calcification levels of the popliteal arterial segment underwent 3D rotational angiography during endovascular revascularization. Image acquisition was performed with the leg straight and with a flexion of 70°/20° in the knee/hip joint. The arterial *centerline and the corresponding branches in both positions were segmented to create 3D reconstructions of the arterial trees. Axial deformation, twisting, and curvatures were quantified. Furthermore, the relationships between the calcification levels and the deformations were investigated. This pilot study is covered in* ***Chapter 2****.*

Following the establishment of the methods necessary to quantify the deformations of the FP artery, utilizing them on a pilot study and comparing the values with previous studies to evaluate the accuracy of the process, the second objective of the thesis was defined as:

Quantifying the deformations of the FP arteries in patients undergoing endovascular revascularization and comparing the effects of primary Nitinol stent implantation on the post-treatment arterial deformations with the effects of percutaneous transluminal angioplasty (PTA).

35 patients with peripheral arterial disease (PAD) were recruited for the study. During endovascular interventions, angiographic images were acquired with the legs straight and with a hip/knee flexion of 20°/70°. Image acquisition was performed before PTA for all patients; after PTA for 17 patients that only underwent balloon angioplasty; and after primary Nitinol stent implantation for the remaining 18 patients. A semi-automatic approach was used to reconstruct the 3D patient-specific artery models from 2D radiographs. Axial shortening and curvature changes in the arteries were calculated in-vivo for the calcified, ballooned and stented regions, as well as the regions that are distal and proximal to the diseased and treated segments. This part is presented in ***Chapter 3****.*

In addition to these objectives to further understand the pre- and post-operative deformations of the FP arteries, another important aim of the thesis was to build an FE framework to investigate the controversial procedure of Nitinol stent oversizing. The contradictory findings between animal and clinical studies, in conjunction with the majority of the numerical studies focusing on balloon-expandable stents, suggests that the efficacy of the procedure remains questionable. Furthermore, there are no studies on the effects of gradual Nitinol stent oversizing on the mechanical behaviors of the FP arteries with clinically relevant levels of PAD. In order to address these issues, the following objectives were defined.

To investigate the structural and hemodynamic effects of Nitinol stent oversizing in geometrically patient-specific FE and CFD models of FP arteries.

The anatomies of the FP arteries of five patients from the pilot study were adopted for the analyses. 3D FE models were reconstructed with a lumen diameter of 5 mm and the fiber-induced material model represented a healthy popliteal artery. Deployment simulations of two different Nitinol stents, with diameters ranging from 5.5 to 9 mm, were performed. Arterial stresses, luminal gains and fatigue behavior of one stent were analyzed. Furthermore, CFD analyses were used to simulate the physiological blood flow inside the stented arteries to obtain WSS parameters. ***Chapter 4*** *deals with this part.*

To study the effects of Nitinol stent oversizing using FE analyses of endovascular therapy of a FP artery model with a clinically relevant level of PAD.

Finite element analyses of endovascular revascularization of an idealized artery with 70% stenosis and three different plaque types have been performed to examine the influence of Nitinol stent oversizing on the arterial stresses and acute lumen gain. The analyses included the simulation of balloon angioplasty to model plaque failure, followed by stent implantation, in which four different oversizing ratios were investigated. This final objective is discussed in ***Chapter 5****.*

Each of the chapters is either published (Chapters 2 & 4), accepted for publication (Chapter 3) or submitted for publication (Chapter 5). As such, they are presented in this thesis as they have been published, with small adjustments made to some of the methodology sections to better explain the concepts behind each study.

Chapter 2

In-vivo Deformations of the Popliteal Artery during Leg Flexion in Subjects with Peripheral Arterial Disease[44]

2.1. Introduction

The obstruction of lower limb arteries, commonly known as peripheral arterial disease (PAD) is mainly caused by atherosclerosis.[47,89] Endovascular therapy is currently considered the primary treatment modality for many PAD patients.[89] Restenosis,[79,102,113] a narrowing of the dilated artery subsequent to endovascular therapy, hampers clinical outcomes following balloon angioplasty of the femoro-popliteal (FP) arterial segment in up to 60% of the patients at one year.[106] Although the introduction of novel Nitinol stents decreased restenosis rates compared to plain balloon angioplasty (POBA),[108] restenosis still remains a significant problem in peripheral arteries.[84,106] In-stent restenosis occurs in up to 30% of the patients subsequent to bare metal Nitinol stent placement[106] and was reported to be associated with stent fractures[65,118] and arterial wall damage.[69,113] Stent failures are clearly associated with the forces exerted on the FP arteries, which are caused by bending, torsion and axial motions during hip and knee flexion.[16,31,63] Moreover, the effects of this mechanical environment, along with different stent designs and material properties, on the stent-artery wall interactions lead to arterial wall damage.[69]

[42] Gokgol, C., N. Diehm, L. Kara, and P. Büchler. Quantification of Popliteal Artery Deformation During Leg Flexion in Subjects with Peripheral Arterial Disease: A Pilot Study. *J. Endovasc. Ther.* 20:825–835, 2013.

To understand the causes of restenosis and improve stent designs, an accurate characterization of this mechanical environment is necessary. Due to the difficulties arising from in-vivo measurement of mechanical forces, previous studies concerned with this characterization focused on the quantification of in-vivo arterial deformations.[16,17,21,31,63,88,117] Although the improvements with each new study are evident, there are certain limitations that may affect their results; namely the use of cadavers[88,117], young[17,31] and healthy subjects,[16,21] and subjects with only mildly or non-calcified arteries.[63] To our knowledge, no data is available concerning arterial deformations in patients with clinically relevant PAD. This information is critical since these patients correspond to the target group for stenting and calcified arteries may deform differently when compared with healthy tissue.

Aim of the present study is to gain a better understanding of the mechanical environment of the atherosclerotically diseased popliteal arterial tract. Based on the above-mentioned limitations of previous studies, it is our understanding that quantifying the deformational change in mild to severely calcified diseased arteries will give a more realistic insight into the mechanical environment created during leg flexion.

2.2. Materials and Methods

2.2.1. Patient Selection

Images were obtained on a clinical indication on five patients (1 female, mean age 71 ± 9) during endovascular therapy for femoro-popliteal arterial obstructions. Clinical characteristics and risk factors are outlined in Table 2.1. Ethics committee approval for the present study was not required since patients were treated according to the regular clinical protocol. In addition, all patients signed a general consent form approved by our institutional review board, thereby agreeing on usage of anonymized data for quality control and retrospective studies.

Table 2.1. Patient demographics, clinical presentation, cardiovascular risk factor profile and level of calcification.

	Patient 1	Patient 2	Patient 3	Patient 4	Patient 5
Age	76	56	65	79	69
Gender	Male	Male	Male	Male	Female
Fontaine stage	IIb	IIb	IIb	IIb	IIb
Hyperlipidemia	No	No	Yes	Yes	No
Diabetes mellitus	Yes	Yes	No	No	Yes
Arterial Hypertension	Yes	Yes	Yes	Yes	Yes
Cigarette smoking	Yes	Yes	Yes	No	Yes
Coronary heart disease	Yes	No	No	Yes	No
Cerebrovascular disease	No	No	No	No	No
Creatinine (μmol/l)	78	85	89	75	58
Level of obstruction	Popliteal	Popliteal	Popliteal	Popliteal	Popliteal
Calcification	Heavy (Level 2)	None (Level 0)	Moderate (Level 1)	Heavy (Level 2)	Moderate (Level 1)
Stenosis vs. occlusion	Stenosis	Occlusion	Stenosis	Stenosis	Stenosis

2.2.2. Image Acquisition

For each patient, 3D rotational angiography of the popliteal arterial segment was performed (AXIOM-Artis, Siemens, Germany) in two natural lower limb positions: with the subjects' lower limb fully extended and during flexion of the knee. 3D rotational angiography was performed utilizing a standard commercially available dyna CT algorithm on the angiographic workstation. Care was taken to standardize knee flexion in all patients, with the help of a specifically designed cast placed under the patients' legs over which the knees were bent (Fig. 2.1). The resulting configuration corresponded to a position in normal walking situation with a 70°/20° flexion in the knee joint.[88]

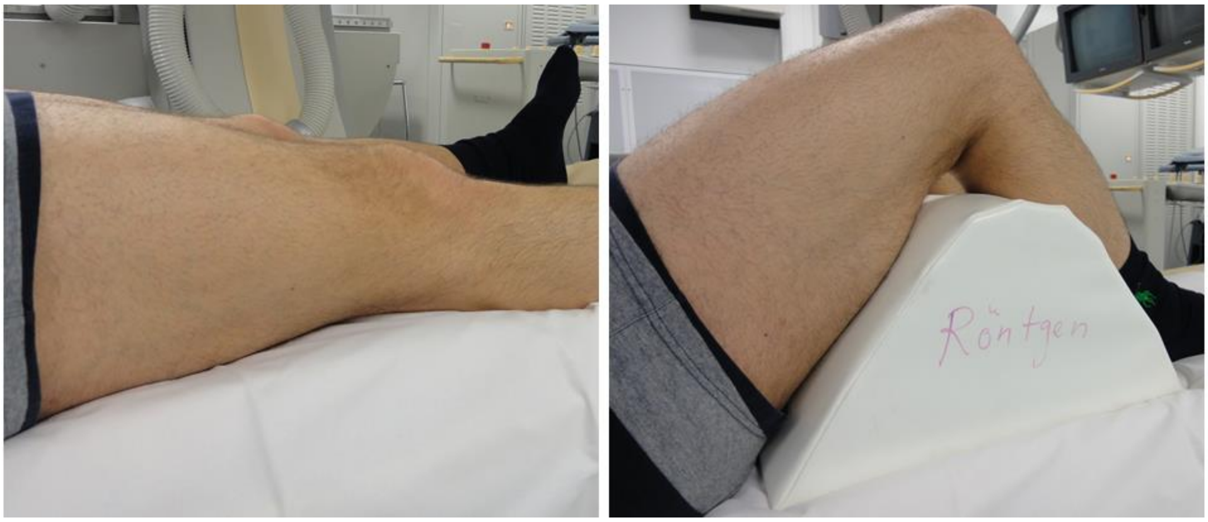

Figure 2.1. Positioning of the leg during 3D rotational angiography: Straight (left) and flexed (right) with the help of a cast designed to simulate the walking condition.

All 3D angiographic examinations were saved digitally and transferred to a workstation (Microsoft Windows operating system) capable of three-dimensional post-processing to quantify the deformation of the arterial tract for each patient. For 4 patients, the investigated segment of the arterial tract started from the descending genicular artery and ended at the superior genicular artery, while it ended at the inferior genicular artery in one patient. Vascular calcification was assessed using a semi-quantitative scoring system: no (0) versus moderate (1) versus heavy calcification (2).

Image Segmentation

For an accurate quantification of the arterial deformations**,** the obtained images were first subjected to pre-processing. In summary, the patients' vasculature and bone structures were segmented on the 3D image datasets using an image-analysis software (Amira 5.2, Visualization Sciences Group SAS). As a result, the 3D vascular tree was obtained for both flexion angles of the leg (Fig. 2.2). Based on these three-dimensional reconstructions, corresponding arterial branches were identified on the two positions. Four landmarks were used to establish the 3D correspondences between the reconstructed arteries at the two angles of flexion dividing the artery into three segments that contain two branches each. The centerline of the whole artery and its respective segments were extracted with the skeletonized feature of Amira. B-splines were used to represent the centerlines, which provided parametric representations of the arteries.

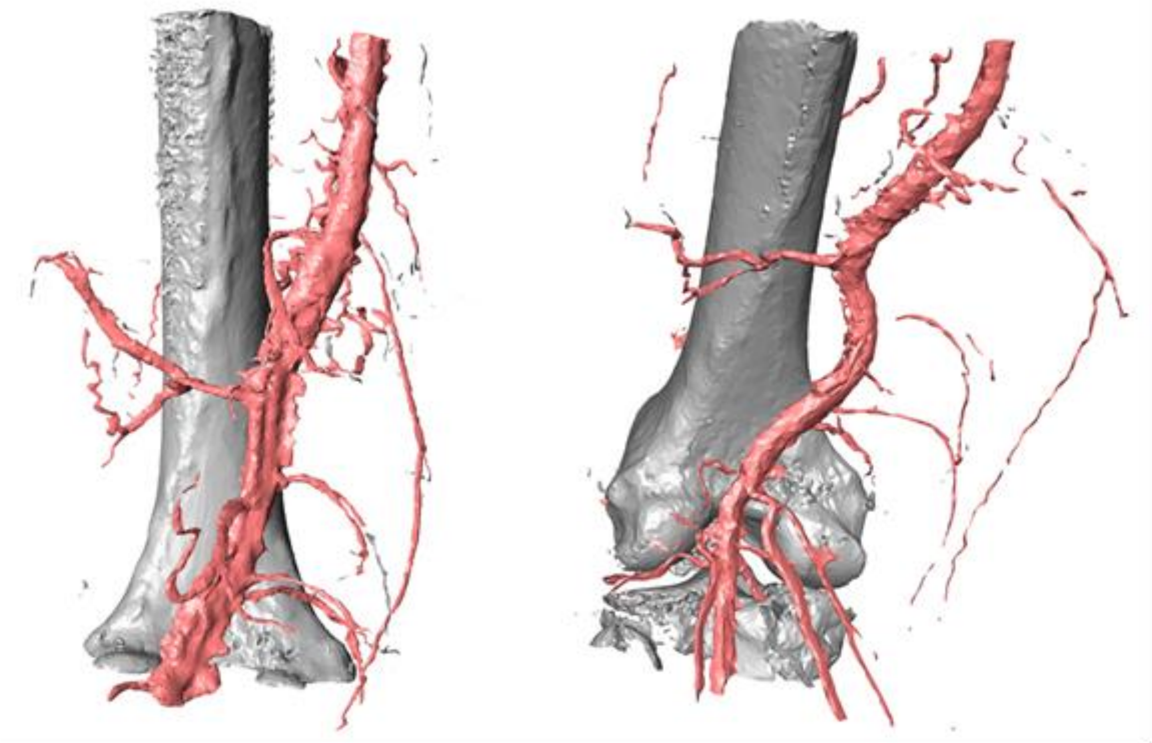

Figure 2.2. Threshold-based segmentation of the bone and artery for patient #1 with the leg in a straight position (left) and after flexion (right).

2.2.3. Quantification of Arterial Deformations

The deformations of the arteries during the flexion were quantified with the axial deformation, the twist angle and the curvature of the artery. The procedure used in this study follows standard techniques previously published,[16,21] but will be summarized here.

Based on the splines describing the arterial centerline, the arc length of the arteries was calculated at each flexion angle. The axial deformation was then measured as the change in the lengths of the segments between straight and flexed positions, divided by the total length of the artery (Fig. 2.3).

For the twist angle quantifications, the “angle of separation” for each segment was calculated by measuring the angle between consecutive side branches. The angle of separation was measured before and after flexion; the angular change induced by the motion corresponded to the twist angle. In addition, the twist angle rate was calculated by dividing the twist angle by the length of the arterial segment. Since the arteries are not straight, the calculations required to obtain the angle of separation must consider the curvature of the arteries. This calculation is done by division of the arterial centerlines into very short sections, such that each section can be assumed to be lying on a plane. The angle between consecutive sections was calculated and used to compensate for the arterial curvature (Fig. 2.3). A detailed description of the mathematical derivation can be found elsewhere.[21]

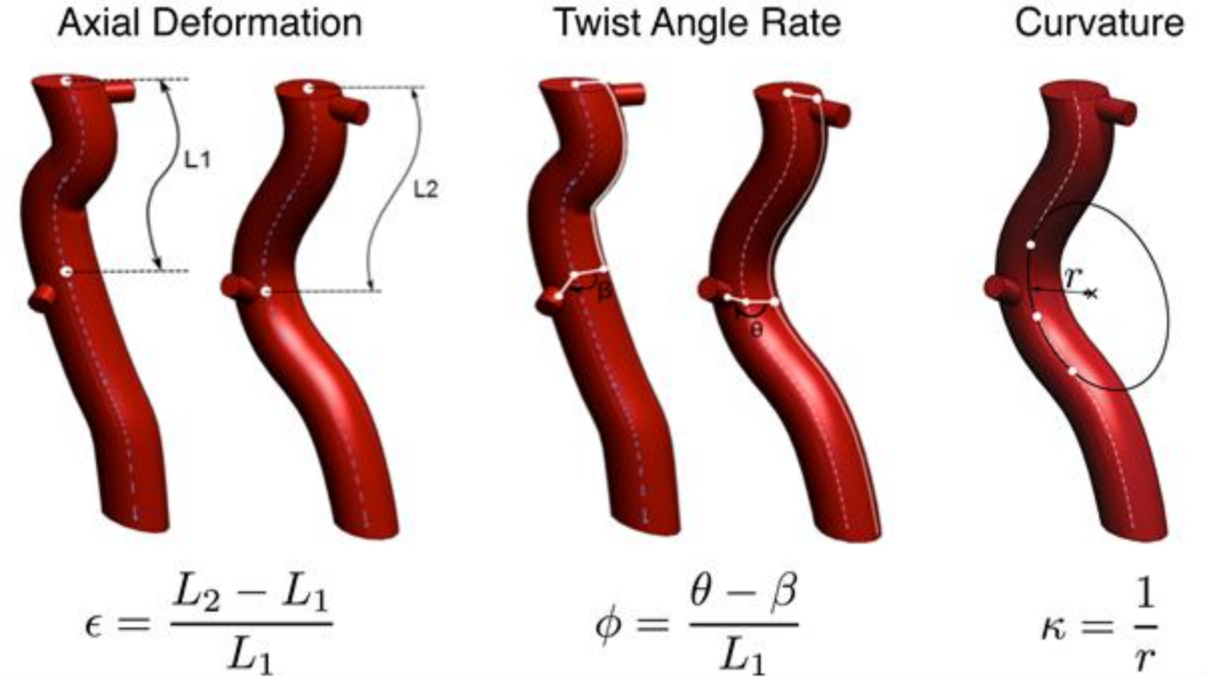

Figure 2.3. Quantification of deformations on the artery: For axial elongation (left), the difference in length of the centerline between the identified landmarks was measured; for torsion (middle), the change in orientation of arterial branches was calculated; and for curvature (right), the inverse of the radius of the circle, defined by three points on the centerline, was calculated.

The arterial curvature was calculated using the osculating circle along the length of the artery. The radius of the circle was defined by three points on the centerline. To avoid measuring insignificant local curvatures, these three points were separated by a distance equal to the arterial diameter. The curvature was defined as the inverse of the radius of the fitted circles. Unlike axial length and twist quantifications, curvatures were calculated along the entire length of the arteries and not for each individual segment (Fig. 2.3).

In addition, the relation between the severity of calcification and the deformation metrics were analyzed. Spearman's rank correlation[95] (ρ) was utilized as a statistical analysis to assess the dependence between these parameters. If an increase in one of the parameters leads to either an increase or decrease in the other one, and if this relation can be defined by a monotonic, but not specifically a linear function, Spearman suggests that these parameters have a positive or negative correlation. A correlation coefficient of +1 means a perfect positive correlation. In this study, the deformation metrics were sorted and ranked in an ascending order, as were the patients' corresponding calcification levels.

2.3. Results

Axial length of the popliteal arterial segment decreased during bending of the leg when compared to the straight leg position in all patients (Table 2.2). Average compression for all patients was found to be 5.9% ± 2.5%; while the average maximum compression was 16.4% ± 8.4%. Moreover, we observed twisting of the arterial segment during leg flexion: The average twist rate was 3.8 º/cm ± 2.3 º/cm, with an average twist angle of 45º ± 25º (in the range of 6º – 71º). The measurements also showed that both the mean and the maximum curvature of the artery increased during flexion of the leg. Arterial twisting was about two times higher after flexion of the knee joint when compared to the curvature measured in the straight position.

Table 2.2. Three-dimensional arterial deformations of the popliteal arterial segment during knee flexion in five patients undergoing endovascular therapy; axial compression, twist rate and curvature.

	Straight to flexed				Curvature (cm^{-1})			
	Axial (%)		Twist rate (°/cm)		Straight		Flexed	
Patient	Mean	Max	Mean	Max	Mean	Max	Mean	Max
1	-4.5	-27.4	5.9	13.2	0.09	0.17	0.23	0.39
2	-7.6	-23.3	5.9	10.9	0.04	0.08	0.08	0.17
3	-6.6	-9.2	0.5	1.3	0.06	012	0.06	0.2
4	-8.4	-11.6	4.5	8.5	0.07	0.13	0.14	0.22
5	-2.4	-10.4	2.2	4.8	0.05	0.08	0.08	0.21
Mean	-5.9	-16.4	3.8	7.7	0.06	0.12	0.12	0.24
± SD	± 2.5	± 8.4	± 2.2	± 4.8	± 0.02	± 0.04	± 0.07	± 0.09

The level of calcification increased from mild to severe among the patients considered. A strong positive correlation was observed between the maximum curvature and the level of arterial calcification, with a ρ factor of 0.97 and 0.98 for straight and flexed positions, respectively (Fig. 2.4). The same correlation was observed between the mean arterial curvatures and the calcification with a ρ factor of 0.98 for both straight and flexed positions. On the other hand, no relationship between the extent of arterial calcification and axial compression or arterial twisting was observed (calculated correlation ρ of 0.40 and 0.43, respectively).

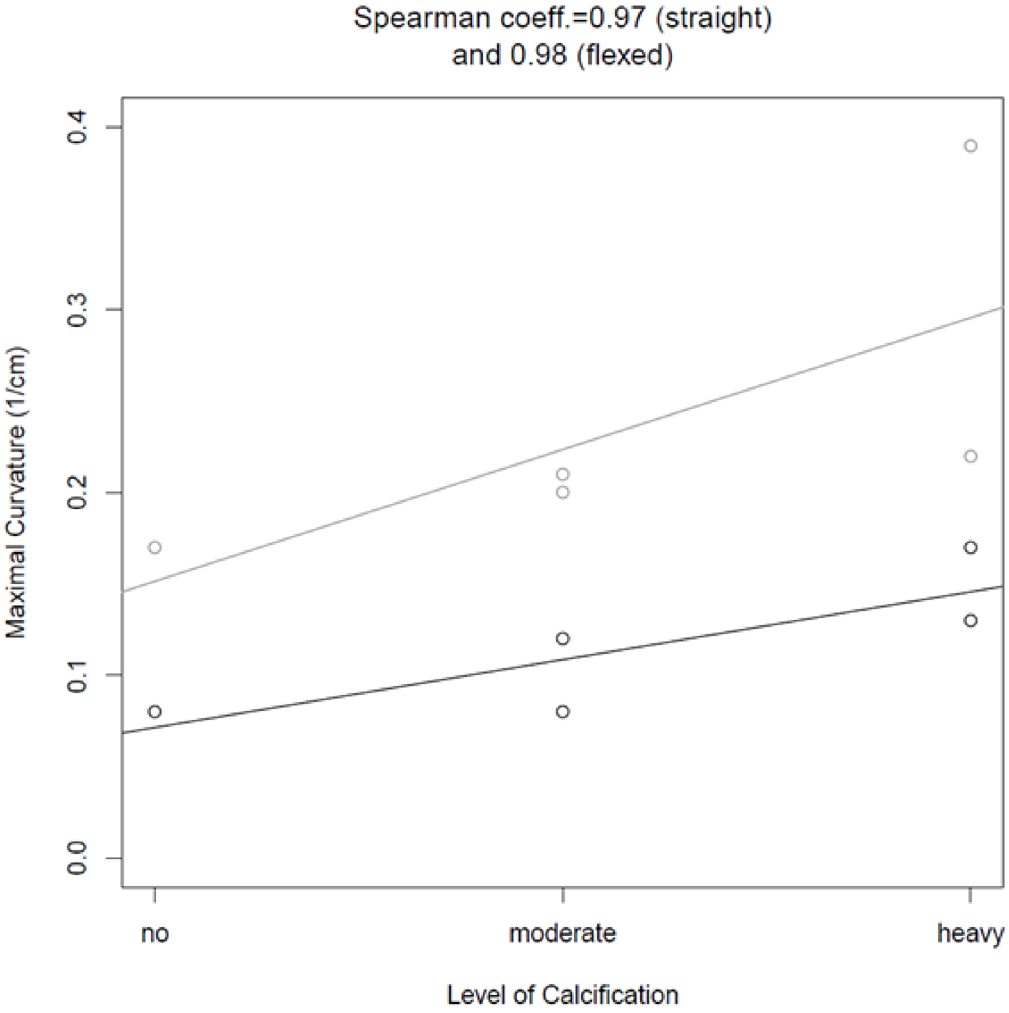

Figure 2.4. Deformation behaviors of the popliteal arterial segments of five patients with respect to different calcification levels for the maximum curvatures (cm^{-1}) in straight (black) and flexed (gray) legs. Vascular calcification was assessed using a semi-quantitative scoring system: no (0), moderate (1) and heavy (2) calcification.

2.4. Discussion

The FP arterial segment is a very challenging territory for endovascular therapy and especially for the placement of stents.[89,106] Excessive biomechanical deformations may constitute possible explanations for the limited success of stents in these arterial segments.[16,31,63] To provide a deeper understanding about the mechanical environment in popliteal arteries during flexion, arterial deformations of five patients with various levels of arterial calcifications ranging from mild to severe were quantified based on 3D rotational CT imaging.

Our results suggest that flexion of the leg in the knee joint induced a decrease of arterial length, an increase of the curvature as well as substantial amount of twisting in the popliteal arterial segment. Furthermore, an increase in the calcification level led to an increase in the maximum curvature observed in both straight and flexed positions, while no change in the amount of arterial twisting and axial deformation was observed for the different levels of calcification.

A direct comparison of these results with previous publications is difficult due to the use of different methodologies, where healthy volunteers were considered with various mechanical configurations and imaging modalities.[16,17,21,31,63,88,117] Although these studies provided important information concerning arterial deformations occurring during various activities, they mostly considered young[17,31] and healthy subjects,[16,21] and subjects with only mild or non-calcified arteries.[63] To our knowledge, the present study is the only one on subjects with clinically relevant PAD; however, the general arterial behavior during the flexion measured in the present work is consistent with previous observations. All published studies reported arterial shortening during leg flexion. The mean amount of shortening reported previously ranges from 15.1% for patients with mild calcifications[63] to 7.4% for healthy subjects[16]. With a 5.9% mean shortening for arteries with moderate to severe calcifications, surements showed a slightly lower axial compression. This confirms the decreased elasticity of the artery from young, healthy subjects to older diseased patients. Concerning the mean twist angle between straight and flexed positions, Klein and coworkers [63] observed a change of 61.1º ± 31.9º in the popliteal arteries of subjects with mild calcifications.. These findings are on par with the mean change of the twist angle of 45.9° ± 25.4° obtained in the present study. Due to the differences in the lengths of the arterial tracts, the comparison of the twist rate is more important than the mean twist angle. The axial twist rate found in the previous studies was between 1.9 °/cm and 3.46 °/cm for the popliteal arteries of patients with clinically different backgrounds.[14] These results compare favorably with our calculation of 3.8°/cm ± 2.3°/cm, since the amount of deformation applied to the leg was in the lower range of the scale.

Due to a limited number of studies on curvature, a satisfactory evaluation of the results, with regard to their accuracy is challenging. Klein and coworkers [63] quantified the mean curvature of the PA segment in straight leg and crossed leg positions as 0.1 cm^{-1} ± 0.02 cm^{-1} and 0.31 cm^{-1} ± 0.1 cm^{-1}. Cheng's findings on curvature vary considerably with respect to the subjects. While no bending was reported in the popliteal arteries of healthy, young subjects;[17] a maximum supine curvature of 0.11 cm^{-1} ± 0.05 cm^{-1} and a maximum flexed curvature of 0.47 cm^{-1} ± 0.24 cm^{-1} were observed along the proximal popliteal arteries of healthy, old subjects.[16] While both our mean and maximum straight curvatures compare with these results, the mean and maximum flexed curvatures of 0.12 cm^{-1} ± 0.07 cm^{-1} and 24 cm^{-1} ± 0.09 cm^{-1} is lower than the reported values. This finding may be attributed to slightly more pronounced knee flexion in the compared studies.[16,63]

The comparison of our results with the previous studies suggest that, although there are significant deformations in the popliteal arteries of diseased patients during leg flexion, the amount of change observed in the PAD patients does not differ significantly from the ones observed in healthy volunteers.[16,17,21] The differences between the published results are likely to be attributed to anatomical variations between patients. Based on this observation, we may conclude that the level of calcification has a limited effect on both the axial deformation and twisting of the popliteal arteries when the leg is flexed. The observed relation between the calcification levels and curvature in both leg positions suggests that as the extent of calcification increases, the curvature of the PA increases. This is in agreement with the observation of Cheng and colleagues[16], which attributes the increased curvature to lower elasticity of arteries impacted by patient age.

One possible and significant use of these measurements with respect to improving the stent designs is in Finite Element (FE) simulations. Since the stents undergo rigorous FE simulations during development, these measurements can be applied as boundary conditions to realistically model the deformation of calcified arteries, even without explicitly modeling the calcification. To our knowledge, the measurements used in the previous FE simulations are all based on cadaveric[35,36,49] or healthy arteries[31] and ignore any possible effect the calcification level may have on the deformation metrics, contrary to what we have showed in the present study. The use of these measurements in FE simulations might have a role in improving stent designs through the analysis of stent behavior and their fracture mechanics under these deformations.

Several limitations of the present study need to be discussed. First, due to size constraints of the angiographic imaging system, we could not consider the entire length of the FP arterial segment, but concentrated on its distal part. Moreover, space constraints in the angiographic system limited the extent of leg motion. Although the flexed position of the leg considered in this study is one of the most important to consider, the procedure could not be extended to more complex physiological situations. Future studies should consider 2D X-ray image acquisitions, which can cover a larger segment of the artery and also allow for higher flexion angles. Although the deformations along the FP arterial segment are not uniform, most of the deformation is expected to take place in the target region analyzed. Future studies should also consider quantifying the entire FP arterial segment to disregard any effect the sizes of the arteries might have on the results. Another limitation concerns the limited number of patients included; however, the typical number of subjects in similar work is between 1 and a maximum of 10.[16,17,21,31,63] In addition, the patients considered in this study covered a large range of arterial calcifications, which is sufficient to provide an assessment of the effect of the PAD on the arterial deformations.

2.5. Conclusion

The study showed that 3D rotational angiography is a method suitable to accurately quantify the deformation of the PA segment in patients. The available workspace is larger than other 3D imaging systems such as MRI, which enables more realistic range of flexion. In addition, it provides a full three-dimensional representation of the tissue and is not limited to bi-dimensional radiographic projections. The measurements were performed on subjects with varying levels of arterial obstruction, in both straight and flexed leg positions thereby representing knee joint positions as observed during walking. We observed significant changes in curvature, twist angle and length of the popliteal arterial segment during leg flexion. The quantifications also lead to a relation of a higher curvature with more severe calcification levels. This implies that the calcification directly affects the curvature, while no such relation with twisting or axial deformation was found. This relation supports the idea that the quantifications help to uncover clinically very important information on the deformation mechanics of the lower limb arteries and may give important insight into stent placement and design. The methodology followed in this pilot study proved to be appropriate to achieve accurate 3D quantifications and can therefore be used to collect data on larger groups of patients.

Chapter 3

In-vivo Quantification of Femoro-popliteal Artery Deformations: Percutaneous Transluminal Angioplasty vs. Nitinol Stent Placement[46,112]

3.1. Introduction

For over a decade, endovascular therapy has been the primary treatment method for most patients with peripheral arterial disease (PAD).[89] The main challenge with this treatment has been to overcome comparatively high restenosis rates in the femoro-popliteal (FP) arteries and the need for target lesion revascularization (TLR). The implantation of Nitinol stents following percutaneous transluminal angioplasty (PTA) using conventional non-coated balloons improved restenosis rates,[30,67,74,115] but led to a new set of problems such as arterial wall damage through stent-artery interactions,[36,96,113] loss of primary patency due to neointimal hyperplasia or stent fractures,[2,65,91] or restriction of the natural deformation behavior of the FP arterial tract.[4,85] The invention of drug-eluting Nitinol stents, along with improved stent designs, partially solved these issues.[27,132,133] The remaining occurrences of

[44] Gökgöl, C., S. Schumann, N. Diehm, G. Zheng, and P. Büchler. In-vivo Quantification of Femoro-popliteal Artery Deformations: Percutaneous Transluminal Angioplasty vs. Nitinol Stent Placement. **Accepted** by *J. Endovasc. Ther.*, August, 2016.

[106] Schumann, S., C. Gökgöl, N. Diehm, P. Büchler, and G. Zheng. The Effect of Stent Implantation on the Deformations of the SFA and the Popliteal Artery: In-Vivo 3D Deformational Analysis from 2D Radiographs. **Accepted** by *J. Vasc. Interv. Radiol.*, April, 2016.

restenosis are hypothesized to have a mechanical origin and to be caused by the stents' effects on the arterial deformations during leg flexion.[4,85]

With the advent of drug-coated balloons, bioresorbable stents and atherectomy devices, the state of the art in the endovascular treatment of FP lesions is moving away from stent placement and towards the so-called "leave-nothing-behind" strategy.[1,103] The motivation behind this approach is to completely resolve the problems caused by the presence of permanent metal scaffolds. A limited number of non-randomized clinical trials addressed the efficacy of this technology and initial results showed superior outcomes than both plain old balloon angioplasty (POBA) and non-coated stents, as well as similar primary patency and TLR rates compared with drug-coated stents.[103,125,132] However, contradictory outcomes among different devices suggest that the technology needs further advancements before it can be considered the gold standard among the available endovascular treatments.[99,125,132] Furthermore, stent placement will continue to be utilized for cases in which PTA fails to provide optimal revascularization. Therefore, there is a need to improve the long-term outcomes of stent implantation in FP arteries. To reduce the risk of restenosis, current stent designs should be adapted to conform to the dynamic mechanical environment in the FP arteries.

In order to observe whether PTA provides better arterial flexibility compared to stent placement, axial deformation and bending behavior of the FP artery following both approaches need to be investigated. While several publications reported the in-vivo deformations of healthy and calcified arteries in both living subjects and cadavers,[16,17,31,44,63,88] only two studies examined the arterial deformations of patients who underwent stent placement.[40,87] However, both studies had limitations that impacted the significance and interpretation of their results. The study from Nikanorov et al. only considered a single Nitinol stent and the measurements were performed on single 2D radiographs, overlooking the three-dimensional nature of the arterial deformations.[87] On the other hand, Ganguly et al. mainly focused on the methodology and validation behind the deformation analyses, and provided limited information concerning the flexion angle, stent types and lesion locations, thereby making it difficult to interpret their findings.[40] Additionally, the implications of plain old balloon angioplasty on the deformation behavior of the FP artery are currently not known. Therefore, the objective of this work was to quantify the in-vivo FP artery deformations of patients undergoing primary Nitinol stent implantation when compared with PTA alone. In addition, by comparing the post-angioplasty deformation behavior with the deformations following stent implantation, current shortcomings of existing stent designs could be identified.

3.2. Materials and Methods

3.2.1. Data Acquisiton

This study was approved by the local ethics committee. Each patient also signed a consent form to accept inclusion into the study and approve the analysis of acquired data, in anonymized form, outside the clinical environment. 35 patients (20 males; mean age: 69 ± 10) scheduled for endovascular therapy were recruited to undergo 2D radiographic imaging of their lower limbs. All patients were classified with a Fontaine stage of IIB and had a mean lesion length of 69 mm ± 9 mm. Information about the anatomical lesion locations, as well as the patients' calcification levels, are presented in Tables 3.1 & 3.2.

The method of treatment for each patient was decided during endovascular therapy. All patients underwent an initial balloon angioplasty, in which the balloon was expanded approximately to 10 atmospheres. Based on a qualitative evaluation of lesion behavior and arterial recoil, primary stent implantation was deemed necessary for 18 patients. With three patients being fitted with two stents, a total of 21 self-expanding Nitinol stents were implanted: Six Pulsar 18 (Biotronik AG, Bülach, Switzerland); one Xpert (Abbott Vascular, Santa Clara, CA, USA); five Zilver PTX (Cook Medical Inc., Bloomington, IN, USA); and nine EverFlex (Ev3 Endovascular Inc., Plymouth, MN, USA) (Table 3.1). Stents were implanted with an overlap of approximately 5 mm into the proximal and distal segments of the lesions. Among the remaining 17 patients who solely underwent PTA, only two patients were treated with drug-coated balloons, and all were subjected to subsequent balloon expansions until an adequate lumen diameter was reached (Table 3.2).

All angiographic images were acquired with a Philips Allura FD 20 Xper X-ray system with Clarity Upgrade (Best, Netherlands). Contrast material was diluted by 50% with saline and injected over the arterial sheath. Prior to the acquisitions, a lightweight calibration phantom was attached to the patients' thighs using a strap. The initial acquisition was performed before treatment in two steps; first with the leg in straight position and then with a knee/hip flexion of 70°/20°. Depending on the chosen treatment method, the acquisition was repeated either immediately after PTA or primary stent implantation. At each configuration, a set of two images, separated by an average view angle of 45 to 60 degrees, was acquired. The images were stored on the workstation in terms of subtraction angiography and cine-images.

Table 3.1. Patient demographics, level of calcification, as well as the description of the lesions and implanted stents in the stent group.

Patient no.	**Age**	**Gender**	**Calcification level**	**Lesion**		**Implanted stents**	
				Location	**Length (mm)**	**Type**	**Size**
1	65	M	Moderate	Mid SFA/ Distal SFA	60	Pulsar-18	Ø6 x 40 mm
2	75	M	Moderate	Distal SFA / Popliteal	180	Pulsar-18	Ø6 x 200 mm
3	56	M	Moderate	Mid SFA/ Distal SFA	50	Xpert	Ø4 x 40 mm
4	68	F	Moderate	Mid SFA	60	Zilver PTX	Ø5 x 80 mm
5	66	F	In-stent re-occlusion	Prox. SFA / Mid SFA	200	EverFlex	Ø5 x 150 mm
6	75	M	Severe	Mid SFA / Distal SFA	180	EverFlex	Ø6 x 200 mm
7	79	F	Severe	Prox. SFA / Distal SFA	350	Pulsar-18 (x2)	Ø5 x 200 mm
8	71	M	Severe	CFA** / Distal SFA	350	Everflex (x2)	Ø6 x 200 mm
9	66	F	Moderate	Prox. SFA / Distal SFA	300	Pulsar-18	Ø5 x 200 mm
10	76	F	Severe	Prox. SFA / Distal SFA	400	Everflex (x2)	Ø6 x 200 mm
11	65	M	Moderate	Distal SFA	100	Zilver PTX	Ø6 x 120 mm
12	71	M	Moderate	Mid SFA / Distal SFA	100	Zilver PTX	Ø6 x 120 mm
13	81	M	Moderate	Popliteal	70	Pulsar-18	Ø5 x 80 mm
14	48	M	Severe	Mid SFA / Distal SFA	50	Everflex	Ø6 x 60 mm
15	79	F	Severe	Mid SFA	80	Everflex	Ø5 x 100 mm
16	61	M	Moderate	Mid SFA	100	Zilver PTX	Ø5 x 120 mm
17	62	M	Moderate	Prox. SFA / Mid SFA	300	Everflex	Ø6 x 200 mm
18	65	M	Moderate	Distal SFA	100	Zilver PTX	Ø6 x 120 mm
Avg ± SD					168 ± 120		168 mm± 131 mm

Table 3.2. Patient demographics, level of calcification, as well as the description of the lesions and PTA-balloons in the PTA group.

Patient no.	Age	Gender	Calcification level	Lesion		PTA-Balloon
				Location	Length (mm)	
19	91	F	Moderate	Distal SFA	50	Ø4 x 40 mm
20	74	M	Moderate	Popliteal	80	Ø3.5 x 150 mm
21	75	M	Severe	Mid SFA / Distal SFA	180	Ø5 x 100 mm
22	66	F	Moderate	Distal SFA	40	Ø4 x 40 mm
23	70	M	Moderate	Mid SFA	40	Ø6 x 60 mm (Drug)
24	57	F	Moderate	Distal SFA	10	Ø4 x 20 mm
25	49	M	Severe	Mid SFA	100	Ø6 x 100 mm
26	71	M	Moderate	Mid SFA / Distal SFA	10	Ø6 x 40 mm
27	80	F	Moderate	Popliteal	40	Ø5 x 40 mm
28	58	M	Moderate	Mid SFA / Distal SFA	50	Ø5 x 40 mm
29	70	F	Moderate	Mid SFA / Distal SFA	40	Ø4 x 60 mm
30	70	F	Moderate	Popliteal	100	Ø4 x 40 mm
31	71	F	Moderate	Popliteal	30	Ø6 x 40 mm (Drug)
32	83	M	Severe	Popliteal	60	Ø3.5 x 40 mm
33	65	F	Severe	Mid SFA / Distal SFA	120	Ø6 x 40 mm
34	75	M	Severe	Mid SFA / Distal SFA	180	Ø5 x 100 mm
35	59	F	Moderate	Distal SFA	10	Ø4 x 20 mm
Avg ± SD					71 ± 53	

3.2.2. 3D Reconstruction of the Arterial Centerline

The 3D reconstruction of the arterial centerlines relies on a pair of angiographic images, which were interactively selected out of the series of images, having a view angle larger than 25°. The initial step is to calibrate the 2D images via the calibration phantom. The phantom consists of 16 radiopaque spherical fiducials which are projected onto the angiographic images as black circular spots (Fig. 3.1). The particular 2D fiducial positions, together with a priori 3D information on the fiducial locations, were used to calibrate each angiographic image[111]. The resulting calibration parameters provide accurate information on the spatial relationship of the acquired images. Based on this spatial relationship, corresponding 2D image locations can be triangulated to a unique 3D position. This triangulation concept was used to retrieve the 3D information of the arterial centerline[112].

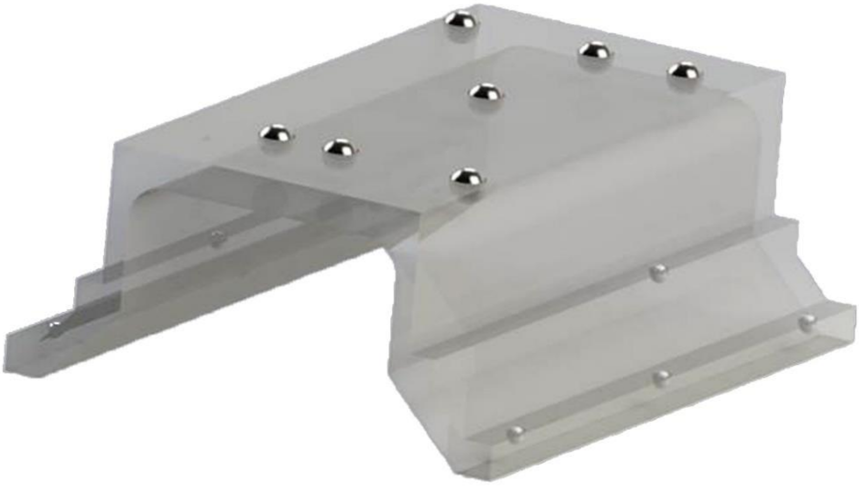

Figure 3.1. The phantom that is attached to the patients' legs during image acquisition is used to calibrate the 2D angiographic images using the fiducials embedded into its surface.

The arterial boundary was defined by picking 2D image points along its projected outline (Fig. 3.2a & 3.2b). After defining the arterial boundary in one image, the beginning and the end of the artery are represented on the second view in terms of two epipolar lines. These lines are used as a guidance to outline the boundary of the artery in the respective other view. The defined boundary points were further interpolated and pairs of opposing boundary points were used to compute respective center points. The set of 2D center points from both views were then triangulated to retrieve the arterial centerline in 3D. A surface model of a reconstructed arterial tree is shown in Fig. 3.2c & 3.2d.

In order to identify the correspondences between straight and flexed positions, certain landmarks have been placed at the stent/balloon ends and to corresponding side-branches between each image using the epipolar constraint. Furthermore, to make sure that the same arterial regions were being considered between pre- and post-treatment images, the landmarks at the stent/balloon ends were projected onto the pre-angioplasty images to accurately identify the lesion ends. All the landmarks were extracted as 3D points.

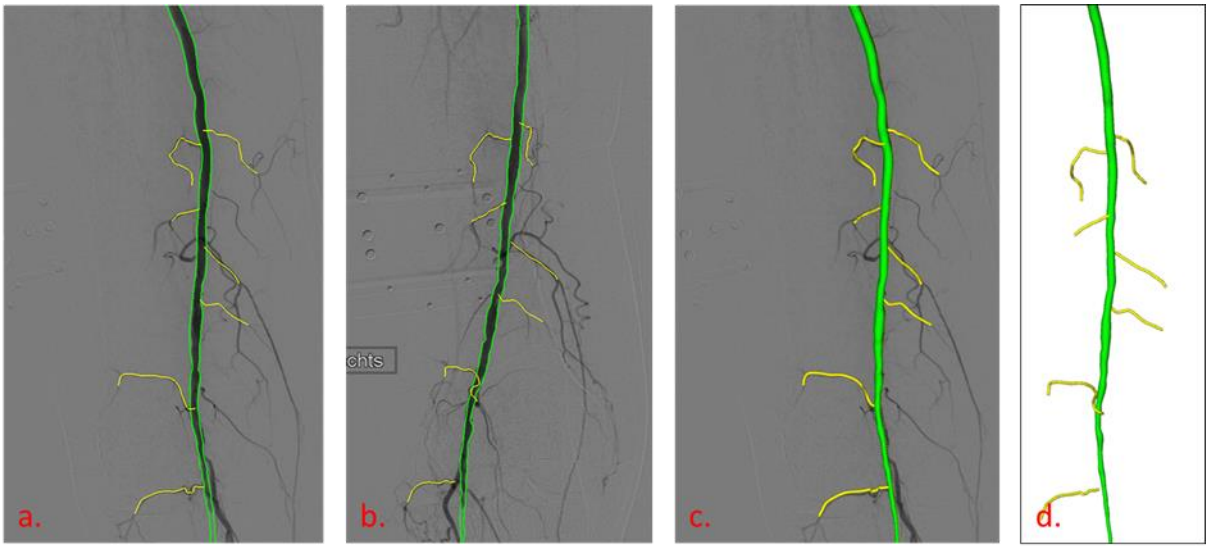

Figure 3.2. Pair of angiographic images with the semi-automatically extracted arterial tree (a) (b); reconstructed 3D arterial tree on top of a radiograph (c); the reconstructed 3D arterial tree (d).

Reconstruction Analysis

To analyze the multi-view reconstruction capability, the forward- and backward projection accuracy of the arterial tree was assessed with respect to an additional validation view. This validation view was also interactively selected, whereas the view direction had to be different (at least 20° apart) than the two views used for 3D reconstruction. The forward projection error results out of the average error distance between the projected points (from the reconstructed model) and the extracted boundary information (defined in the validation view). The backward-projection error is determined by computing epipolar lines for each 2D centerline point (of main branch and side-branches) of the validation view and computing the distance to the closest vertex of the reconstructed model.

3.2.3 Arterial Deformations

A previously established methodology has been adopted to estimate the arterial deformations.[21] The calculations were directly performed on the reconstructed arterial centerlines. The centerline was divided into 3 segments defined by the landmarks that were used to identify the correspondences between straight and flexed positions (i.e. proximal to lesion, lesion center and distal to lesion for the pre-treatment measurements; and proximal to treated region, stented/ballooned region and distal to treated region for post-treatment measurements). The sample sizes for each segment is reported in Table 3.2.

The arterial deformations that were investigated in this study were the changes in length and curvature due to flexion of the leg. The lengths of the individual arterial segments were estimated by calculating the total linear distance between the landmarks defining the boundaries of each segment. As such, the axial deformation was defined as the change in length between flexed and straight positions, divided by the undeformed length in the straight position.

The curvature at a single location was measured by fitting a circle to 3 consecutive points on the centerline[21]. The distance between each consecutive point corresponded to the average arterial diameter and was updated with respect to the investigated FP region. The curvature was defined as the inverse of the radius of the circle. By moving this circle along the entire centerline, the complete curvature profile of an arterial segment was obtained. Both the mean and maximal curvature changes were then calculated as the difference between the curvature profiles in the straight and flexed positions.

Statistical significance regarding the effects of leg flexion, as well as the influences of stent implantation and balloon angioplasty, on arterial deformations were assessed using paired t-tests with a level of 5%.

3.3. Results

For each of the 18 patients, four angiographic datasets (pre- and post-angioplasty in straight and flexed position) were analyzed. For one patient (patient 2), the artery reconstruction was not possible in the pre-angioplasty stage as the main branch was only partially visible due to severe arterial calcification. 19 datasets were available for assessing the reconstruction accuracy. The average angle between a pair of views used for 3D reconstruction was 37.9 ± 8.0° and between the validation view and its closest view used for reconstruction was 28.5 ± 9.1°. The forward projection error was 1.18 ± 0.28 mm on average (max. error: 1.44 mm) and the average backward reconstruction error was 1.03 ± 0.15 mm (max. error: 1.24 mm).

Prior to endovascular treatment, the arterial segments of all samples shortened with leg flexion (Table 3.3). Within the lesion, the average shortening was higher for the stent group (-6.4% ± 3.4%) than the PTA group (-4.6% ± 3.0%). However, this difference was not statistically significant (*P*: 0.11). Furthermore, it was not possible to make a relevant comparison in the proximal regions as there was only one patient data for the pre-stent proximal group.

Regardless of the treatment method, the shortening behavior was preserved for all segments after the operation. For the patients treated only with PTA, the average shortening within the ballooned regions (-7.6% ± 4.9%) increased compared to the diseased regions (5.0% ± 2.3). On the other hand, patients that have received stents showed a statistically significant decrease in the average shortening within the stented regions as opposed to their pre-treatment counterparts (post-stent: -3.2% ± 2.9% vs. pre-stent: -6.4% ± 3.4%, *P*: 0.005). Consequently, a statistically significant increase in the axial flexibility of the treated arterial segment was observed when the treatment did not involve primary stent implantation (post-balloon vs. post-stent *P*: 0.004).

The mean and maximal curvatures of all the arterial segments increased with leg flexion. For both the diseased and treated regions, the average curvature values nearly doubled with the flexion (Table 3.3). Prior to the treatment, there were no statistically significant differences between the curvature behaviors of the stent and PTA groups either within the lesion or distal to the lesion. Likewise, the average curvature values in these regions were similar before and after treatment (Table 3.3). However, similar statements for the proximal regions could not be made due to limited data in the pre-stent proximal group.

Table 3.3. The axial deformation and the mean and maximal curvatures of the FP arteries due to a hip/knee flexion of 20°/70° within the lesions and regions that are proximal or distal to the lesions. The measurements correspond to the average deformations performed prior to PTA, divided into their respective groups of only ballooned (Pre-PTA) and stented (Pre-Stent) after PTA only (post-PTA); and following primary stent implantation (post-stent). The *P* values show the effect of leg flexion on the mean and maximal curvatures of the arteries obtained from paired t-tests.

	Sample Size	**Axial Deformation (%)**	**Curvature (cm^{-1})**							
			Mean				**Maximal**			
			Straight	**Flexed**	**Δ**	***P***	**Straight**	**Flexed**	**Δ**	***P***
Pre-PTA	17									
Proximal to lesion	14	-5.0 ± 2.3	0.05 ± 0.02	0.07 ± 0.02	0.02 ± 0.01	0.031	0.10 ± 0.03	0.14 ± 0.05	0.08 ± 0.05	0.041
Lesion	17	-4.6 ± 3.0	0.07 ± 0.02	0.12 ± 0.08	0.05 ± 0.07	0.028	0.13 ± 0.05	0.26 ± 0.17	0.18 ± 0.16	0.025
Distal to lesion	14	-11.5 ± 4.0	0.06 ± 0.02	0.17 ± 0.16	0.11 ± 0.15	0.060	0.11 ± 0.04	0.30 ± 0.25	0.24 ± 0.25	0.038
Pre-Stent	18									
Proximal to lesion	1	-8.0	0.06	0.17	0.11	-	0.11	0.34	0.28	-
Lesion	18	-6.4 ± 3.4	0.05 ± 0.02	0.09 ± 0.04	0.04 ± 0.03	0.004	0.12 ± 0.04	0.19 ± 0.08	0.12 ± 0.04	0.008
Distal to lesion	15	-12.9 ± 3.6	0.06 ± 0.02	0.16 ± 0.05	0.10 ± 0.06	0.005	0.13 ± 0.05	0.33 ± 0.12	0.28 ± 0.14	0.004
Post-PTA	17									
Proximal to lesion	14	-4.4 ± 3.6	0.04 ± 0.02	0.06 ± 0.01	0.01 ± 0.02	0.097	0.08 ± 0.02	0.11 ± 0.03	0.05 ± 0.05	0.036
Lesion	17	-7.4 ± 5.3	0.07 ± 0.02	0.13 ± 0.07	0.06 ± 0.06	0.003	0.13 ± 0.03	0.25 ± 0.15	0.19 ± 0.12	0.005
Distal to lesion	15	-11.6 ± 4.3	0.06 ± 0.02	0.20 ± 0.18	0.15 ± 0.17	0.120	0.11 ± 0.04	0.29 ± 0.23	0.25 ± 0.21	0.130
Post-Stent	18									
Proximal to lesion	14	-8.7 ± 8.7	0.05 ± 0.02	0.13 ± 0.09	0.08 ± 0.10	0.094	0.10 ± 0.04	0.24 ± 0.19	0.18 ± 0.19	0.082
Lesion	18	-3.2 ± 2.9	0.06 ± 0.02	0.09 ± 0.05	0.03 ± 0.04	0.003	0.11 ± 0.05	0.21 ± 0.16	0.16 ± 0.14	0.004
Distal to lesion	15	-9.3 ± 6.7	0.07 ± 0.02	0.16 ± 0.08	0.09 ± 0.07	< 0.001	0.13 ± 0.04	0.30 ± 0.16	0.24 ± 0.18	< 0.001

Within the regions proximal to the treated segments, the mean and maximum curvature values in the flexed positions were significantly higher with stented arteries than when only PTA was performed (mean curvature: *P*: 0.008; max curvature: *P*: 0.02). For the remaining arterial segments, the average curvature values did not show any significant differences between different treatment methods. Despite this, stent implantation resulted in notable arterial kinking in seven patients (Fig. 3.3). The kinking almost always occurred when the stents were implanted towards the popliteal artery and within 1 cm of the distal stent end. The only exception was that of one patient who had the stent implanted along the full length of the popliteal artery, which resulted in the kinking to occur in the distal SFA, 1 cm to the proximal end of the stent. There was no visible evidence of arterial kinking in the arteries treated with PTA.

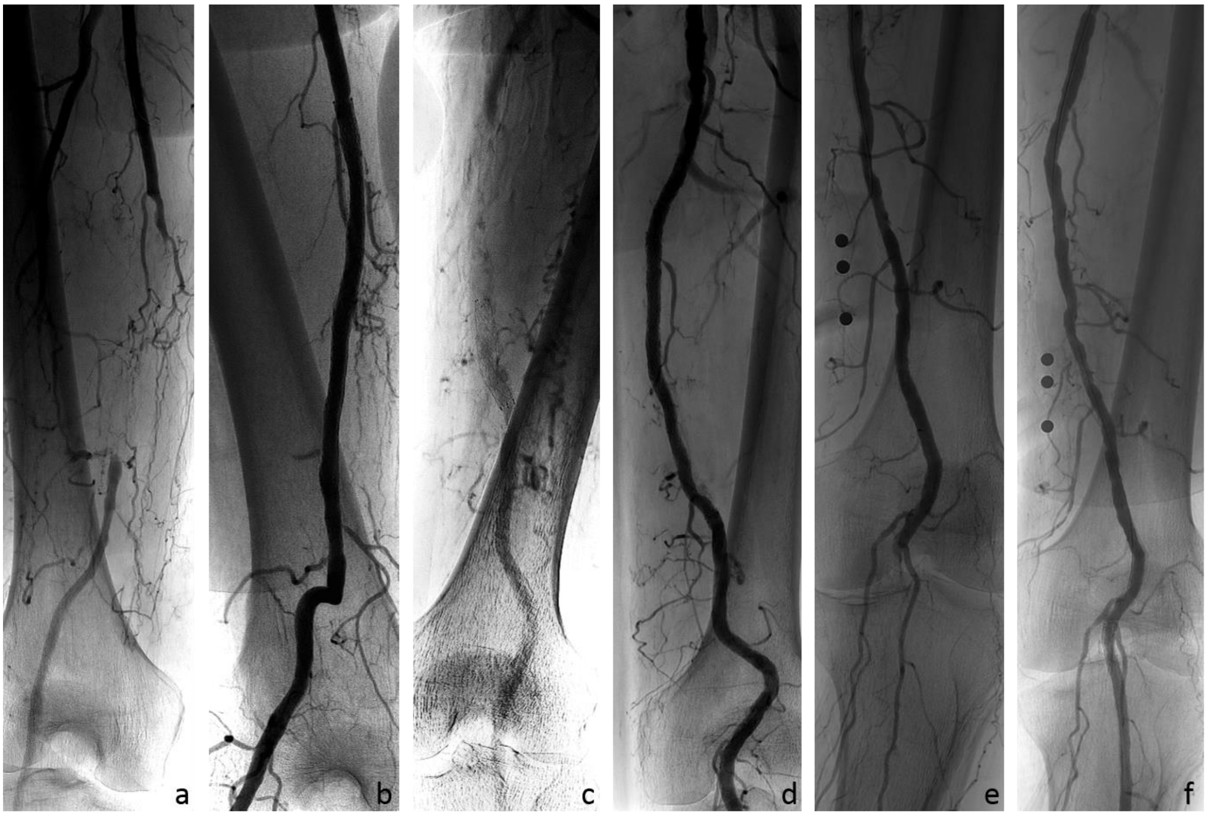

Figure 3.3. Angiographic images of the FP arteries of 4 patients acquired prior to PTA (a, c, e) and following primary stent implantation (b, d, f) and with a hip/knee flexion of 20°/70°. For all cases, the placement of the stents in the higher deformational segments of the FP artery increased the arterial curvatures compared to the pre-treatment phase, leading to extreme deformations, such as arterial kinking, with leg flexion.

With regards to the different anatomical sections along the FP artery, the average maximal curvature change in the popliteal artery (pre-angioplasty: 0.32 ± 0.18; post-balloon: 0.29 ± 0.13; post-stent: 0.34 ± 0.16) was always significantly higher than both the distal-SFA (pre-angioplasty: 0.11 ± 0.08; post-balloon: 0.07 ± 0.02; post-stent: 0.16 ± 0.16) and mid-SFA (pre-angioplasty: 0.07 ± 0.05; post-balloon: 0.07 ± 0.07; post-stent: 0.12 ± 0.11). No significant differences were found in the bending behaviors between the distal-SFA and mid-SFA. Finally, based on unpaired t-tests conducted between the stent groups of Pulsar-18, Everflex and Zilver-PTX, the differences between the arterial deformations caused by different stent designs were not found to be statistically significant.

3.4. Discussion

The main drawback of endovascular therapy in the FP arterial tract is the risk of restenosis.[74,89] Recent clinical trials reported the long-term restenosis rates in that challenging arterial segment to be 17% with drug-eluting stents[27] and 20% with drug-coated balloons.[132] While these numbers are an improvement over the long-term outcomes obtained with non-coated devices,[103,115] they also further underline the hypothesis that the persisting restenosis rates can be attributed to the mechanical deformations of the FP artery.

The healthy FP artery deformations have been the subject of numerous studies[16,17,31,63,88]. However, comparisons between these studies (i.e. old vs. young patients; living vs. cadaveric subjects) show that the deformations are heavily dependent on the composition of the arteries.[16,88] As such, these studies can only present limited information to improve current treatment methods and devices. To this end, it is crucial to analyze the deformations of arteries with PAD prior to and after endovascular treatment. Such studies would not only provide information on the arterial deformations of the target population, but also on the mechanical state of the artery resulting from different treatment modalities. Therefore, the aim of this study was to estimate the in-vivo deformations of 35 FP arteries with PAD prior to endovascular treatment and immediately after PTA or primary stent implantation.

The reported reconstruction errors correspond well with data published in literature. Based on 4-5 projections of the coronary artery, Liao et al. reported a mean back-projection error of 1.18 mm.[71] The RMS forward projection error of the FP arterial centerline was reported by

Klein et al. to be 2.13 mm for the leg in straight position and 1.61 mm for the leg in flexed position.[62]

For all FP segments, the lengths of the arteries shortened and their mean and maximum curvatures increased as the leg moved to a flexed position (Table 2). This general deformation behavior was found to be similar before and after acute stent implantation and balloon angioplasty. Furthermore, both the axial deformation and curvature behaviors within the lesion showed no significant differences between the pre-stent and pre-PTA groups. This suggests that the choice of the treatment method was not influenced by the arterial deformations of the diseased arteries.

The treatment had a statistically significant effect on the axial deformation behaviors of the diseased segments due to leg flexion. Performing plain balloon angioplasty resulted in increased axial shortening, while primary stent implantation led to decreased axial compressibility. On the other hand, both procedures had a limited impact on the axial deformations of the regions distal to the diseased segments. Similarly, PTA had no effect on the axial behavior of the artery in the proximal regions.

Stented arteries had a significantly higher mean and maximum curvature values compared to the arteries that underwent only PTA in the regions proximal to the treated segments. However, there was only one valid patient data corresponding to the segment proximal to the lesion in the pre-stent group. As a result, it’s not clear if the statistically significant differences observed between the mean and maximum curvatures of stented and ballooned arteries were already present prior to the treatments or are caused by the different treatment methods. Within the treated and distal-to-the-treated segments, the average bending behavior of the FP arteries due to leg flexion was similar between the two treatment methods. However, 40% of the patients that received stents exhibited arterial kinking either distal or proximal to the stent ends immediately after the procedure (Fig. 3.3). In contrast, arteries that were only treated with PTA were not associated with kinking and, in one patient, the procedure was even found to resolve an identified case of kinking observed before treatment, resulting in a smoother bending behavior (Fig. 3.4).

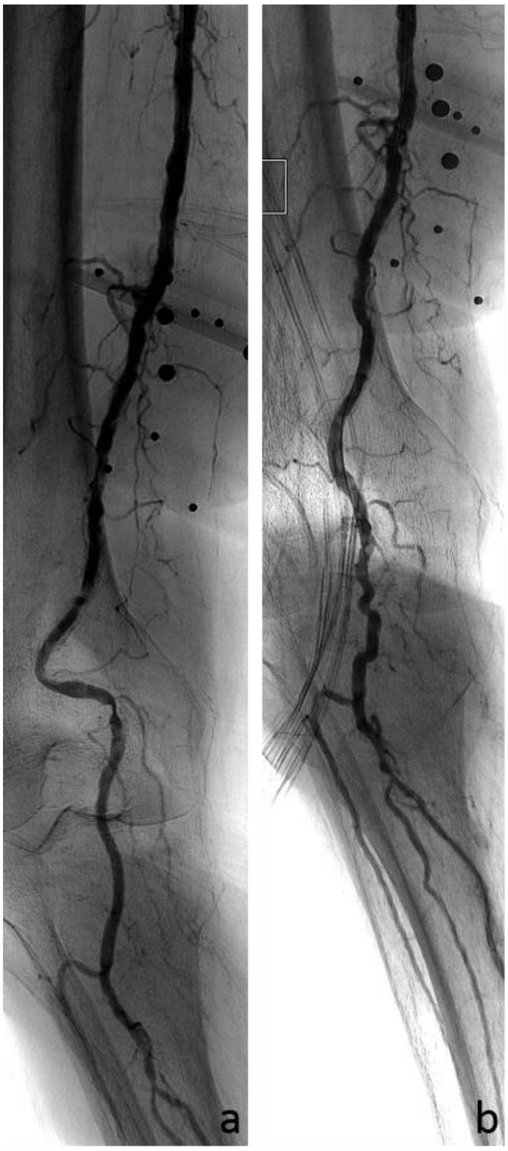

Figure 3.4. Angiographic images of the FP artery of one patient acquired prior to (a) and following (b) PTA and with a hip/knee flexion of 20°/70°. Performing PTA resolved the arterial kinking observed in the pre-treatment phase and returned the artery to a more natural deformation behavior.

Our results suggest that the restrictions imposed by the stents on the axial shortening capabilities of the arteries are liable to produce extreme arterial deformations. Due to the FP artery's posterior location to the knee joint, the overall arterial length is expected to decrease during flexion. If the artery is not able to compress axially, the additional tissue would either form a curve of its own or join a pre-existing curve, resulting in an increased curvature profile and, possibly, arterial kinking. This is especially true for the cases, in which stent implantation occurs in the segments of the FP artery that undergoes greater deformation with leg flexion, such as the distal-SFA and the popliteal artery[40,63,87,112]. The comparisons between the two treatment methods further support the relation between arterial kinking and increased axial stiffness of the artery due to stent placement.

Previous clinical studies have suggested that chronic arterial kinking may disrupt the natural blood flow, leading to restenosis or reocclusions.[4] In our case, 20% of the patients showed symptoms of restenosis within six months following the operation. Among them, four patients exhibited arterial kinking following treatment. This distribution of the data results in an odds ratio of 5.0, suggesting that the possibility of restenosis increases with the presence of arterial kinking. Based on this observation, the “leave-nothing-behind” strategy could be considered as the optimum treatment approach, as performing only balloon angioplasty helped restore the natural deformation behavior of the FP arteries. However, bail-out stenting will continue to be utilized for arteries that are suspected to collapse without the presence of a stent. Therefore, to decrease the possible restenosis rates caused by stent implantation, future stents would benefit from designs that enable axial shortening during leg flexion. Another, albeit a more controversial, solution, would be to place an additional stent into the arteries that experience kinking. This would help smoothen the transition of the mechanical stiffness between the stented segment and the adjacent bare artery. The major risk with this approach concerns the formation of stenosis due to stenting a healthy artery, which may be prevented to a certain extent by using drug-eluting stents.

Due to the limited number of studies and the differences between their methods, a direct comparison of our results with previous publications is difficult. The average axial shortening and mean and maximum curvatures from the pilot study presented in Chapter 2 compare favorably with our current pre-angioplasty measurements within the lesion.[44] However, contrary to the outcomes observed from that pilot study, no correlation between the curvature behavior and level of calcification was observed. Nikanorov et al. measured the axial elongation, bend radius and deflection angle on 17 patients that were only implanted with the Absolute (Abbott Vascular, Santa Clara, CA, USA) self-expanding stent.[87] With a 70°/20° knee/hip flexion, they reported a mean axial compression of 2.4% ± 0.4% in a combined segment of the SFA/proximal popliteal (2 patients) and a mean curvature of 0.1 cm^{-1} in the popliteal artery (6 patients). Finally, Ganguly et al. reported a mean axial shortening of 4% ± 3% and a mean curvature change of 0.05 cm^{-1} in the stented femoral arteries (unknown stent types) of 13 patients with an unknown degree of leg flexion.[40] The results from both studies compare favorably with our observations. The differences can be attributed to the number of patients included in the study, to the different stent designs implanted in the patients and to the different methods used to perform the measurements.

The main limitation of the present study concerns the reconstruction of the 3D models from only two 2D radiographic images. Due to the sparse number of views the identification of corresponding side-branches was not possible in most cases. Besides changes to the artery's length and curvature, leg flexion also causes twisting of the FP artery. However, the twist angle could not be measured as it requires the accurate position of the side branches and their deviation from the main branch. Due to mismatched field of views between the angiographic images, the severity of the calcifications and, in some instances, the lengths of the lesions, it was not always possible to identify the proximal and distal regions, leading to varying reductions in the sample sizes of these sub-groups. However, with the exception of one sub-group, the inclusion was above 80%, thereby providing a sufficient number of datasets to allow for relevant statistical evaluations. All the calculations were performed on two static positions, so the measurements actually represent the arterial deformations at a single point that is found during the walking cycle rather than considering a dynamic walking situation, which includes the effect of muscle contraction on the arterial shape. Finally, a follow-up study is needed to further support the hypothesis that arterial kinking significantly increases the risk of restenosis.

3.5. Conclusion

The current study showed the different effects of the available endovascular treatment methods on the FP artery deformations. In this context, PTA was observed to help in recovering the natural deformation behavior of the artery. On the other hand, stent implantation limited the artery's axial compressibility during leg flexion, which led to arterial kinks when the stents were implanted in the segments of the FP artery that are normally subject to large deformations. As arterial kinking is associated with restenosis and reocclusions, our results would favor the leave-nothing-behind approach for the FP artery revascularizations. However, for arteries that require stent implantation, the current stent designs should be improved to allow for greater shortening with leg flexion.

Chapter 4

Nitinol Stent Oversizing in Patients Undergoing Popliteal Artery Revascularization: A Finite Element Study[45]

4.1. Introduction

Peripheral arterial disease (PAD) is commonly treated by endovascular means.[47] Restenosis remains the major drawback of endovascular revascularization and may affect up to 70% of patients undergoing plain balloon angioplasty of the femoro-popliteal (FP) arteries.[107] The introduction of self-expanding Nitinol stents has reduced restenosis rates within these arterial segments to about 40% depending on arterial lesion morphology.[108] Two main explanations have been proposed to explain the restenosis subsequent to Nitinol stent placement; stent fractures[105] and chronic irritation of arterial walls during or following stent deployment.[51] While stent fractures may be explained by the high mechanical loads acting upon the stent during flexion of the leg[44], arterial wall damage may result from oversizing of Nitinol stents, which is frequently performed to achieve large luminal gain and to prevent stent migration.[101,137]

Several investigations have been performed to evaluate the effect of stent diameter on the risk of restenosis.[11,61,93,101,137] A correlation between Nitinol stent oversizing and restenosis

---

[43] Gökgöl, C., N. Diehm, F. Rikhtegar, and P. Büchler. The Effects of Nitinol Stent Oversizing in Patients Undergoing Femoro-popliteal Artery Revascularization: A Geometrically Patient-specific Finite Element Study. *Ann. Biomed. Eng.* 43:2868–2880, 2015.

has been evaluated using animal models, for which oversized stents have been implanted in healthy arteries of Yucatan swine[137], mini-pigs[101], canines[11,61] and humans.[93] Based on these studies, it is difficult to assess the clinical effect of Nitinol stent oversizing a few months following endovascular intervention. In some studies, stent oversizing was associated with adequate luminal gain immediately during the implantation, but ultimately led to excess neointimal hyperplasia and restenosis.[11,101,137] Other authors reported limited restenosis months after implantation of oversized stents.[61,93]

A better description of the biomechanical implications of oversizing on arterial tissues may help to understand the mechanisms responsible for restenosis and therefore help the clinicians to select the appropriate stent size during intervention. There are various structural finite element (FE) analyses on stent deployment.[22,37,81,96,135,138] Similarly, computational fluid dynamics (CFD) simulations have been widely used to investigate the hemodynamic properties of stented arteries and their implications for neointimal hyperplasia.[15,18,60,66,94,114] However, the only numerical studies conducted on stent missizing were found to be on balloon-expandable stents deployed in straight cylindrical models of healthy[15,66] or calcified coronary arteries.[128] Due to the significant differences in their deployment procedures, the results from these studies could not be adopted for self-expandable Nitinol stents. Thus, the aim of the present study was to quantify the biomechanical effects of Nitinol stent oversizing using numerical models of non-calcified popliteal arteries obtained from patients undergoing endovascular revascularization. Two main aspects were considered; the mechanical effect of the stent on arterial walls and hemodynamic alterations induced by stents of varying size. We hypothesized that wall stresses increase with increasing stent size, which may lead to chronic arterial wall damage. Moreover, we suggested that the presence of an arterial curvature would aggravate the effects of oversizing by further increasing arterial stress levels. Finally, we hypothesized that oversizing could trigger neointimal hyperplasia in the arterial walls by reducing wall shear stress (WSS) and by increasing oscillatory shear index (OSI).

4.2. Materials and Methods

Reconstruction of the Patient-Specific Arterial Geometries

The anatomies of the arterial models were obtained from five patients (4 men and 1 woman; age, 56-79 years; mean age 69 ± 9.1 years) undergoing intra-arterial 3D rotational digital subtraction angiography (AXIOM-Artis, Siemens, Germany) prior to endovascular revascularization of FP arteries.[44] For 4 patients, the investigated segment of the arterial tract started from the descending genicular artery and ended at the superior genicular artery. For the remaining patient, the segment ended at the inferior genicular artery. Ethics committee approval had been obtained prior to the start of this investigation. Further information about the patients and the acquisition process could be found in a previous study.[44]

All 3D angiographic examinations were saved digitally and transferred to a workstation capable of 3D post-processing. Following the segmentation of the vasculatures on the 3D image datasets with an image analysis software (Amira 5.2; FEI Visualization Sciences Group, Burlington, MA, USA), arterial centerlines were extracted and shortened to only have the section with the maximal curvatures (mean length of 53 mm, with a range of 47-59.5 mm). Each centerline was described by 108 points. For each patient, the FE mesh of the artery was reconstructed around these centerlines using a script in Matlab (The Mathworks Inc., Natick, MA, USA). For each node on the centerline, the script generated 5 rings, each with 128 nodes. This meshing approach resulted in the same number of nodes and elements for all the arterial models. Furthermore, for longer centerlines, the distance between the rings were adjusted so that the element size around the region of stent implantation would be the same as the shorter centerlines. Apart from the patient-specific arteries, a sixth arterial model was created from a straight centerline to represent a generic, straight artery. The arteries were assumed to have a circular cross section of constant diameter. Three concentric arterial layers were reconstructed; the intima (5mm – 5.3mm), the media (5.3mm – 5.9mm) and the adventitia (5.9mm – 6mm). All of the arterial models had 54,874 linear hexahedral reduced integration (C3D8R) elements; 13,696 elements in both intima and adventitia and 27,392 elements in the medial arterial layer. The validity of the mesh was confirmed through a mesh sensitivity analysis, in which the maximum circumferential stresses in each layer of the artery changed by 3% at the diastolic and systolic points of a cardiac cycle.

Material Model of the Arteries

The material model adopted for the artery was an anisotropic, hyper-elastic model that represented two families of collagen fibers.[42,52] The strain energy density function was based on the constitutive laws proposed by Gasser et al., which allows not only the specification of fiber orientations, but also the inclusion of fiber dispersions within each layer.[42] The material parameters for the model were taken from experiments performed on non-calcified iliac arteries (Table 4.1).[42,52] The two families of fibers were symmetrically arranged with respect to the arteries' circumferential directions. In accordance with previous findings[42], the fibers within media were perfectly aligned in circumferential direction (κ = 0); whereas the fibers within intima and adventitia were modeled as slightly (κ = 0.02) and highly dispersed (κ = 0.226), respectively.

Table 4.1. Material parameters for the individual layers of the artery; intima, media and adventitia.

	Adventitia	Media	Intima
C_{10} (kPa)	7.64	15	31
k_1 (kPa)	996.6	4	51
k_2	524.6	2.3	1.1
$\delta_1 = \delta_2$ (°)	50	7	5
κ	0.226	0	0.02

Numerical Models of the Nitinol Stents

The arterial models were implanted with two commercially available, self-expanding stents: Astron-Pulsar and Astron (Biotronik AG, Bülach, Switzerland) (Fig. 4.1). Both stents were made of the same shape memory Nitinol, whose material coefficients were provided by the manufacturer (Table 4.2). Nevertheless, the stents exhibited different mechanical behaviors due to their different designs, with the Astron having larger strut width, thickness and outer diameter (119µm, 245µm and 5 mm, respectively) than the Astron-Pulsar stent (80µm, 155µm and 3.5 mm, respectively). FE meshes of both stents were produced with 173,160 and 91,248 C3D8R elements for Astron-Pulsar and Astron, respectively. The number of elements used to mesh the stents were determined by sensitivity analyses, in which the maximum principal strain values changed less than 2.5% in the stents' crimped configurations.

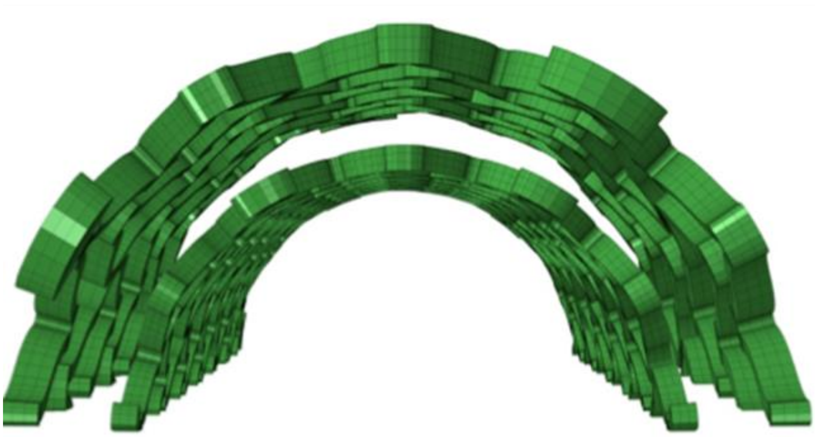

Figure 4.1. The production geometries of the Astron-Pulsar and the Astron stents showed that the Astron had a larger strut width, thickness and outer diameter than the Astron stent. Despite the geometrical differences, both stents had the same patterns.

Table 4.2. Material parameters for the Nitinol model obtained from the laser-cut stent.

Austenite elasticity E_A (MPa)	65,000
Austenite Poisson's ratio ν_A	0.33
Martensite elasticity E_M (MPa)	23,500
Martensite Poisson's ratio ν_M	0.33
Transformation strain ε^L	0.046
Loading $(\delta\sigma/\delta T)_L$ [MPa T^{-1}]	0
Start of transformation loading σ_L^S (MPa)	465
End of transformation loading σ_L^E (MPa)	535
Reference temperature T_0($°C$)	37
unloading $(\delta\sigma/\delta T)_U$	0
Start of transformation unloading σ_U^S (MPa)	227
End of transformation unloading σ_U^E (MPa)	187
Start of transformation stress in compression σ_{CL}^S (MPa)	582
Volumetric transformation strain ε_V^L	0.046

Structural Simulation Parameters

Due to the discontinuities induced by the large number of complex contact interactions between several components of the model, the structural analyses were conducted with

Abaqus/Explicit (Dassault Systemes, Simulia Corp., RI, USA). A semi-automatic stable time increment of $4\text{x}10^{-6}$ was defined to control mass scaling. This increment ensured that the ratio of kinetic to internal energy in the system remained below 5% to avoid dynamic effects, which guaranteed that the analysis remained quasi-static. To leave the stents constraint free and let them find their own mechanical equilibriums, all displacement boundary conditions were applied onto the nodes of two rigid cylinders that were meshed with 4 node quadrilateral shell elements, with reduced integration (S4R). They surrounded the inner and outer surfaces of the stents and acted as expansion and crimp tools (Fig. 4.2). While the undeformed diameter of the expansion tool corresponded to the inner diameter of the Astron-Pulsar stent; the initial size of the crimp tool was sufficiently large to only contact with the stents when this one reaches its unconstrained diameter. The contact between the surfaces was defined as a frictionless, hard contact. Additionally, arteries were fixed at both ends with the exception of the local radial directions. A total of four cases were considered for each artery, where stents with unconstrained diameters of 5.5, 6, 7 and 9 mm were used.

Preliminary FE Analyses

Prior to the oversizing analyses, the validity of the arterial model had been evaluated. Rectangular strips of each individual arterial layer were subjected to uniaxial extension and their mechanical behaviors in axial and circumferential directions had been compared with published experimental data.[53] Another evaluation of the proposed arterial model was performed by calculating the compliance of the artery. The compliance was calculated as the ratio of the maximum nominal strain to the maximum pressure change during a cardiac cycle and the numerically obtained value was compared with in vivo measurements.[122] The precision of the models used to simulate the stents was also evaluated. The radial force generated by the stents was calculated while crimping the stents to a 1.8 mm diameter followed by an expansion to their unconstrained diameters of 9 mm. The radial force was compared with experimental measurements provided by the stent manufacturer. Finally, in order to ensure a 5 mm lumen at a mean blood pressure of 120 mmHg, the arterial models were run through an iterative process[38], in which the arterial expansion was estimated under the target pressure. The unloaded arterial geometry obtained following the last iteration was considered as the stress-free configuration.

FE simulations of Stent Deployment

Accurate calculation of the deployment requires considering the complete stress-strain history of the Nitinol stents. Therefore, full stent deployment, involving the preconditioning of the stents, was performed for all cases (Fig. 4.2). In the first step, the only active contact in the model was between the inner surface of the stent and the outer surface of the expansion tool. By radially displacing each node of the rigid tool, the stent was expanded to its desired unconstrained diameter. At this stage, the stent was subjected to annealing; a procedure used to remove the existing stresses, while preserving the deformed shape. Subsequently, the previous contact pair of stent-expansion tool was replaced with a contact interaction between the outer-surface of the stent and the inner-surface of the crimp tool. In the next step, the stent was crimped to its deployment diameter (1.25 mm for Astron-Pulsar and 1.88 mm for the Astron stent) by applying displacements to the nodes of the crimp-tool. During this step, a uniform pressure load of 120 mmHg was applied to the inner surface of the arteries to expand the lumen diameters to exactly 5 mm, which corresponded to the average lumen diameter of healthy arteries in physiological blood pressures.[120] Following crimping, the crimp tool was deformed into the shape of the arterial centerline to simulate stent insertion. The contact pair was modified to include an interaction between the outer-surface of the stent with the inner-surface of the artery in addition to the existing stent-crimp tool pair. Consequently, during the tool's radial expansion to its final configuration (which depends on the unconstrained stent diameter for each oversizing case), the stent smoothly detached from the tool when it came into contact with the inner wall of the artery. After deployment, a cyclic blood pressure of ±40 mmHg (i.e. pressure between 80mmHg and 160mmHg) was applied to the inner surface of the artery for a total of 3 cycles to simulate a case of isolated systolic hypertension, which has been reported to be the most frequent form of hypertension in patients suffering from PAD.[100]

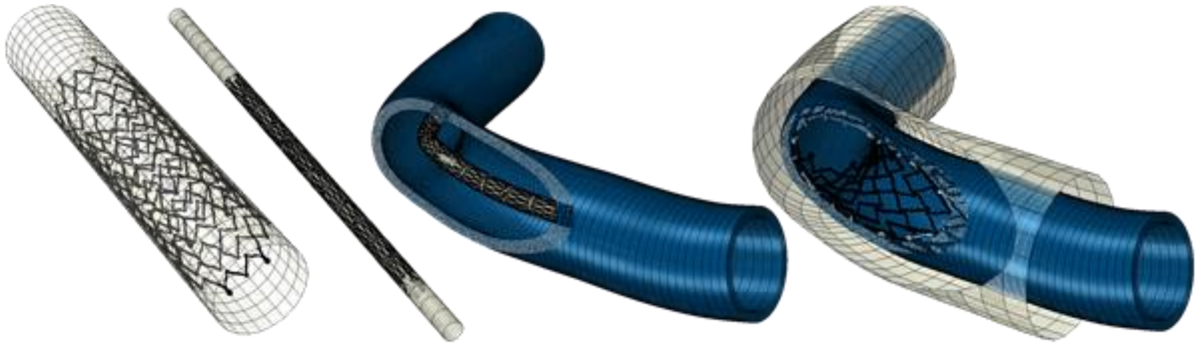

Figure 4.2. The preconditioning and deployment of a Nitinol stent into a patient-specific popliteal artery. By radially displacing the nodes of the expansion tool (not shown), the Astron-Pulsar stent is expanded to its unconstrained diameter of 7mm (left). After annealing, the stent is crimped to its deployment diameter of 1.2 mm by radial displacement of the nodes of the crimp tool (middle-left). The insertion to the patient's artery is achieved by a displacement-controlled deformation of the crimp tool into the shape of the arterial midline (middle-right). The crimp-tool is then expanded to its initial diameter, which corresponds to the deployment of the stent as it is detached from the tool to contact the arterial walls (right).

CFD Simulations

Blood flow computations investigated the effects of different oversizing ratios and the performances of both stents in a patient-specific artery. Following stent deployment, the deformed meshes of the artery and the stents were exported from Abaqus as open file formats (.obj) and converted to surface .stl models using Solidworks 2013 (Dassault Systemes, Simulia Corp., RI, USA). These geometries were used for the generation of the computational volumetric grids, consisting of approximately 4.5 million tetrahedral elements, in ANSYS ICEM CFD (ANSYS Inc., Pittsburg, PA). The computational domain is adequately refined near the stent struts and different sizes of the computational grid are tested in a steady-state solution to ensure that the results are independent of the applied spatial discretization scheme. The analyses were performed with the finite volume code CFX 14.0 (ANSYS Inc., Pittsburg, PA), where the following continuity and Navier-Stokes equations are discretized with second order accuracy in space and time:

$$\nabla . u = 0 \quad (1)$$

$$\rho \frac{\partial u}{\partial t} + \rho u . \nabla u = -\nabla p + \mu \nabla^2 u \quad (2)$$

where *u* is velocity (m/s), *t* is time (s), *ρ* is density (kg/m^3) and *p* and *μ* are pressure (Pa) and dynamic viscosity (Pa.s), respectively.

Physiological blood flow was simulated as a transient flow condition by applying the MRI-measured volumetric flow rate at the inlet of the artery.[126] The artery outlet was set to have zero pressure and a no-slip boundary condition was prescribed at the arterial wall and stent struts. Consequently, the outlet was extended enough to minimize the effects of boundary conditions on the accuracy of the simulations. As the plug-flow profile is applied at the inlet, it was also extended to reach a realistic blood flow profile. This way, a fully developed parabolic flow profile was guaranteed. Blood was modeled as an incompressible Newtonian fluid with a density of 1050 kg/m^3 and a viscosity of 3.5x10^{-3} Pa.s.[78] Three cardiac cycles were calculated using a time step size 0.01 s. Each time step was assumed converged, when residuals reduced to 10^{-6} of their initial values.

Analysis of Results

A relation between restenosis and arterial stresses has previously been suggested, with high arterial stresses acting as a predictor of restenosis.[129] On the other hand, the lack of an exact stress threshold that marks the beginning of such a process would only lead to indirect suggestions for a safe oversizing ratio. A better approach would be to define an oversizing limit based on tissue failure, which could be correlated by experimental findings.[53] As a result, the maximum circumferential stresses in each layer were compared with their respective ultimate experimental stresses to specify the most failure-prone layer in the artery. Subsequently, the maximum circumferential stresses in this layer were evaluated to establish a correspondence between arterial stresses and unconstrained stent diameters.

The application of cyclic blood pressures following deployment provided the means to conduct fatigue analyses on the stents. The main aim was to calculate the factor of safety ($FOS_{Nitinol}$) of the Nitinol stents, which represented the structural integrity of the implanted device. Since Nitinol is strain driven, mean strains and strain amplitudes were calculated at all integration points. Using the strain amplitude obtained from the 3rd cycle and a Nitinol endurance limit of 0.4%[90], $FOS_{Nitinol}$ was determined as:

$$\frac{1}{FOS_{Nitinol}} = \frac{0.4}{\varepsilon_{amp}} \tag{3}$$

where ε_{amp} represents the maximum strain amplitude and was calculated as the difference of the maximum principal strains between the systolic and diastolic blood pressures. A FOS value below +1 corresponds to material failure.

Spatial and temporal variations of arterial endothelial WSS are believed to play a critical role in hemodynamics of intact and stented arteries.[97] WSS parameters such as Time-Average WSS (TAWSS) and Oscillatory Shear Index (OSI) were derived from the numerically-calculated transient WSS field using an in-house MATLAB script and visualized by Tecplot (Tecplot Inc., Bellevue, WA). To obtain results independent of the temporal cycles and simulation initialization, the data of only the last cardiac cycle was evaluated. TAWSS, as a crucial factor to evaluate the hemodynamic status of the stented artery, was defined as[56]:

$$TAWSS = \frac{1}{T}\int_0^T \left|\vec{\tau}_w\right| dt \tag{4}$$

where, $\left|\vec{\tau}_w\right|$ is the CFD-calculated magnitude of the instantaneous WSS vector (Pa) and T is the duration of one cardiac cycle (s). To include the effect of transient oscillation of the blood flow, OSI was defined as[56]:

$$OSI = \frac{1}{2}\left(1 - \frac{\left|\int_0^T \vec{\tau}_w \, dt\right|}{\int_0^T \left|\vec{\tau}_w\right| dt}\right) \tag{5}$$

To provide a less-sensitive hemodynamic performance indicator, the surface area exposed to low TASSW and high OSI was normalized with respect to the luminal surface area.

4.3. Results

The preliminary simulations have been performed to validate the numerical models proposed for the artery and the Nitinol stents. The compliance of the arterial tract calculated with the model was 7.1% $\mathrm{mmHg}^{-1} \times 10^{-2}$, which corresponded to experimental measurements acquired on the popliteal artery of subjects without evidence of PAD.[122] Simulations of the arterial tissues showed a good agreement with uniaxial traction experiments conducted on each individual arterial layer (Fig. 4.3).[53] In addition, the radial forces of the stents calculated with the model corresponded to the forces measured experimentally (Fig. 4.3). Furthermore, mechanical comparison of the two stents revealed that the Astron had a higher radial force compared to the Astron-Pulsar during its expansion from 1.8 to 7 mm, thereby making it stiffer at the point of contact (about 5 mm) with the artery (Fig. 4.3).

Following stent deployment, results indicated that adventitia was the arterial layer supporting most of the mechanical load (Fig. 4.4). Moreover, adventitia was the most failure-prone layer, reaching up to 60% of its ultimate stresses[53] for a normal-sized stent and up to 100% of the ultimate stresses when the oversizing ratio was 1.8. For all cases, the maximum circumferential stresses in this layer increased non-linearly with respect to the unconstrained diameters of the Astron-Pulsar stent (Fig. 4.5). Furthermore, the relationship between acute luminal gain and stent diameters was also observed to be non-linear. Thus, when stents of 5.5, 6, 7 and 9 mm diameters were implanted, acute luminal gains were reported to be 7%, 10%, 11% and 11.5%, respectively (Fig. 4.5).

The non-linear increase in arterial stresses and lumen gains was similar for both stents in all arteries (Fig. 4.5). Due to its higher radial force, the Astron stent produced higher stresses in the arteries when compared with the Astron-Pulsar stent at each pressure level (Fig. 4.6). In the straight arterial model, the maximum difference between the stresses produced by the two stents was about 30% for both normal-sized and oversized stents. This difference increased to more than 40% in patient-specific arteries (Fig. 4.6). The artery also had a greater expansion with the Astron stent, in which the maximum increase of the lumen gain was 1.5% and 2.5% for straight and patient-specific arteries, respectively (Fig. 4.6).

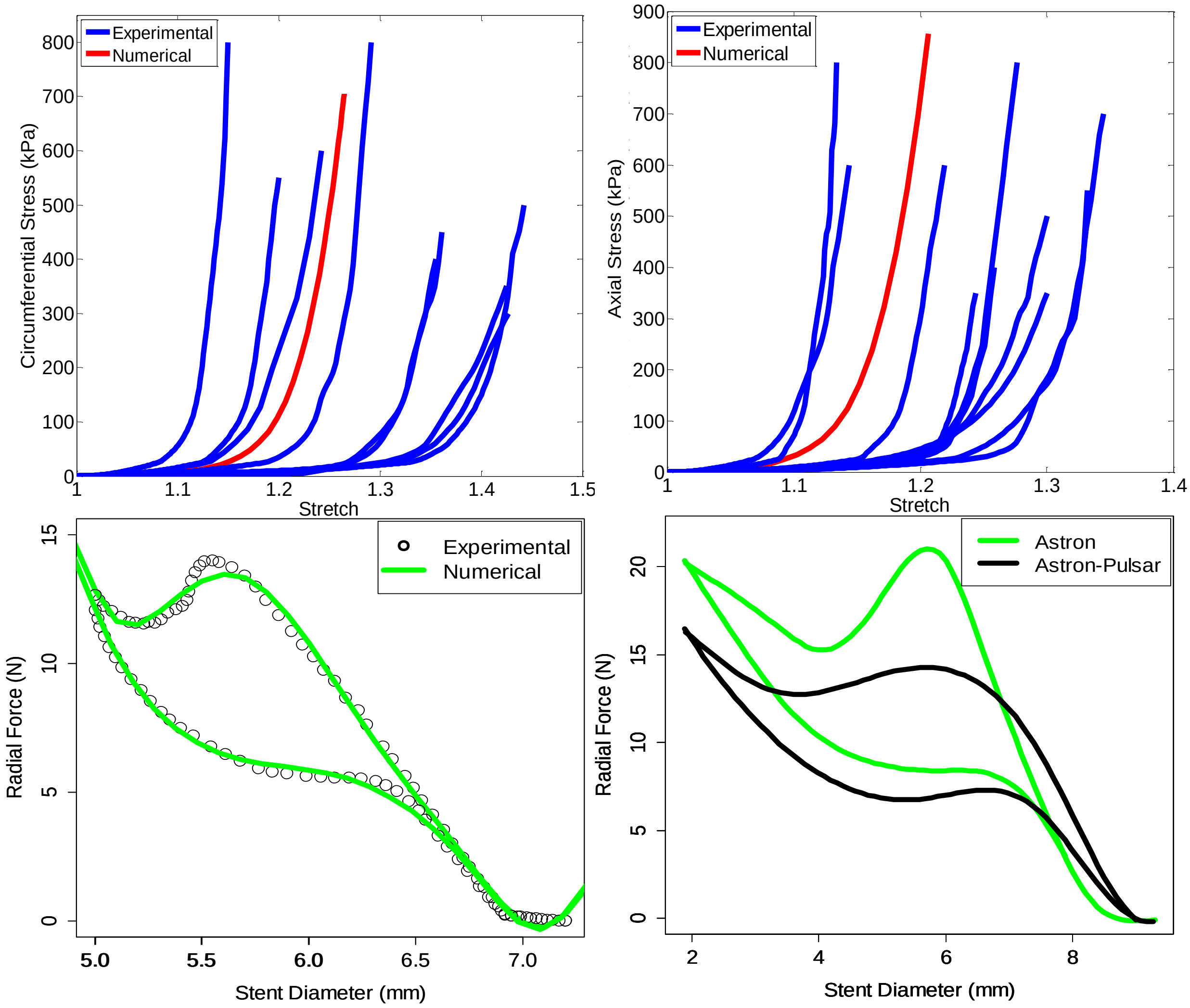

Figure 4.3. Uniaxial extension tests of the adventitial layer excised in circumferential (top left) and axial (top right) directions are numerically modeled and the resultant stress-strain relationships (red) are found to be in range of the diverse mechanical behaviors obtained via experiments (blue). The numerically obtained radial forces (green) of the Astron-Pulsar stent correspond to the experimental measurements (black) (bottom left). Additionally, the comparison of the radial forces of Astron-Pulsar (black) and Astron (green) stents highlights the stiffer nature of the Astron stent (bottom right).

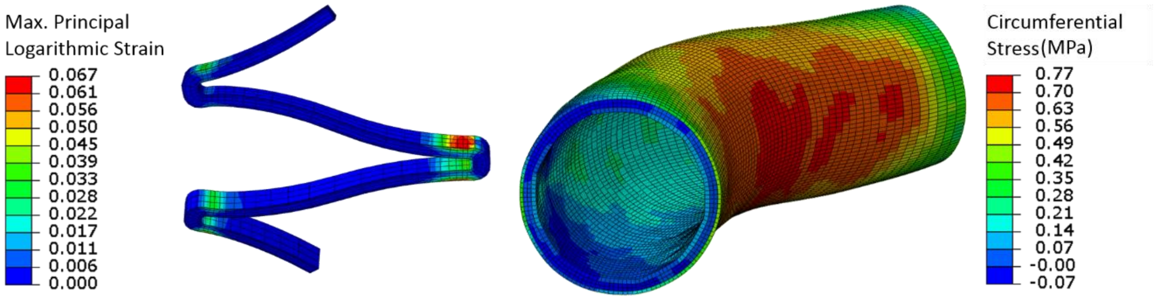
Max. Principal
Logarithmic Strain
0.067
0.061
0.056
0.050
0.045
0.039
0.033
0.028
0.022
0.017
0.011
0.006
0.000
Circumferential
Stress(MPa)
0.77
0.70
0.63
0.56
0.49
0.42
0.35
0.28
0.21
0.14
0.07
-0.00
-0.07

Figure 4.4. Following deployment, strains are concentrated at the outer sides of the struts (left) and stress distribution in different layers of the artery demonstrates the load-carrying behavior of the adventitia (bottom-right).

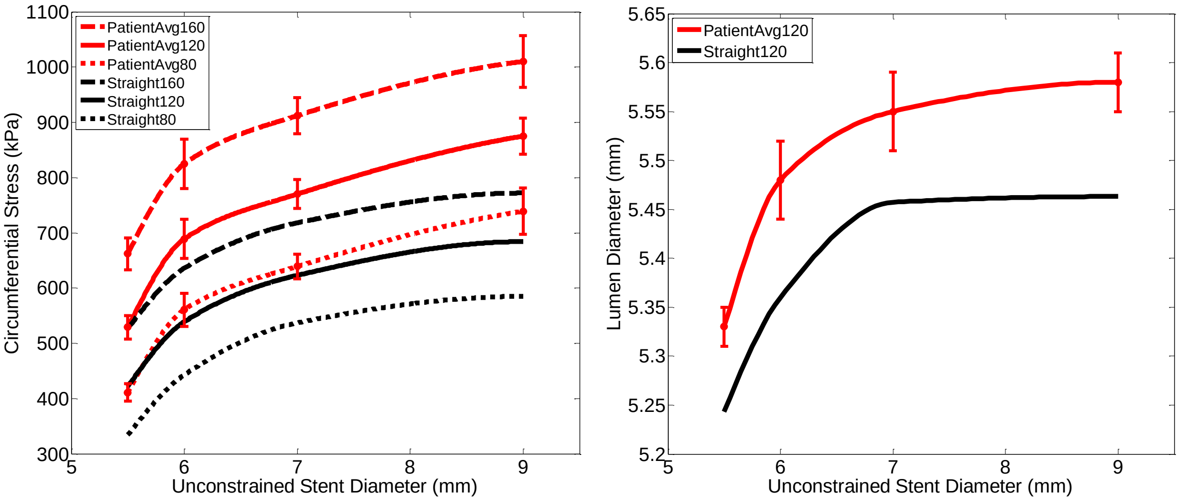

Figure 4.5. The average maximum arterial circumferential stresses of the patient-specific arteries (red) exceed the stress levels observed in a straight artery (black) and show a less emphasized non-linear behavior for all blood pressure values (range: 80 mmHg – 160 mmHg) (left). Regardless of the arterial geometries, a very small lumen gain is achieved by oversizing the stents (right).

Regardless of the arterial geometry, the fatigue behavior of the Astron-Pulsar stent showed similar behaviors. Increasing the unconstrained stent diameters led to an increase in the mean strains at the integration points; with the average maximum values being reported as 1.70% ± 0.51%, 3.38% ± 0.89%, 6% ± 0.07% and 7.07% ± 0.11 for 5.5, 6, 7 and 9 mm, respectively (Fig. 4.7). In contrast, there was a smaller increase in the strain amplitude with increasing oversizing ratios. Consequently, the factor of safety of the stent was found as 5.28 ± 0.1, 4.94 ± 0.11, 3.64 ± 0.27 and 1.18 ± 0.11 for 5.5, 6, 7 and 9 mm, respectively. A similar gradual decrease in the safety factor of the stent was observed for the Astron as well.

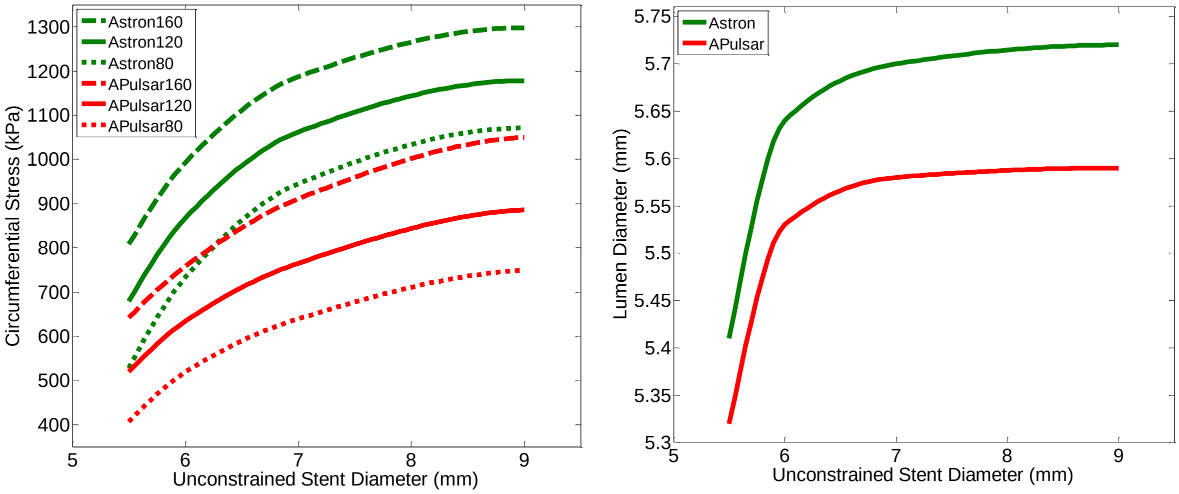

Figure 4.6. The stent with a higher radial force, Astron (green), was found to create significantly higher stress levels than the Astron-Pulsar stent (red) (left). In comparison, a very limited increase in lumen gain is observed to create a mismatch in arterial stress-lumen relationship (right). Regardless of the stent designs, a very small lumen gain is achieved by oversizing the stents (right).

For all deployment cases and for both stent models, spatial structure of blood flow and instantaneous patterns of WSS were found to be complex and varying during the cardiac cycle (Fig. 4.8). Throughout the cardiac cycle and for the time-integrated parameter, localized areas of atheroprone low WSS (less than 5% of maximum WSS i.e. < 0.5 Pa) were seen in regions of flow separation, e.g. near the stent struts and inner side of curved artery. Regions of high WSS, on the other hand, were likely to occur on the outer side of the arterial curvature and on the in-lumen-protruded side of the stent struts. Independent of the stent stiffness, length and geometry, larger areas were exposed to low WSS at proximal portions of the stented segments. Furthermore, the distribution of OSI, as a measure of temporal WSS change, in both stents showed similar traits with the TAWSS distribution. High values of OSI (more than 20% of maximum OSI i.e. >0.1) were seen in the vicinity of stent struts, inter-strut connectors, proximal segment of stented artery and distal inner wall of the curved artery.

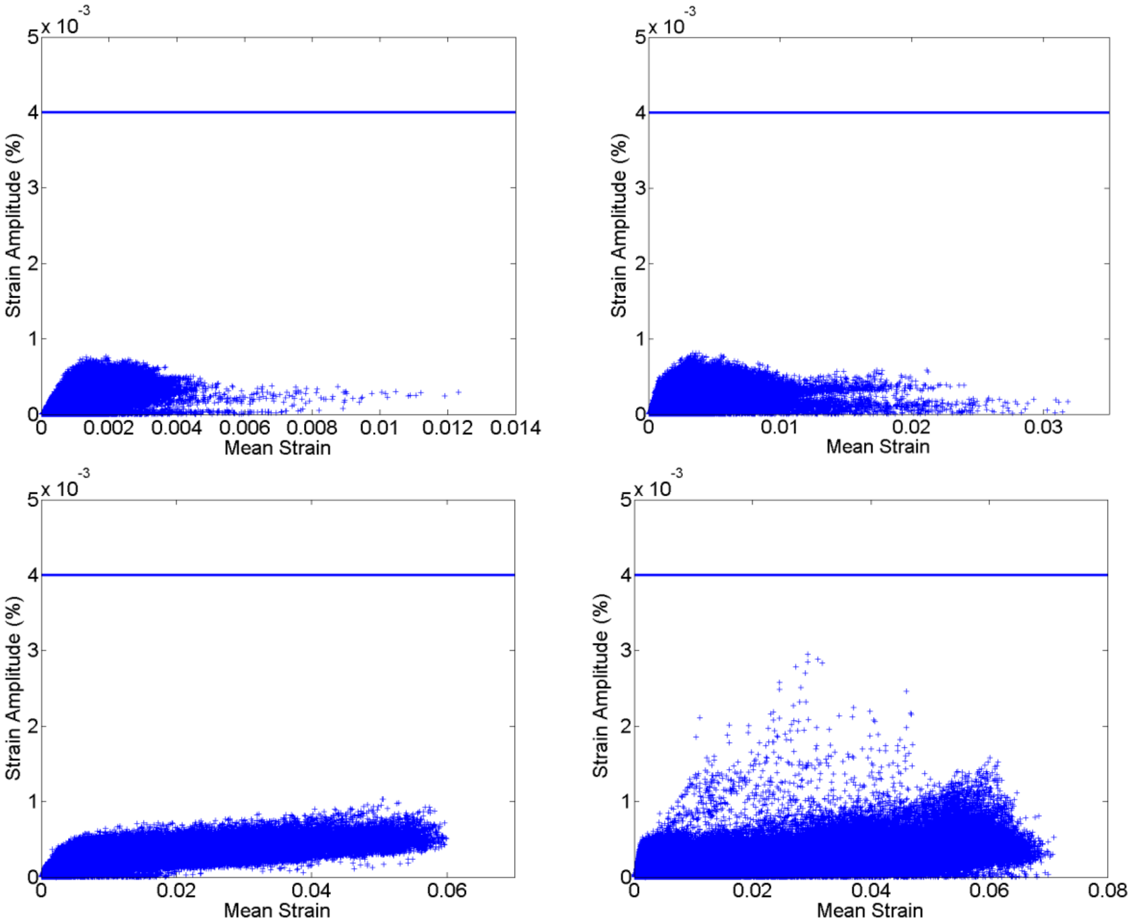

Figure 4.7. The fatigue behavior of the Pulsar stent when deployed into a geometrically accurate artery with unconstrained stent diameters of 5 mm (top left), 6 mm (top right), 7 mm (bottom left) and 9 mm (bottom right): As the oversizing ratio is increased, the strain amplitude of more points are found to migrate towards the Nitinol safety limit of 0.4; thereby decreasing the safety factor of the stent.

A direct comparison of all cases showed that increasing the stent-induced arterial diameter would raise the normalized surface area exposed to low TAWSS (less than 0.5 Pa), which was concurrently more pronounced for the cases stented with the Astron (Fig. 4.9). In addition, the deployment of Astron definitively assured that the surface area exposed to high atheroprone values of OSI would be bigger than with the Astron-Pulsar (Fig. 4.9). No clear relation between the oscillatory features of blood flow and different lateral expansion rates was observed.

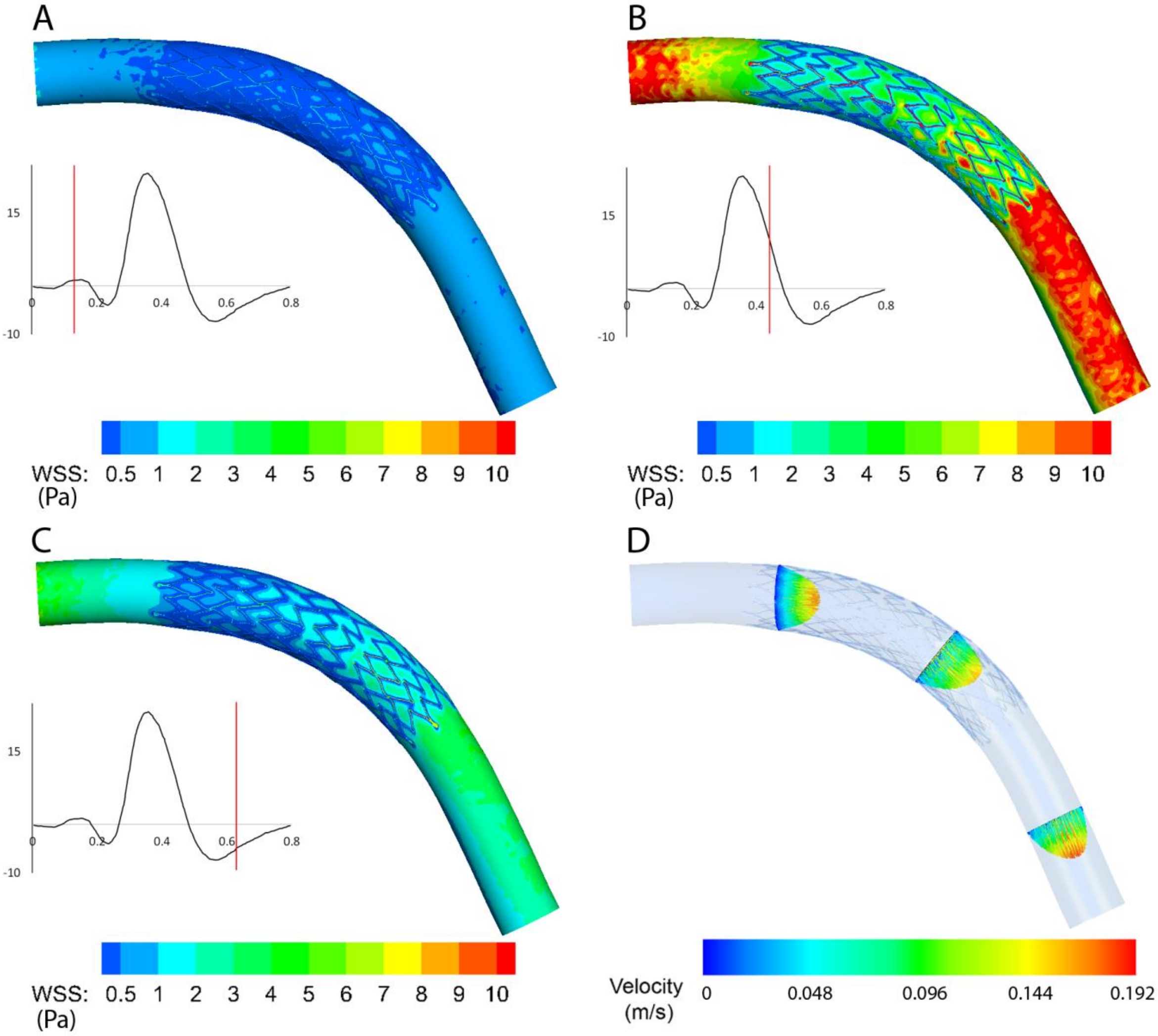
A
B
C
D
15
-10
0
0.2
0.4
0.6
0.8
WSS: (Pa)
0.5 1 2 3 4 5 6 7 8 9 10
Velocity (m/s)
0
0.048
0.096
0.144
0.192

Figure 4.8. Instantaneous pattern of WSS distribution on stented popliteal artery at different instants of a cardiac cycle marked by solid red line on a flow rate profile inset. WSS is shown at: (A) t = 0.13 second (B) t = 0.44 second and (C) t = 0.64 second. Panel (D) shows how the symmetric velocity profile is distorted toward the outer wall owing to arterial curvature. This affects the WSS distribution considerably.

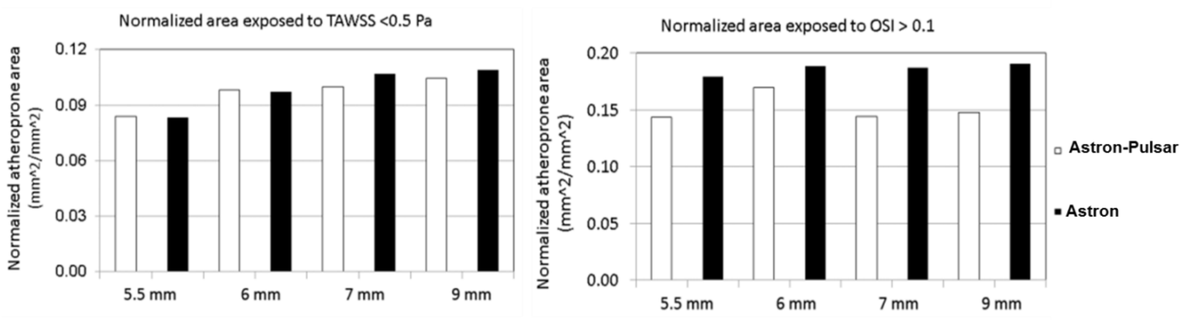

Figure 4.9. Normalized surface area exposed to TAWSS of less than 0.5 Pa (left) and OSI of more than 0.1 (right). Oversizing leads to larger areas being exposed to low TAWSS and more prominent atheroprone conditions at the arterial wall, which is more noticeable for the cases with the stiffer Astron stent. On the other hand, while the local mechanical environment induced by oscillatory characteristics of blood flow significantly increase with the deployment of Astron, they are not directly affected by stent oversizing.

4.4. Discussion

Nitinol stent oversizing is commonly performed during endovascular procedures; however, currently, stent sizing mostly relies on the expertise of the clinicians and is defined by stent manufacturers and not by objective criteria. While oversizing a stent will undoubtedly increase acute luminal gain, it can also create a hostile chronic environment for the artery through stent-to-arterial wall interactions, which may ultimately lead to arterial damage, neointimal/adventitial hyperplasia and restenosis.[101,137] With previous clinical studies reporting controversial findings on the subject[15,61,93,101], the efficacy of oversizing remains an issue to be answered. Thus, to improve the understanding of mechanical effects of stent oversizing in the popliteal arterial tract, numerical analyses have been performed within the present investigation.

The hypothesis behind stent oversizing is that oversized stents will limit possible arterial restenosis due to acute lumen enlargement. However, results of this study showed a non-linear relationship between the lumen gain and oversizing ratio (Figs. 4.5 & 4.6). Increased oversizing led to a small lumen increase, while generating rapidly increasing arterial stresses. This mismatch between the limited lumen gain and elevating stresses can be illustrated by a 3% lumen vs. 30% stress increase for the Astron-Pulsar stent (4% vs. 33% for the Astron) when the stent-to-artery ratio is transitioned from 1.1 to 1.2. Therefore, our results suggest that instead of providing an additional lumen gain, stents with higher oversizing ratios inflict greater chronic arterial damages through increased chronic arterial stresses.

A comparison between the numerical and experimental results indicated that increased oversizing, the level of arterial stresses came close to the failure limits of the tissues, which have been obtained via uniaxial extension tests .[53] Independent of the stent design, adventitia was found to be the most vulnerable layer due to its highly nonlinear mechanical response at pressures above 80 mmHg.[110] The high risk of failure in this layer further suggests that normal sized stents are more favorable to protect arterial walls from chronic damage and, consequent, neoadventitial hyperplasia.[110]

Results of the numerical calculations showed that both the maximum arterial circumferential stresses and the luminal gains increased non-linearly with respect to the unconstrained stent diameters regardless of arterial geometries and stent designs (Fig. 4.5). Comparisons between straight and patient-specific geometries showed that the latter exhibited slightly less pronounced non-linear increase of the mechanical parameters with increased oversizing. This may be explained by distinctive deformations exerted onto different arterial geometries during stent deployment. While the straight artery was only displaced radially, the curved arteries were subjected to straightening alongside radial expansion. This effect not only caused an overall increase of the circumferential stresses for each oversizing ratio, but also led to higher stress differences between oversized and normal-sized arteries.

The successful outcome of an endovascular procedure not only lies in selecting the correct stent size, but also in selecting the correct stent design. In the present study, the disproportionate increase between lumen gain and arterial stresses for successive oversizing ratios was similar for both stents (Fig. 4.6). On the other hand, oversizing the Astron stent to the ratio of 1.2 increased the risk of failure considerably when compared with the Astron-Pulsar stent. Furthermore, a maximum difference of 2.5% was observed between the lumen gains achieved at this oversizing ratio (Fig. 4.6). This value remains small when compared with their corresponding stress difference of 37% (Fig. 4.6). Therefore, this mismatch between the changes in the stresses and lumen diameters suggests that radial force would have an impact on the processes observed during clinical follow-up, as stents with higher radial forces would likely inflict more chronic irritation to arterial walls when compared with their less stiff counterparts.

Individual patient anatomies in the present study all showed different curvatures. However, no relation between the fatigue behavior of either the Astron-Pulsar or the Astron and arterial geometries was observed. Instead, the stents performed similarly for all curved arteries. This may be explained by the fact that an identical systolic-diastolic pressure behavior was applied to all models.[96] The safety factor of the Astron-Pulsar stent was found to decrease with increasing oversizing ratio, which can be explained by the higher deformations exhibited by oversized stents due their incomplete expansions at deployment. Although the calculated fatigue criterion remained below the failure level, stents with 9 mm diameters came close to the Nitinol endurance limit of 0.4% (Fig. 4.7)[90], without even considering the mechanical forces acting on the stent due to the physiological loading present in lower limb arteries[44]. This result suggests that oversizing increases the risks of stent failures, which has been directly related with restenosis.[65]

Physiological stressors such as near-wall flow, which directly perturb intra- and extracellular signaling, proved to be a reliable predictor for local biological responses of stented arteries[12]. Thus, studying the hemodynamic performance of implanted stents and considering procedural variabilities, such as oversizing, could be used to provide clinicians with accurate observations on the causes of adverse biological effects. Local flow patterns are proved to affect the neointimal formation, in-stent restenosis and thrombosis in stented arteries. Therefore, computed indices of flow were calculated here to support the hypothesized drawback of stent oversizing. The critical values of low WSS and high OSI, which are reported to correlate with adverse clinical outcomes[97], were found to be similar to already published studies.[98] Stent oversizing considerably perturbed the local flow patterns, specifically the near-wall flow, due to the abrupt change in the proximate bounding geometry. The procedure was found to increase the normalized surface area exposed to low TAWSS, leading to a large area of the stented artery to be susceptible to unfavorable biological responses. The abrupt change of arterial size and the expanded cross-section would decrease the blood flow and the WSS in the vicinity of the stented wall (Fig. 4.8). For cases where significant lumen gain is not achieved, this would depress the hemodynamic efficiency of the oversized stent and seriously question its clinical expediency. In contrast, the larger surface area exposed to high OSI was not affected by the stent-to-artery ratio (Fig. 4.9). This may be mainly related to the specific shape of the stent and curvature of the artery, wherein the secondary flow generated by the arterial curvature and recirculation zones induced by the stent will have a combinatory effect on the oscillatory characteristics of the blood flow. For the cases implanted with the Astron stent, larger deformations were induced in the artery walls around the stent struts, which resulted in a larger alteration of near-wall flow compared to the more flexible Astron-Pulsar stent. Consequently, computed indices of flow such as velocity and WSS are more affected when stiffer stents are used. In conclusion, stent-induced oversizing of the arterial wall, independent of the stent type, would deteriorate the hemodynamic performance of peripheral stents, wherein the arteries fitted with stiffer stents become more vulnerable.

The validity of the proposed arterial model was verified by comparing the numerical simulations with published experimental data. The individual behaviors of each arterial layer obtained via traction simulations, as well as the overall compliance of the artery, matched well with existing measurements (Fig. 4.3).[53,122] Furthermore, the mechanical behavior of the adventitia is similar to previous reports[110], as it became the mechanically predominant layer when the physiological blood pressure of 13.3 kPa is exceeded. These comparisons indicated that the present arterial model is appropriate to evaluate arterial stenting. Finally, the immediate lumen gain values obtained from the deployment simulations were compared with a clinical investigation that performed Nitinol stent oversizing in the femoral arteries of Yucatan swines[137]. These clinical findings compared favorably with the lumen gains obtained in our study for high oversizing ratios (>1.4). On the other hand, numerical models with lower oversizing ratios (<1.4) predicted a larger lumen gain, which can be attributed to the difference between the numerical and clinical arterial diameters prior to stenting.

Several limitations to the present study need to be discussed. Only healthy arteries were modeled and stented, while stents are generally implanted in diseased arteries. The inclusion of plaques into the model would not only change the stress/strain values, but would also have an impact on the location of maximum stress/strain concentrations in the arterial models. However, based on current understanding, deployed stents usually overlap with the non-obstructed parts of an artery, thereby exerting potential effects caused by stent oversizing on both healthy and diseased sections. Moreover, pre-clinical investigations have so far used healthy animal arteries to investigate the effects of oversizing. Thus, the results could easily be compared to validate the numerical models. Only two stent designs were used in this study. Although the effects of oversizing are not expected to change with different stent designs, the level of stress and lumen expansion may show differences. Performing similar calculations for different designs could work towards achieving an average value for a safe oversizing ratio.

Since the present study focused on the parametric evaluation of the stenting procedure, the same material model was used for all patient-specific arteries. Due to this parametric approach, the conclusion on the effect of oversizing should remain identical for each patient, although the exact level of strain may differ. Finally, the residual strains for the arteries were not modeled, which may suggest a possible overestimation of the arterial stresses. Nonetheless, the nonlinear stress behavior with increasing stent diameters would be the same. The accuracy of blood flow simulations depends on the chosen boundary conditions. In order to obtain more realistic results, direct experimental measurements should be used to define the boundary conditions for blood velocity or pressure at the inlet and outlet. In this study, a generic dataset obtained from MRI measurement was applied at the inlet of the domain. However, a simplified boundary condition was used at the outlet with a zero pressure. To limit the error introduced by this approximation, the outlet was extended to maintain realistic flow profiles.

4.5. Conclusion

The effects of Nitinol stent oversizing in geometrically patient-specific popliteal arteries were evaluated through numerical analyses. A gradual increase of the stent-to-artery ratio from 1.1 to 1.8 showed the development of both the structural and hemodynamic properties of arteries with respect to the normal and oversized stent diameters, while providing the framework for fatigue analyses of the stents. The results showed that oversizing had a very limited impact on the immediate lumen gains achieved following stenting. At the same time, transition to a higher oversizing ratio led to a significant increase in structural and WSS in arteries, which can be associated with arterial damage and disruption in the blood flow. Since self-expanding stents will continuously apply radial forces to the arterial walls in order to reach their nominal diameters, these damages will continue to accumulate, creating a mechanical environment prone to induce restenosis. Therefore, to increase the success rate of an endovascular procedure in a FP arterial tract that includes healthy popliteal segments, clinicians should take care not to oversize Nitinol stents and allow them to contribute to a late lumen gain in the arteries.

Chapter 5

Numerical Modeling of Nitinol Stent Oversizing in Arteries with Peripheral Arterial Disease: The Influence of Plaque Type[43]

5.1. Introduction

Endovascular treatment of Peripheral Arterial Disease (PAD) is either performed by percutaneous transluminal angioplasty (PTA) or through primary stent implantation following revascularization.[47,89] In the case of the latter, choosing the correct stent size is crucial to simultaneously counteract arterial recoil and prevent extensive damage to the arterial tissues.[101,137] However, due to a lack of established guidelines, the current clinical practice consists of the qualitative selection of the proper stent size based solely on recommendations provided by the stent manufacturers. As a result, Nitinol stent oversizing is frequently performed to maintain full wall apposition and prevent stent migration.[61,93,101,137] Despite these perceived advantages, the large stresses inflicted onto the arteries due to oversizing might lead to arterial damage and, ultimately, to restenosis.[22,51,96,129]

The number of studies on Nitinol stent oversizing in the peripheral vasculatory system are scarce. To date, there have only been two animal investigations that have studied the implications of coated and non-coated Nitinol stent oversizing in Yucatan swine and mini-

[41] Gökgöl, C., N. Diehm, and P. Büchler. Numerical Modeling of Nitinol Stent Oversizing in Arteries with Clinically Relevant Levels of Peripheral Arterial Disease: The Influence of Plaque Type on the Outcomes of Endovascular Therapy. (**Submitted** to *Ann. Biomed. Eng.*, August, 2016)

pigs.[101,137] Both studies have defined over-sized arteries as having a stent-to-artery ratio, i.e. the ratio of nominal stent diameter to lumen diameter of the artery, above 1.4 and suggested that while all the arteries have shown neointimal proliferation, only the oversized arteries (stent-to-artery ratio > 1.4) were damaged enough to exhibit restenosis. However, these studies were performed in healthy arteries and, as such, the results might not be applicable to the patient population that undergoes endovascular therapy of the lower limbs. A clinical study on stenosed carotid arteries supports this hypothesis, as the results suggest that oversized arteries (stent-to-artery ratio between 1.4 and 2.0) yield better outcomes in terms of late lumen loss compared to normal-sized arteries (stent-to-artery ratio below 1.4).[93] These contradictory outcomes can be attributed not only to the differences in the vasculature systems, but also to the different morphologies and mechanics between healthy and diseased arterial layers. Therefore, to understand the effects of Nitinol stent oversizing on the actual clinical practice, the procedure should be evaluated on peripheral arteries with PAD.

Numerical analyses are routinely used to support or replace experiments with the intention to analyze the fatigue life of stents.[32,75,76,91] They are also frequently used to understand the mechanical and hemodynamic behaviors of both healthy and diseased arteries due to stent implantation.[8,22,45,55] In this instance, the numerical approach is a suitable substitute to performing clinical investigations that would be ethically questionable due to a high risk of damage to both the plaque and healthy arterial tissues. The majority of the previous numerical studies on stent mis-sizing have focused on balloon-expandable stents in coronary arteries.[14,15,54,66] These studies have shown that stent implantation tends to disrupt the natural flow patterns and that oversizing (stent-to-artery ratio > 1.0) negatively impacts the Wall Shear Stress (WSS) parameters and, consequently, increases the risk of restenosis. However, the results are not directly adaptable either to the endovascular procedures performed in lower-limbs or to the common clinical practice due to the differences in stent types, their deployment techniques and the use of healthy arterial models. On the other hand, the limited number of studies that cover Nitinol stent oversizing in peripheral arteries performed the analyses on non-calcified arteries.[45] As such, the effects of Nitinol stent oversizing on the mechanical behavior of arteries with calcified plaques are currently not known. Therefore, the main aim of this study was to investigate the changes in arterial stresses and acute lumen gains associated with gradual stent oversizing. The numerical investigation was performed using finite element (FE) analyses of endovascular therapy in an artery model that included clinically relevant PAD. A secondary objective was to observe whether the effects of oversizing were influenced by the degree of lesion calcification.

5.2. Materials and Methods

Components of the FE Simulations

Five parts were required for the FE modeling of the endovascular therapy; the diseased artery, the angioplasty balloon/s, the Nitinol stent, and the expansion and crimp tools. The artery was idealized as a straight cylinder with completely healthy sections at both ends and a mix of healthy and atherosclerotic tissue at the center for a total length of 35 mm (Fig. 5.1). Each healthy section had a length and lumen diameter of 5.0 mm[122] and were made of 3 layers[55]; intima, media and adventita with thicknesses of 0.15 mm, 0.25 mm and 0.1 mm, respectively.[116,119] The diseased section was created by increasing the thickness of the intimal layer to reach a luminal diameter that corresponded to 30% of the healthy lumen, which is indicative of a clinically relevant PAD. By modifying the mechanical tissue properties of the thickened intimal layer to represent an atherosclerotic plaque, the stenosed tissue had been directly embedded into the artery. This approach enabled a geometrically smooth transition between the healthy and diseased sections and the resultant configuration corresponded to a symmetric plaque (Fig. 5.1a). As it was previously shown that femoral plaques are typically heavily calcified[24,29,50,70], the plaque only included calcification and not any underlying sections of lipid pool or fibrotic tissues. Each layer, including the plaque, was discretized with linear hexahedral reduced integration elements (C3D8R). In each healthy section, the number of elements in intima, media and adventitia were approximately 4,000, 7,000 and 4,000, respectively. For the diseased section, the number of elements in the medial and adventitial layers were increased by approximately 2 times their healthy counterparts, while the plaque was meshed with approximately 50,000 elements. A mesh sensitivity analysis was performed to verify that the mesh was sufficiently dense to satisfy the convergence criteria defined in a previous study.[45]

The initial geometry of the angioplasty balloon corresponded to its fully-expanded configuration with a diameter of 5.0 mm and a length of 25 mm (Fig. 5.1b). The balloon had 4,000 linear quadrilateral membrane elements with reduced integration (M3D4R). A commercially available Nitinol stent, Astron-Pulsar (Biotronik AG, Bülach, Switzerland), with production dimensions of 80µm strut width, 155µm strut thickness, 3.5 mm outer diameter and 25 mm length was considered for the simulations (Fig. 5.1d). These dimensions represented the configuration right after the stent was laser-cut from a Nitinol tube and before the in-silico expansion and annealing. The number and type of elements for the stent were previously verified and corresponded to 170,000 linear reduced integration elements (C3D8R).[45] The rigid expansion and crimp tools, which were used for the preconditioning and deployment of the stent, were both meshed with linear quadrilateral shell elements with reduced integration (S4R). The expansion tool had the same initial diameter as the inner diameter of the stent. Conversely, the diameter of the crimp tool corresponded to the unconstrained stent diameter achieved at the end of the preconditioning state and, as such, varied with each oversizing case (Fig. 5.1d).

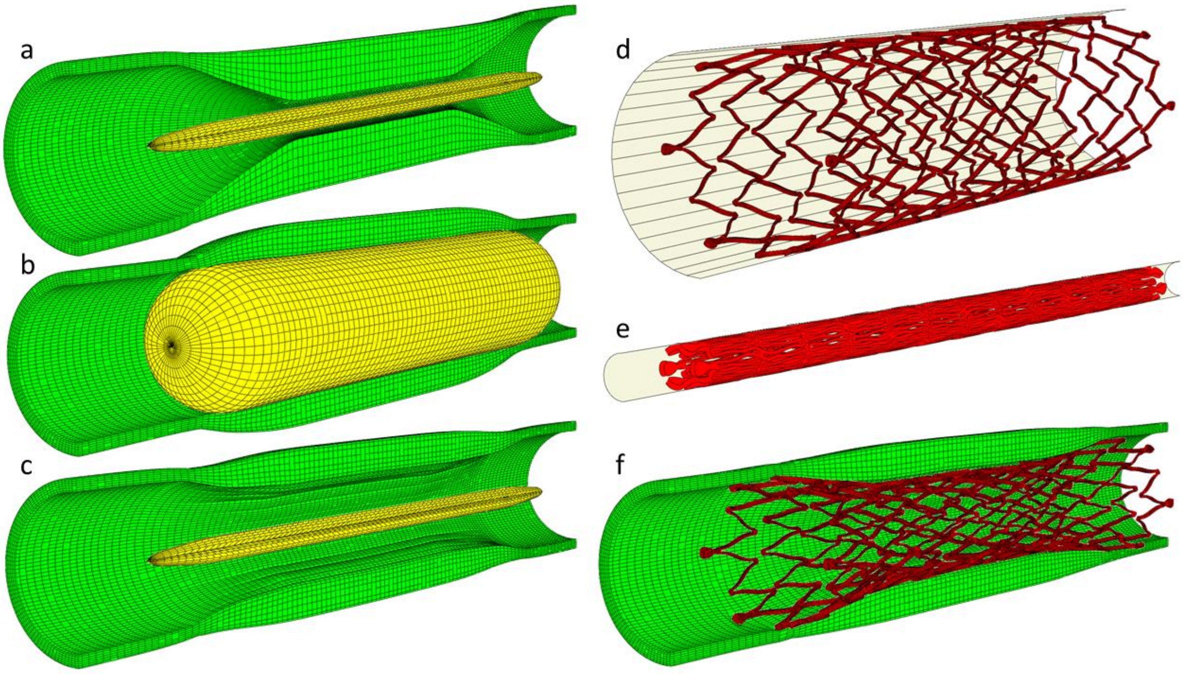

Figure 5.1. The complete procedure of an endovascular therapy in an artery with a clinically relevant level of PAD (70% stenosis): The pressurization of the artery with the physiological blood pressure of 120 mmHg and the positioning of the angioplasty balloon (a), unfolding of the angioplasty balloon with a pressure of 7 atm to simulate plaque failure (b), folding of the angioplasty balloon and evaluation of the expanded lumen diameter (c), representation of the Nitinol stent and the crimp tool in their unconstrained diameters prior to crimping of the stent (d), crimping of the Nitinol stent to a crimp diameter of 1.2 mm to simulate insertion into the artery (e), and the deployment of the stent into the artery (f).

Consitutive Models

The healthy arterial layers were represented with the Holzapfel-Gasser-Ogden (HGO) model; an anisotropic, hyper-elastic material model that includes two collagen fibre families.[42,52] The material parameters were obtained from uniaxial tensile tests performed on the healthy portions of a single diseased external iliac artery acquired from autopsy. The exact values, including the fibre orientations and fibre dispersions within each layer, have been reported previously.[45,52]

The atherosclerotic tissue was modeled as isotropic, hyper-elastic using a 3rd order reduced polynomial form (Yeoh) based on the uniaxial experimental data performed on 20 samples of human atherosclerotic femoral plaques (Table 5.1).[25] The fitting was performed in Abaqus v.6.12 (Dassault Systemes, Simulia Corp., RI, USA) by providing the experimental data as the input for the material model. Three plaque groups (lightly calcified, moderately calcified and heavily calcified) were considered for the analyses. The experimental data showed that the lightly calcified plaque underwent high stretch until tissue failure (0.3 MPa at a nominal strain of 1.15); while the moderately calcified plaque reached a higher ultimate tensile stress (0.43 MPa) at a nominal strain of 0.75. This suggests that the moderately calcified plaque was stiffer compared to the lightly calcified plaque. On the other hand, both the ultimate tensile stress and stretch values for the heavily calcified plaque were lower than the other plaque types (0.16 Mpa at a nominal strain of 0.55). This behavior has been associated with the unique morphology of the heavily calcified plaque, which differs not only from the other femoral plaques, but also from the heavily calcified plaques from other anatomical regions.[83] However, as a result of its low failure stress and strain, the elastic mechanical response of the heavily calcified plaque prior to failure was very similar to the lightly calcified plaque.

Similar to previous studies that modeled plaque failure during endovascular therapy, a perfect plasticity model was adopted to represent tissue damage.[19,22,23,32,92] This method allows the plaque to undergo plastic deformation, while preventing an increase in its stresses. Once the plastic limit is reached, the loads exerted onto the artery are transferred to the healthy layers. Upon unloading, the plaque is plastically deformed and the lumen diameter is permanently increased. At that point, the stresses in the healthy layers are determined by the extent of plastic deformation in the atherosclerotic tissues. The plasticity thresholds in this current study corresponded to the failure stress levels of each plaque group (Fig. 5.2).[25,26] A justification for using failure stresses as yield stresses in the perfect plasticity model is provided in the discussion.

Table 5.1. Material parameters (C10, C20 and C30) of the Yeoh SEF model for the arteries with lightly, moderately and heavily calcified plaques represent the average mechanical behavior of the plaque tissue under uniaxial extension tests[25,26]. The plasticity threshold corresponds to the failure stress of the tissues.

-	**C10 (MPa)**	**C20 (MPa)**	**C30 (MPa)**	**Plasticity Threshold**	
Calcification				**Stress (MPa)**	**Strain**
Light	$5.9\ 10^{-2}$	$4.4\ 10^{-3}$	$-2.7\ 10^{-4}$	$3.0\ 10^{-1}$	1.15
Moderate	$1.4\ 10^{-1}$	$3.1\ 10^{-2}$	$-1.6\ 10^{-2}$	$4.3\ 10^{-1}$	0.75
Heavy	$4.7\ 10^{-2}$	$1.5\ 10^{-2}$	$-1.3\ 10^{-2}$	$1.2\ 10^{-1}$	0.55

The angioplasty balloon was modeled with a linear, elastic material model. The material parameters, as well as a mass proportional Rayleigh damping coefficient, which was assigned to make the folding and inflation of the balloon more stable, were taken from literature.[22] The material parameters for the super-elastic Nitinol model were provided by the manufacturer.[45] Finally, the rigid crimp and expansion tools were represented with a linear, elastic model (Young's modulus $\boldsymbol{E}$: 210,000 MPa; Poisson's ratio $\boldsymbol{v}$: 0.3).

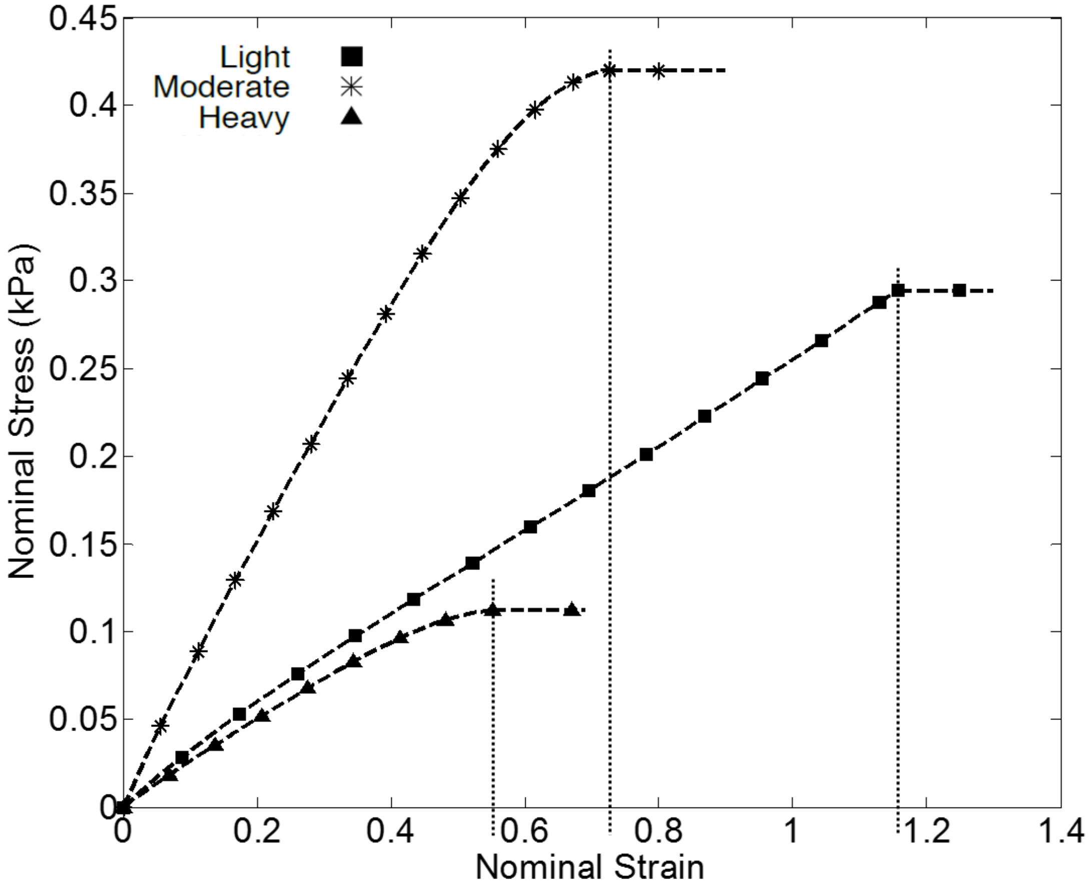

Figure 5.2. The average stress-strain behaviors of the lightly (n=3), moderately (n=5) and heavily (n=12) calcified femoral plaque types under uniaxial tensile tests show that the moderately calcified plaque have the highest stiffness; while the lightly and heavily calcified plaque types have similar mechanical behaviors prior to tissue failure.[25] The tissue damage was modeled using perfect plasticity with the heavily calcified plaque reaching its constant stress threshold the earliest (160 kPa at a nominal strain of 0.55) and the lightly calcified plaque reaching it the latest (300 kPa at a nominal strain of 1.15) (Table 5.1).

Simulation Parameters

The simulations were performed using Abaqus/Explicit with a user-defined, semi-automatic stable time increment of 4 x 10^{-6}. This value ensured that the kinetic energies of each individual part and the whole assembly remained below 5% of their corresponding internal energies at any given time during the analyses. As a result, the quasi-static nature of the analyses was preserved at all time points of the simulations. A symmetry boundary condition was defined at the middle of the angioplasty balloon to prevent it from moving axially during the folding/unfolding steps. Finally, the artery was constrained at both ends to prevent movement in the longitudinal axis. A hard, frictionless contact was defined for the interactions between the balloon and the artery, as well as between the stent and the artery, using the general contact algorithm. On the other hand, the interactions between the tools and the stent were established with a surface-to-surface contact methodology, which ensured a proper separation of the surfaces.

Preliminary Analyses

Prior to the main analysis of endovascular therapy and stent oversizing, the initial configurations of the stent, the balloon and the artery were prepared through three standalone simulations. The first one was stent preconditioning, which consisted of an initial expansion of the stent to its unconstrained diameter, followed by an annealing procedure that was performed to remove the stresses and preserve the expanded shape. A total of four oversizing ratios, 1.0, 1.2, 1.4, and 1.8, were investigated in this study. The unconstrained stent diameter for each case was calculated by multiplying these ratios with the healthy lumen diameter (i.e. 5 mm, 6 mm, 7 mm and 9 mm). For this simulation, the contact interaction between the outer surface of the expansion tool and the inner surface of the stent was activated. Subsequently, the stent was expanded by applying velocity boundary conditions to the nodes of the expansion tool. The second simulation was the folding of the angioplasty balloon by applying a negative pressure to the balloon's inner surface. The third and final simulation was an iterative process to determine the stress-free diameter of the artery, such that the healthy lumen diameter corresponded to the average diameter of the popliteal artery (i.e. 5 mm) under the physiological blood pressure of 120 mmHg.[120] The deformed, stress-free configurations of the stent, the balloon and the artery were, then, brought together in a new assembly for the main analysis. In addition to these preparation simulations, the changes in the radial force profile of the stent with respect to different oversizing ratios were evaluated through further analyses, where the stents were crimped to their insertion diameter of 1.2 mm and expanded back to their unconstrained diameters.

Simulation of Endovascular Therapy

The main analysis included the clinical processes of balloon angioplasty and stent implantation (Fig. 5.1). In the first step, the artery was pressurized by applying the physiological blood pressure of 120 mmHg on the inner surface of the artery (Fig. 5.1a). Next, the contact pair of balloon-artery was activated, and balloon angioplasty was simulated by applying a positive pressure of 7 atm. to the inner surface of the balloon (Fig. 5.1b). Subsequently, the balloon was folded and the minimum lumen diameter was checked to evaluate the success of the angioplasty (Fig. 5.1c). If the lumen diameter was below 70% of the healthy lumen diameter,[32] then an additional angioplasty was performed using a larger balloon diameter. Following the adequate expansion of the lumen, the contact interaction between the inner surface of the crimp tool and the outer surface of the stent was activated and the stent was crimped to its insertion diameter of 1.2 mm by radially displacing each node of the crimp tool (Fig. 5.1e). Finally, the contact pair of stent-artery was activated and the stent was expanded by radially expanding the crimp tool to its original position. As the stent came into contact with the artery, it detached from the crimp tool and was deployed into the artery (Fig. 5.1f).

Data Analysis

The effects of Nitinol stent oversizing were evaluated by analyzing the stress distribution (in particular, the 95th percentile) along the circumferential direction in the healthy layers surrounding the diseased region and the minimum lumen diameter at the end of pressurization, after balloon angioplasty and post stent deployment.

It is hypothesized that high arterial stresses possibly lead to adverse outcomes in patients.[45,129] Since a stress threshold that puts the artery at risk is unknown, previous studies have investigated the effects of stent implantation based on tissue failure[22,23], which could be corroborated by experimental findings. Similarly, in this study, the 95th percentile stresses calculated with the numerical model were compared to the ultimate experimental stresses[42] in the circumferential directions for the healthy layers surrounding the atherosclerotic tissue. The arterial layer identified as the most failure-prone was analyzed to establish the effects of endovascular therapy and Nitinol stent oversizing.

For the calculation of the minimum lumen diameter, the position of each node at the arterial lumen interface was extracted from Abaqus and exported to Matlab. Along the length of the artery, circles were fitted to each of the 108 rings of nodes representing the arterial lumen. The diameters of the circles corresponded to the lumen diameters along the length of the artery and the smallest one determined the minimum lumen diameter.

Additionally, the equivalent plastic strain (PEEQ) distributions in the atherosclerotic tissue were reported to quantify plaque failure among the 3 different plaque types.

5.3. Results

The complete radial force profile of the stent clearly showed the super-elastic behavior of the Nitinol material,[121] where the stent's outward force remained near-constant across a wide range of diameters during crimping and deployment into the artery (Fig. 5.3). Increasing the oversizing ratio resulted in a higher radial force to be applied by the stent onto the artery during deployment. This difference was highest between the unconstrained stent diameters of 5 and 6 mm, which exhibited a 40% increase in the stent's radial force. The difference in the radial force was smaller – approx. 20% - when the unconstrained stent diameter increased from 7 to 9 mm. In contrast, the change in stent's radial force is nominal (approx. 5%) between the unconstrained stent diameters of 6 and 7 mm.

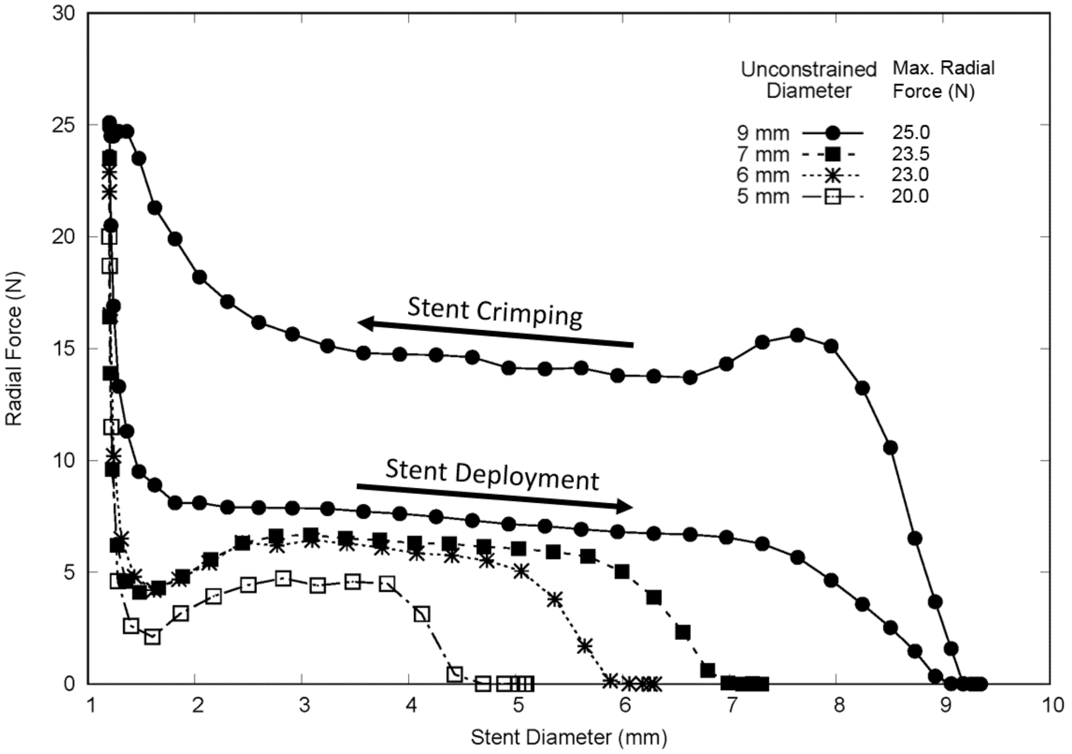

Figure 5.3. The radial force profiles of the Nitinol stent for each of the unconstrained stent diameters showed that increasing the oversizing ratio led to an increase in the radial force of the stent during crimping and deployment into the artery. As a result, the 9 mm stent exerted the highest radial force onto the artery, whereas the 5 mm stent exerted the lowest. On the other hand, the difference between the radial forces of the 6 and 7 mm stents during deployment was found to be marginal. For visualization purposes, the full radial force profile during the crimping and deployment of stent is only shown for the 9 mm stent.

Under the physiological blood pressure of 120 mmHg, the circumferential stresses in the healthy layers surrounding the diseased region, as well as the minimum lumen diameters, were comparable between the different plaque groups (Table 5.2). This suggested that all the artery models were in a similar mechanical condition prior to balloon angioplasty. The initial PTA with a 5 mm angioplasty balloon yielded different outcomes for the three plaque types. The minimum lumen diameters for the vessels with lightly, moderately and heavily calcified plaques were 2.5 mm, 3.2 mm and 3.4 mm, respectively (Table 5.3). At this stage, only the vessel with heavily calcified plaque satisfied the requirement to continue with stent implantation, as it was the only arterial model that reached a diseased lumen diameter corresponding to 70% of the healthy lumen diameter.[32] This can be explained by the low stress-strain threshold (0.16 Mpa at a nominal strain of 0.55) required to start the plastic deformation process in the heavily calcified plaque. As a result, the heavily calcified plaque underwent greater plastic deformation than both the moderately and lightly calcified plaques, which reached their constant stress thresholds at considerably higher strain values of 0.75 and 1.15, respectively (Fig. 5.2).

To satisfy the deployment criteria, the arteries with lightly and moderately calcified plaques underwent a second PTA. The additional PTA of the artery with moderately calcified plaque using a 5.5 mm balloon yielded a lumen diameter of 3.5 mm. On the other hand, even with a 6 mm balloon, only a 3.0 mm lumen diameter could be reached for the artery with lightly calcified plaque, resulting in a partially successful balloon angioplasty. This can be attributed to the high amounts of stretch required to plastically deform the lightly calcified plaque.

Table 5.2. The circumferential stresses (95th percentile) in the adventitial layer following the pressurization of the artery with a physiological blood pressure of 120 mmHg (Pre-Angio), balloon angioplasty and stent implantation for the arteries with lightly, moderately and heavily calcified plaques.

	Circumferential Stresses (kPa) (95th Percentile)						
	Pre-Angio (@ 120 mmHg)	**Post 1st Balloon Angioplasty**	**Post 2nd Balloon Angioplasty**	**Post Stent Implantation**			
				Unconstrained Stent Diameter			
				5 mm	**6 mm**	**7 mm**	**9 mm**
Calcification							
Light	0.6	32	140	371	458	485	543
Moderate	0.1	161	356	559	590	600	641
Heavy	0.8	303	-	732	833	851	922

Table 5.3. The minimum lumen diameter following the pressurization of the artery with a physiological blood pressure of 120 mmHg (Pre-Angio), balloon angioplasty and stent implantation for the arteries with lightly, moderately and heavily calcified plaques.

	Minimum Lumen Diameter (mm)						
	Pre-Angio (@ 120 mmHg)	**Post 1st Balloon Angioplasty**	**Post 2nd Balloon Angioplasty**	**Post Stent Implantation**			
				Unconstrained Stent Diameter			
				5 mm	**6 mm**	**7 mm**	**9 mm**
Calcification							
Light	1.46	2.51	2.98	3.45	3.50	3.51	3.57
Moderate	1.39	3.16	3.49	3.68	3.71	3.71	3.74
Heavy	1.48	3.44	-	3.83	3.89	3.90	3.95

The PEEQ distributions in the atherosclerotic tissues following PTA support these observations (Fig. 5.4). Among the different plaque types, the heavily calcified plaque had the highest plastic strain not only at the lumen interface, but also along the thickness of the plaque after the initial balloon angioplasty (Fig. 5.4c). In line with the achieved lumen gains, the lightly calcified plaque exhibited the least amount of plastic strain within the complete atherosclerotic tissue (Fig. 5.4a) while the plastic strain in the moderately calcified plaque were in between the two groups (Fig. 5.4b). A 2nd PTA significantly affected the plastic strain distribution in the moderately calcified plaque. The procedure increased the overall plastic strain level and led to an increase in the volume that underwent plastic deformation (Fig. 5.4e). Performing a 2nd PTA also had a similar effect on the distribution of plastic strain in the lightly calcified plaque (Fig. 5.4d). However, the overall plastic strain was still lower than the other plaque groups.

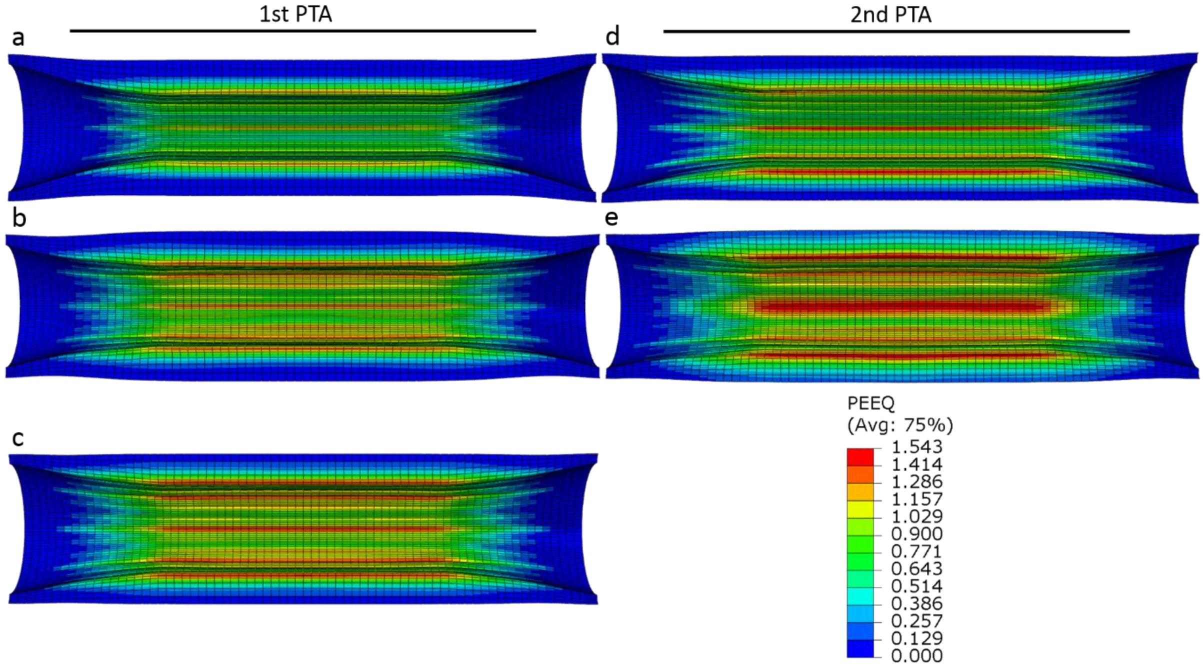

Figure 5.4. The PEEQ distributions in the atherosclerotic tissues following the 1st PTA showed that the heavily calcified plaque had the largest plastic strain and, as such, the largest plastic deformation (c). The extent of plastic deformation was followed by the moderately calcified plaque (b) and, finally, the lightly calcified plaque (a). Performing a 2nd PTA resulted in a significant increase in the plastic strain level of the moderately calcified plaque (e). On the other hand, while the 2nd PTA also increased the extent of plastic deformation experienced by the lightly calcified plaque; the overall plastic strain was still lower than the other plaque types (d).

Following PTA, the arteries with heavily and moderately calcified plaques were in high stress states (Table 5.2). Additionally, they had similar stress values in the healthy layers surrounding the plaque. These can be attributed to the high levels of plastic strain observed in both plaque types. Comparatively, the stresses in the artery with lightly calcified plaque were significantly lower as its atherosclerotic tissue underwent a smaller plastic deformation than the other plaque types.

The implantation of a Nitinol stent further increased the stresses and lumen diameters in all the artery models (Tables 5.2 & 5.3). However, compared to PTA, the procedure did not cause any additional plastic deformation. As a result, the additional stresses and lumen gains produced by stent implantation are directly influenced by the hyperelastic behavior, i.e. the mechanical stiffness, of the plaque, since the plaque tissue continued to support the loads exerted onto the artery following PTA.

Regardless of the oversizing ratio, the artery with heavily calcified plaque always had the highest circumferential stresses and lumen diameter (Fig. 5.6). This can be attributed to the high stress-state of the artery following PTA and the low stiffness of the plaque (Fig. 5.2). On the other hand, while the lightly calcified plaque had a similar stiffness as the heavily calcified plaque, the artery always had the lowest circumferential stresses and lumen diameter. This low level of stress directly results from the low stress-state following balloon angioplasty.

Stent implantation has led to a narrow distribution of the stresses in the arteries with lightly and moderately calcified plaques (Fig. 5.6). Again, this can be attributed to the low stiffness of the plaque tissues, allowing a uniform deformation and stress increase along the entire tissue. In contrast, the stress distribution in the artery with moderately calcified plaques was much wider, with lower minimum values than the stress levels observed in the arteries with lightly calcified plaques. This can be explained by the higher stiffness of the moderate plaque, acting as a stronger barrier that limits the amount of load transferred to the healthy tissues.

For all plaque groups, increasing the oversizing ratio led to a linear increase in the circumferential stresses (Fig. 5.7). Similarly, a linear relationship was observed between the oversizing ratio and the lumen diameter (Fig. 5.7). The artery with heavily calcified plaque, followed by the artery with lightly calcified plaque, exhibited the largest increase in arterial stresses with increased oversizing. Correspondingly, these two plaque types had the largest increases in the acute lumen gains with oversizing. The similar behavior between these two arterial models can be attributed to the similar stiffness of the lightly and heavily calcified plaques (Fig. 5.2). In comparison, the artery with moderately calcified plaque was the least affected in terms of arterial stresses and lumen gain due to the high stiffness of its plaque.

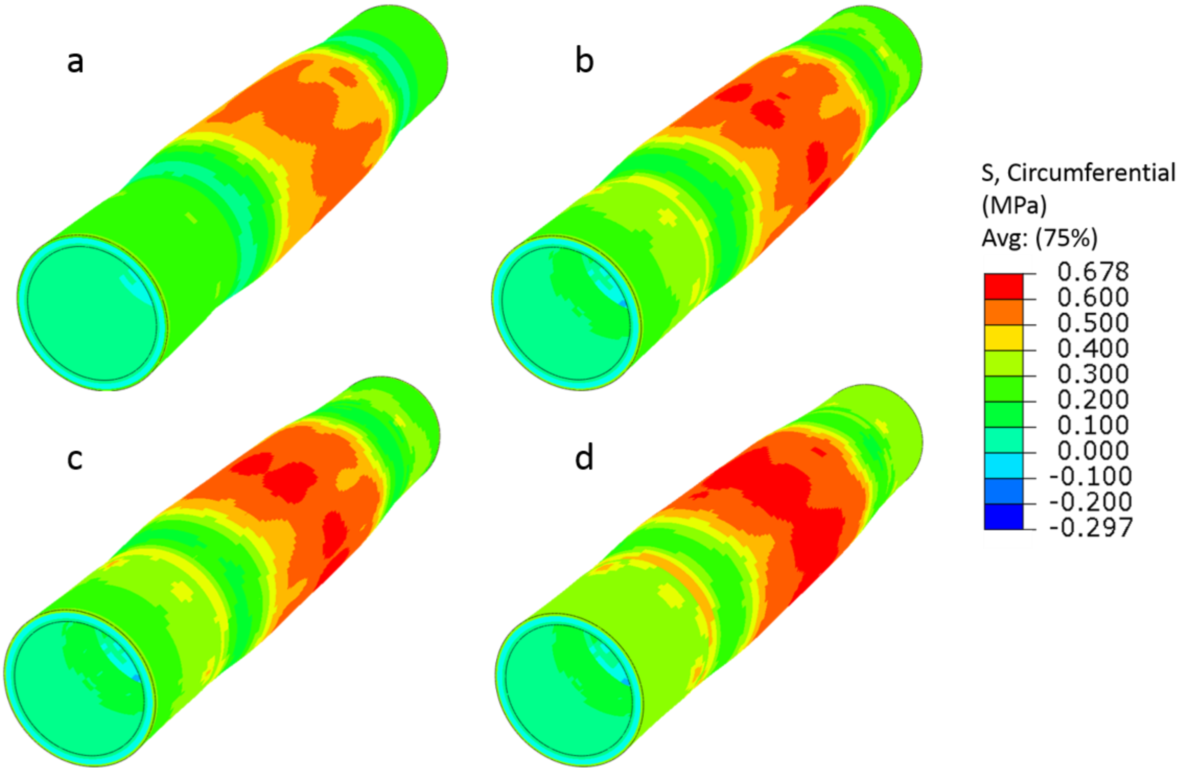

Figure 5.5. The stress distribution in the artery with moderately calcified plaque following stent implantation showed that, regardless of the oversizing ratio, the most failure-prone layer was the healthy adventitia over the diseased region. Increasing the oversizing ratio led to an increase in the circumferential stresses of the artery, with the 9 mm stent (d) producing the highest stress, followed by the 7 mm stent (c), the 6 mm stent (b) and, finally, the 5 mm stent (a).

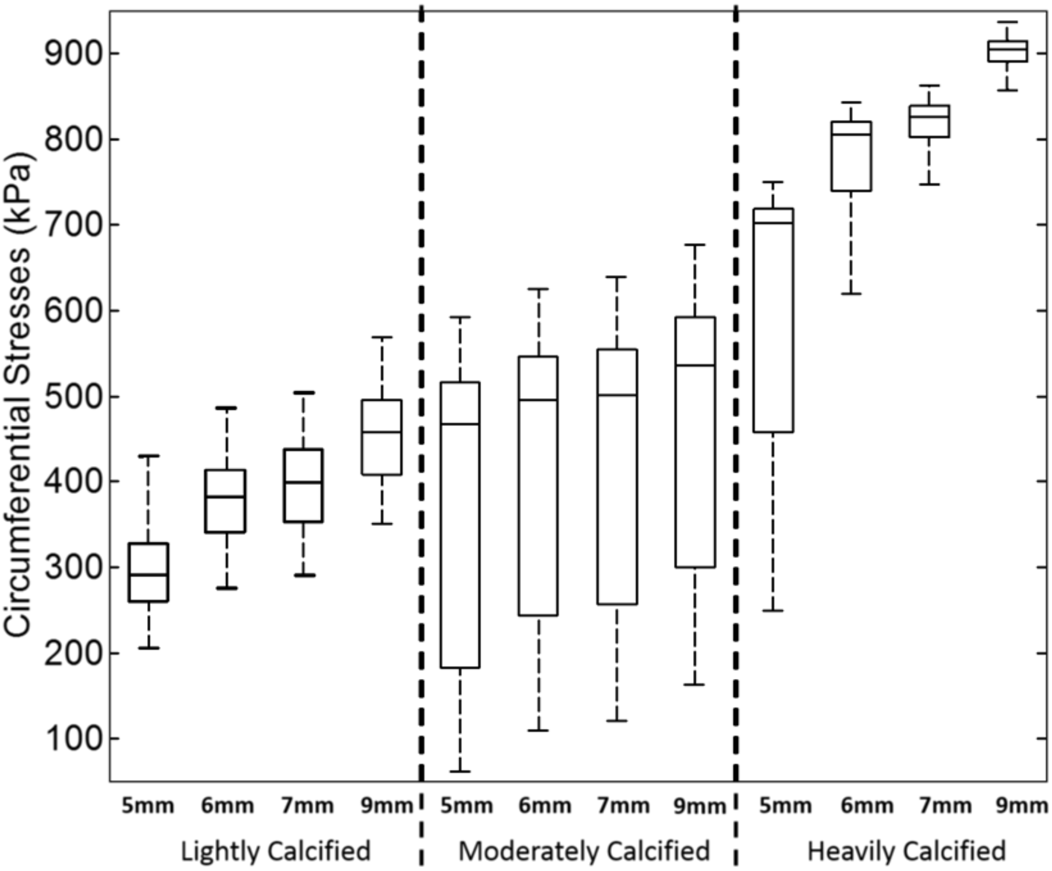

Figure 5.6. The stress distribution in the healthy adventitia has been reported for the different plaque types and oversizing ratios. Similar to the 95th percentile, the average stresses were lower for the artery with the lightly calcified plaque, followed by the arteries with moderately and heavily calcified plaques. The stress values in the adventitia showed a larger scattering for the artery with the moderately calcified plaque than for the other types of calcification. The wider distribution can be attributed to the plaque stiffness. Despite these differences, there was a linear relationship between the unconstrained stent diameters and the circumferential stresses (the 95th percentile, the 75th percentile, as well as the median values) for all the artery models.

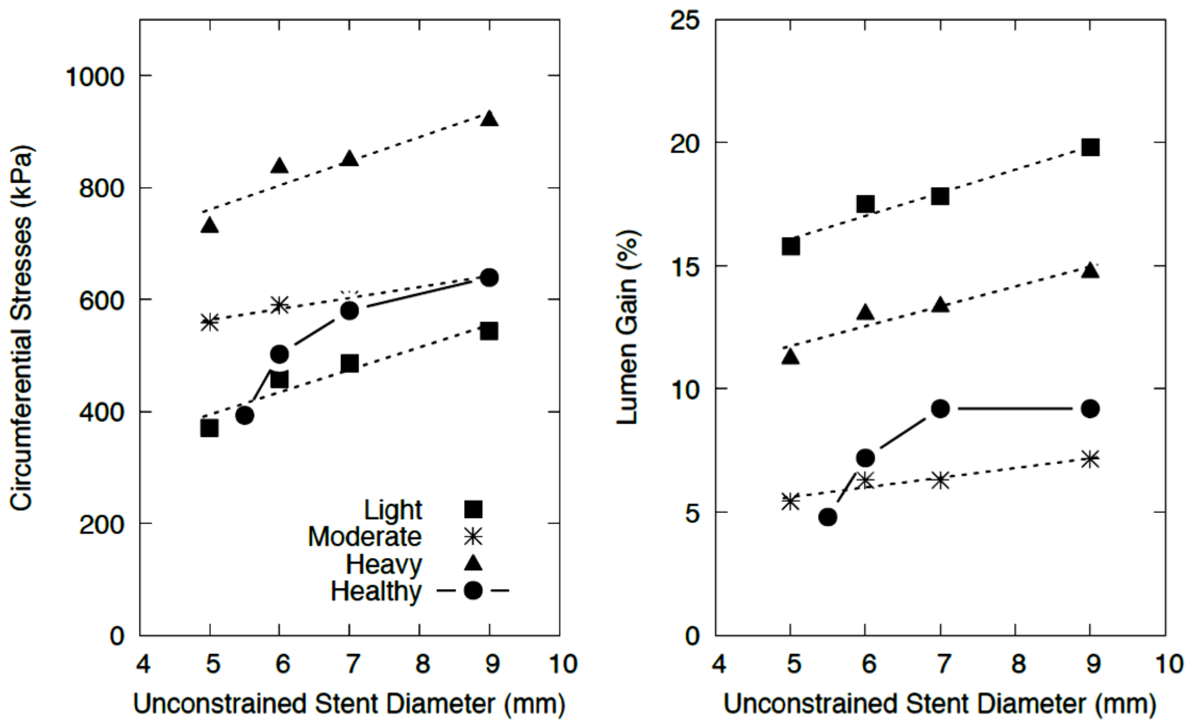

Figure 5.7. Regardless of the plaque type, Nitinol stent oversizing resulted in a linear increase in both the arterial circumferential stresses (left) and the lumen gains (right). For each oversizing ratio, the highest circumferential stresses were found to be in the artery with heavily calcified plaque, while the lowest were in the artery with lightly calcified plaque. On the other hand, the highest lumen gain was reported to be in the artery with lightly calcified plaque, followed by the arteries with heavily and moderately calcified plaques. In comparison, oversizing in a non-calcified artery resulted in a non-linear increase in arterial stresses, as well as in the lumen gain. Furthermore, diseased arteries were found to be less sensitive to oversizing than healthy arteries due to a smaller increase in the arterial stresses between each oversizing ratio.

5.4. Discussion

Nitinol stent oversizing is a term used to describe the ratio and, in extreme cases, the mismatch between healthy lumen and stent diameters.[101,137] The procedure can occur either on purpose, by selecting a stent diameter that is larger than the healthy lumen diameter, or inadvertently, by implanting a single long stent over a considerably long lesion (>300 mm), which results in a mismatch between the constant stent diameter and the narrowing lumen.[20,61] Currently, stent manufacturers provide a stent-specific value as the recommended oversizing ratio. However, the bases for selecting these values are unclear. With no objective guidelines, clinicians either avoid oversizing and, as a result, do not utilize the procedure's possible advantages (i.e. preventing stent migration, achieving a desirable lumen gain immediately after implantation etc.),[93] or they tend to oversize the stents and risk arterial damage. More recently, animal studies and numerical analyses have been conducted to define an ideal oversizing ratio for the peripheral arteries.[101,137] However, they were limited by the use of healthy arteries, whose morphologies are considerably different than diseased arteries. Thus, to understand the real-world implications of Nitinol stent oversizing, these studies should primarily be conducted on diseased arteries. Therefore, the aim of this study was to investigate the effects of Nitinol stent oversizing on the mechanical behavior of peripheral arteries by performing in-silico analyses of endovascular therapy in arterial models with a clinically relevant model of PAD. Furthermore, three different plaque types were considered in the model to evaluate whether the severity of plaque calcification has any influence on the treatment outcomes. The mechanical behavior of the artery during PTA is strongly affected by the plaque type. Between the lightly and moderately calcified plaques, the former had to undergo a comparatively higher stretch to reach its plastic limit (Fig. 5.2). On the other hand, the stress and strain values associated with the plasticity threshold of the heavily calcified artery was considerably lower than the other plaque types. These strain values (Table 5.1)[26] directly defined the configurations of the arteries following PTA. Thus, two of the artery types required a 2nd balloon angioplasty to achieve a satisfactory lumen diameter due to the high stretch that was necessary to start plastic deformation in their plaques. A 2nd PTA increased the amount of plastic strain in the moderately calcified plaque (Fig. 5.4d) to similar levels observed in the heavily calcified plaque after one PTA (Fig. 5.4c). This meant that both plaque types experienced similar amounts of plastic deformation, which can also be inferred from the similar lumen diameters and arterial stresses between the two artery types (Tables 5.2 & 5.3). For the lighly calcified artery, even a second PTA was insufficient to reach the level of strain needed to undergo the same level of plastic deformation as the other plaque types. As a result, the arteries with moderately and heavily calcified plaques were both in a higher stress state compared to the artery with lightly calcified plaque following PTA.

The type of plaque also affected the outcomes following Nitinol stent implantation. Due to the use of perfect plasticity as a damage model, the deformed plaque continued to support the loads exerted onto the artery by the stent. However, unlike the situation during PTA, only the hyper-elastic behavior of the plaque influenced the final configuration of the artery, as no additional plastic deformation was observed during stent deployment. As a result, the lumen gain obtained following stent implantation was considerably lower than the one achieved after PTA. The artery with heavily calcified plaque had a substantial increase in adventitial stresses following stent implantation due to its low mechanical stiffness in the elastic region (Table 5.2). Although being at a comparatively lower stress state after PTA, the artery with lightly calcified plaque also had a significant increase, which can be attributed to the similar mechanical stiffness of the two plaque types (Fig. 5.2). On the other hand, the artery with moderately calcified plaque had the least increase in adventitial stresses with stent implantation due to the higher stiffness of the moderate plaque. These outcomes were accordingly reflected in the lumen gains observed following stent deployment, with the arteries with heavily and lightly calcified plaques achieving a similar and higher lumen gain compared to the artery with moderately calcified plaque (Table 5.3) (Fig. 5.7). For all plaque types, the increases in adventitial stresses and acute lumen gains with respect to Nitinol stent oversizing were heavily dependent on the stent's radial force profiles for different oversizing ratios (Fig. 5.3). A larger increase in the radial force of the stent has led to a correspondingly large increase in both arterial stresses and lumen diameters. As such, increasing the oversizing ratio from 1.0 to 1.2 (5 mm to 6 mm) or from 1.4 to 1.8 (7 mm to 9 mm) had a bigger effect on the mechanical response of the artery compared to the similar outcomes obtained with increasing the ratio from 1.2 to 1.4 (6 mm to 7 mm) (Tables 5.2 & 5.3). Despite this, the relationship between the arterial stresses (the 95th percentile, the 75th percentile and the median values) and the oversizing ratio, as well as the relation between the acute lumen gains and the unconstrained stent diameters, was found to be well approximated with a linear function for all plaque groups (Figs. 5.6 & 5.7). However, a mismatch between the increases in arterial stresses and lumen gain was also present with oversizing (i.e. 31% stress increase vs. 4% increase in the lumen gain when the oversizing ratio was increased from 1.0 to 1.8 for the artery with lightly calcified plaque).Comparison of the results with an oversizing study conducted in healthy peripheral arteries showed that the outcomes of the procedure differed significantly between the two artery types.[45] Oversizing of healthy arteries led to nonlinear increases in both arterial stresses and lumen gains (Fig. 5.7). Furthermore, regardless of the plaque type, diseased arteries were less sensitive to oversizing, showcased by a smaller increase in adventitial stresses between each oversizing ratio. This can be explained by the difference in the distribution of the loads between the healthy and diseased arteries. Whereas the adventitia primarily supported the majority of the mechanical load in the healthy artery; in the diseased arteries, the load was distributed between the plastically deformed plaque and the adventitia.

Following stent implantation, the arteries with moderately and heavily calcified plaques exhibited higher stresses compared to the healthy artery. This result can be attributed to the revascularization of the artery with PTA. This procedure was only performed in the diseased arteries and determined the arterial stresses prior to stent deployment. By comparison, the stress levels in the arteries with moderately and heavily calcivited plaques after PTA corresponded to the stresses calculated in the healthy artery with an oversized stent of 5.5 mm. At this stage, deploying a stent in the arteries with moderately and heavily calcified plaques further increased their high stress levels and ensured that their final stress states would be higher than the healthy artery. On the other hand, the artery with lightly calcified plaque was at a low stress state after PTA and the additional stresses produced by stents did not exceed the stress levels in the healthy arteries.

In terms of lumen gain, the results suggested that the adventitia acted as a protective layer and prevented the artery from significant expansion in healthy arteries[45,53]. In the diseased arteries, however, the stent continued to push against the plaque, without producing any additional plastic deformation. As such, the resultant lumen gain was determined by the stiffness of the plaque tissue. Since the arteries with lightly and heavily calcified arteries had a low mechanical stiffness, they produced higher lumen gains than the non-calcified arteries. Despite these differences, the mismatch between the low lumen gain induced by stent oversizing and the large increase of the arterial stresses was also observed for the healthy arteries.

Several assumptions had to be made within the current numerical framework. Within the diseased region, the intimal layer was replaced with the plaque tissue. However, since the adventitia becomes the mechanically predominant layer under high pressures (following PTA),[110] the influence of the intimal layer on the mechanical behavior of the artery would be small and can be neglected. The artery was not pre-stressed, which may decrease the final values of the stresses observed after stent implantation. However, arterial pre-stressing would not affect the linear relation between the oversizing ratio and either the stresses or the lumen gain.

The model of perfect plasticity that is used for reconfiguring the plaque tissue represents a simplified approach to the failure of the calcified plaque. Although not exactly a failure model, perfect plasticity is commonly used to model plaque failure during endovacular therapy.[19,22,23,32,92] The majority of these studies have set the stress threshold at 400 kPa[19,22,23], which corresponded to an average value of plaque failure under uniaxial tensile tests.[73] The remaining studies have used 270 kPa, which represented the rupture stress of a single atheresclerotic plaque.[32,92] Conway et al. have justified using the ultimate tensile stresses as the plastic stress threshold by conducting a parametric study with different values.[23] Their results showed that the variances in the stress threshold had a marginal effect on the mechanical behavior of the artery; changing the yield stress from 200 kPa to 400 kPa resulted in less than a 5% change in vessel recoil for all plaque types. Recently, Chiastra et al. have used the same methodology to simulate PTA and stent implantation in numerical models of coronary bifurcation.[19] A combination of CT angiography and Optical Coherence Tomography (OCT) was used to validate the simulations. The results showed approximately 15%-20% error between the calculated shape of the artery and the experimental reconstruction based on the Hybrid OC-CT methodology. The results from both of these studies suggested that using failure stresses as a plastic threshold is a suitable approximation to model plaque failure.

In any case, there is no information in the literature that suggests the plaque actually behaves the way it is modeled in this study during balloon angioplasty. Furthermore, with this model, the deformed plaque continues to support the loads that are exerted onto the artery by the stent, which may lead to an underestimation of the arterial stresses. Experimental and clinical studies that focus on understanding the failure behavior of the plaque should be undertaken to improve the existing knowledge and modeling of the failure characteristics of the atherosclerotic tissues. Finally, the results provide an overview of Nitinol stent oversizing based on a single stent design. Although we believe that the general behavior would be similar for other designs, the actual stress values and lumen diameters would likely be different.

5.5. Conclusion

Despite Nitinol stent oversizing being routinely performed during endovascular interventions, the number of experimental and numerical studies that investigate the effects of the procedure has been limited. Furthermore, the studies have been performed almost exclusively on healthy arterial models, completely overlooking the plaque tissue, the procedure of balloon angioplasty and the effect of the reconfigured calcification on the outcomes of stent deployment. Therefore, this study used calcified arterial models in order to give some insights on the implications of Nitinol stent oversizing in patients undergoing endovascular revascularizations. Both PTA and stent implantation were responsible for a significant increase in adventitial stresses. However, PTA alone was the primary force behind achieving a substantial lumen gain. Among the different plaque types, oversizing seems not be critical for the lightly and moderately calcified arteries; due to the former being at a lower stress state and the latter having the least increase in adventitial stresses with oversizing. However, for both cases, the procedure only produces a marginal lumen gain. For the heavily calcified arteries, oversizing should be avoided as it only acts to increase an already high stress state following PTA towards the failure limit of adventitia.[52] These results further support the notion that stents are inherently made to act as scaffolds and not as instruments to facilitate additional lumen expansion.

Chapter 6

Conclusion & Outlook

The main objectives of this thesis were to characterize the deformation behavior and mechanical response of the femoro-popliteal (FP) arterial tract through clinical and numerical investigations. The motivation behind the clinical part of the thesis was based on the high restenosis rates that continue to negatively affect the long-term outcomes of endovascular procedures in the lower-limb arteries.[27,58,115] Based on the limitations in the literature, there was a clear need to improve the existing knowledge of the complex deformations the FP artery undergoes during routine activities, such as walking and stair-climbing.[16,40,63,87] Although there has been a specific focus on FP artery deformations for the last two decades, previous works were mainly conducted on subjects that did not represent the population targeted for endovascular therapy.[16,17,62] As such, utilizing these results to improve current implantation procedures and stent designs would be erroneous. On the other hand, the low number of works that included patients with Peripheral Arterial Disease (PAD) had methodological limitations that, at best, can lead to incorrect interpretations of the reported outcomes and, at worst, can affect the accuracy of their results.[40,87] Currently, there are no works that show the effects endovascular therapy has on the deformation behaviors of the PAD-afflicted FP arteries by comparing the pre- and post-intervention deformations on the same patients. Furthermore, none of the studies have made comparisons between the effects of different endovascular procedures (i.e. Percutaneous Transluminal Angioplasty (PTA) vs. Nitinol stent implantation) on arterial deformations, which may be used to inform about possible improvements to existing stent designs. Therefore, the clinical part of the study was designed to investigate the effects of PAD, PTA and stent implantation on the deformations of the FP arteries during leg flexion.

Initially, a pilot study was performed on five patients with PAD using 3D rotational angiography.[44] The data revealed that, not unlike the healthy FP arteries, the diseased popliteal arteries undergo significant shortening and twisting, and experience a notable increase in their curvature profiles with leg flexion. Additionally, the change in the curvature was found to be directly affected by the extent of arterial calcification. This study showed that 3D rotational angiography is able to fully characterize the FP arterial deformations. However, the imaging modality is time consuming and induces additional radiation to the patients.

Therefore, a technique that is able to provide an accurate reconstruction of a 3D model of the FP artery based on multiple 2D angiographic images was developed.[112] This approach has the benefit of allowing more freedom concerning the type of leg flexion that the patient can perform and it could be easily integrated to the clinical workflow. Based on this method, the arterial deformations of 35 patients, diagnosed with PAD, were quantified prior to endovascular therapy and following either PTA or primary Nitinol stent placement.[46] Through direct comparisons with the pre-angioplasty measurements, the results showed that the choice of the treatment method substantially affects the post-interventional axial deformations of the FP arteries. Performing only PTA produced a more flexible artery, while the implantation of a stent further restricted the arteries' shortening capabilities.

The arterial deformations obtained from the clinical studies provide greater insight into the mechanical environment of the diseased FP arteries and how they are affected by the available endovascular procedures currently being employed to treat PAD. The major significance of these studies lies in their utilization to improve existing stent designs. Three different stents were found to impact the natural shortening behavior of the artery during leg flexion. This information can directly be used to reevaluate the performance of other stents that are placed in the FP arteries and additional modifications can be made to replicate the effects of performing PTA. The deformations can easily be adapted to be used in in-vitro studies to investigate the commercially available stents' fatigue behaviors. Instead of applying generic forces to replicate the in-vivo conditions, these deformations would give a more accurate description of the arterial deformations that the stents would actually undergo once they are implanted in the PAD-afflicted arteries. Similarly, the deformations can easily be used in numerical analyses that aim to investigate the mechanical behaviors of the arteries and stents, as well as stent-artery interactions, during leg flexion. Although some of the numerical studies use clinical images to generate accurate models of the legs, the contact interactions and boundary conditions they adopt to simulate leg flexion have no clinical basis (simple boundary conditions, the absence of a stent model, no validation).[31,36,49,85,86,96] By combining the 3D reconstructed shapes of each artery with their corresponding deformations, patient-specific numerical models, which can support the clinical outcomes and present results unobtainable through conventional means, can be generated and validated. This information can be used to improve the understanding of the surgeon on each of his patients to help him adapt the treatment strategy for the specific situation. In the future, this information can lead to predictive models and optimize the surgery based on numerical tools. Additionally, these patient-specific models could be used to optimize stent designs, select correct stent lengths and placement to minimize the risk of restenosis.

The motivation behind the numerical part of the thesis was mainly based on the contradictory outcomes between the animal and clinical studies concerning Nitinol stent oversizing.[61,93,101,137] Furthermore, the studies that focused on the FP arterial segment only investigated the responses of the healthy arteries to this controversial procedure and none of the studies were supported with numerical analyses. To date, the implications from these studies were being used to derive conclusions on the procedure’s effects on diseased arteries, and the actual mechanical behavior of the PAD-afflicted arteries under Nitinol stent oversizing was not known. Therefore, a validated FE framework was generated, healthy FP arteries with patient-specific geometries and idealized arteries with clinically relevant levels of PAD. Based on the artery model, either only stent implantation or the complete endovascular therapy (PTA + stent implantation) was simulated. The analyses provided important observations concerning Nitinol stent oversizing in FP arteries. Regardless of the presence of a plaque tissue, results showed that Nitinol stent oversizing was found to produce a marginal lumen gain in contrast to a significant increase in arterial stresses. For the lightly and moderately calcified arteries, oversizing was found to be non-critical; whereas for healthy and heavily calcified arteries, the procedure should be avoided due to a risk of tissue failure. These adverse effects to both the artery walls and stents may create circumstances for restenosis. Although the ideal oversizing ratio is stent-specific, the studies showed that Nitinol stent oversizing has a very small impact on the immediate lumen gain, which contradicts the clinical motivations of the procedure.

The major limitation of the numerical framework concerns the mechanical behavior of the plaque under PTA. Although endovascular treatment of the FP arteries has been the subject of numerous numerical studies, the parameters corresponding to this step of the procedure are generalized and based on assumptions.[19,32] Clinically, balloon angioplasty is expected to "crack" the lesion, and redistribute the diseased material along the arterial walls. However, the process behind this "cracking", as well as the final anatomical configuration of the residual stenosis, remains unclear, resulting in numerical models that are based on qualitative information from angiographic images and clinicians. In addition, the mechanical process resulting in the permanent deformation of the lesions is mostly unknown. Several mechanisms have been proposed such as elasto-plastic deformation or stress softening.[22,26] Up to now, among the limited number of experimental studies conducted on the atherosclerotic femoral plaques, none of the experimental findings could be used to determine the most appropriate approach.[25] This information is crucial to having an accurate model of the PTA and the subsequent step of stent implantation. A possible approach to understand and implement this behavior within the numerical framework would be to perform Intravascular Ultrasound (IVUS) or Optical Coherence Tomography (OCT) imaging. By taking IVUS or OCT-images prior to and following PTA, the changes in the anatomy of the lesion could be quantified. The direct and accurate reconstruction of the shape of the tissue after balloon angioplasty will help address open questions concerning the mechanism of re-vascularization, will provide a validation step for the numerical analyses, as well as an accurate representation of the anatomical configuration before stent placement.

The current hypothesis suggests that the restenosis in FP arteries following stent implantation is mainly associated with adverse changes in the deformation behavior and mechanical response of the artery due to the introduction of a device that disrupts the artery's natural deformations during leg movement. We believe that the natural extension of this hypothesis is the prediction of restenosis through specific mechanical markers derived from patient-specific numerical models, which require precise information on the anatomy, mechanical properties and boundary conditions. As shown in this thesis, the boundary conditions that are needed to simulate leg flexion can be acquired through in-vivo measurements using 2D X-ray angiography. The rest, however, cannot be readily obtained; i.e. the imaging modalities used in this thesis only allow for the reconstruction of patient-specific curvatures. As such, additional imaging technologies, such as OCT, is necessary to reconstruct the lumen of the artery, and determine the thickness, type and composition of the lesions. Furthermore, OCT images acquired following stent implantation can be used to validate the results of the numerical analyses. An in-vivo characterization of the material properties of the artery, in the form of compliance measurements, can be performed using IVUS. The combination of these different imaging methodologies with consistent follow-up studies and a numerical framework, similar to the one introduced in the 2nd part of this thesis, can provide an overall structure to determine the relationship between the mechanical markers (such as stent wall apposition, level of arterial damage, un-physiological arterial deformations, stress and strain distributions) and restenosis.

The techniques described here will hopefully help clinical practice by improved understanding of the basic biomechanical properties of the commonly involved FP arteries. In addition, the expected outcomes will provide novel information required to design enhanced stents and improved placement strategies into the arteries. Ultimately, insights from the present research protocol may help predict and prevent possible cases of in-stent restenosis at the baseline based on post-treatment arterial deformations, improve long-term outcomes for patients that have undergone PAD treatment and reduce the need for repeated revascularization procedures, thereby providing relief for healthcare systems.

Bibliography

1. Adams, B. Y. G. L., and O. J. Mendes. DCBs in the United States. *Suppl. to Endovasc. Today* 13:14–16, 2014.

2. Adlakha, S., M. Sheikh, J. Wu, M. W. Burket, U. Pandya, W. Colyer, E. Eltahawy, and C. J. Cooper. Stent fracture in the coronary and peripheral arteries. *J. Interv. Cardiol.* 23:411–419, 2010.

3. Arena, F. J. Long Nitinol Stenting in the Femoropopliteal System. *Endovasc. Today* 55–9, 2005.

4. Arena, F. J. Arterial kink and damage in normal segments of the superficial femoral and popliteal arteries abutting nitinol stents--a common cause of late occlusion and restenosis? A single-center experience. *J. Invasive Cardiol.* 17:482–486, 2005.

5. Auricchio, F., M. D. I. Loreto, and E. Sacco. Finite-element Analysis of a Stenotic Artery Revascularization through a Stent Insertion. *Comput. Methods Biomech. Biomed. Engin.* 4:249–263, 2001.

6. Babalik, E., M. Gülbaran, T. Gürmen, and S. Oztürk. Fracture of popliteal artery stents. *Circ. J.* 67:643–645, 2003.

7. Becquemin, J.-P., J.-P. Favre, J. Marzelle, C. Nemoz, C. Corsin, and A. Leizorovicz. Systematic versus selective stent placement after superficial femoral artery balloon angioplasty: a multicenter prospective randomized study. *J. Vasc. Surg.* 37:487–94, 2003.

8. Boland, E. L., J. a. Grogan, C. Conway, and P. E. McHugh. Computer Simulation of the Mechanical Behaviour of Implanted Biodegradable Stents in a Remodelling Artery. *Jom* 68:1198–1203, 2016.

9. Bosiers, M., G. Torsello, H.-M. Gissler, J. Ruef, S. Müller-Hülsbeck, T. Jahnke, P. Peeters, K. Daenens, J. Lammer, H. Schroë, K. Mathias, R. Koppensteiner, F. Vermassen, and D. Scheinert. Nitinol stent implantation in long superficial femoral artery lesions: 12-month results of the DURABILITY I study. *J. Endovasc. Ther.* 16:261–269, 2009.

10. Cejna, M., S. Thurnher, H. Illiasch, W. Horvath, P. Waldenberger, K. Hornik, and J. Lammer. PTA versus Palmaz stent placement in femoropopliteal artery obstructions: a multicenter prospective randomized study. *J. Vasc. Interv. Radiol.* 12:23–31, 2001.

11. Cha, S.-H., M. Hee Han, Y. Ho Choi, C. Jin Yoon, S. Kug Baik, S. Jin Kim, and K.-H. Chang. Vascular Responses in Normal Canine Carotid Arteries. *Invest. Radiol.* 38:95–101, 2003.

12. Chatzizisis, Y. S., A. U. Coskun, M. Jonas, E. R. Edelman, C. L. Feldman, and P. H. Stone. Role of Endothelial Shear Stress in the Natural History of Coronary Atherosclerosis and Vascular Remodeling. Molecular, Cellular, and Vascular Behavior. , 2007.

13. Chen, H. Y., J. Hermiller, A. K. Sinha, M. Sturek, L. Zhu, and G. S. Kassab. Effects of stent sizing on endothelial and vessel wall stress: potential mechanisms for in-stent restenosis. *J. Appl. Physiol.* 106:1686–1691, 2009.

14. Chen, H. Y., B.-K. Koo, D. L. Bhatt, and G. S. Kassab. Impact of stent mis-sizing and mis-positioning on coronary fluid wall shear and intramural stress. *J. Appl. Physiol.* 115:285–292, 2013.

15. Chen, H. Y., a. K. Sinha, J. S. Choy, H. Zheng, M. Sturek, B. Bigelow, D. L. Bhatt, and G. S. Kassab. Mis-sizing of stent promotes intimal hyperplasia: impact of endothelial shear and intramural stress. *AJP Hear. Circ. Physiol.* 301:H2254–H2263, 2011.

16. Cheng, C. P., G. Choi, R. J. Herfkens, and C. A. Taylor. The effect of aging on deformations of the superficial femoral artery resulting from hip and knee flexion: potential clinical implications. *J. Vasc. Interv. Radiol.* 21:195–202, 2010.

17. Cheng, C. P., N. M. Wilson, R. L. Hallett, R. J. Herfkens, and C. A. Taylor. In vivo MR angiographic quantification of axial and twisting deformations of the superficial femoral artery resulting from maximum hip and knee flexion. *J. Vasc. Interv. Radiol.* 17:979–987, 2006.

18. Chiastra, C., S. Morlacchi, D. Gallo, U. Morbiducci, R. Cárdenes, I. Larrabide, and F. Migliavacca. Computational fluid dynamic simulations of image-based stented coronary bifurcation models. *J. R. Soc. Interface* 10:, 2013.

19. Chiastra, C., W. Wu, B. Dickerhoff, A. Aleiou, G. Dubini, H. Otake, F. Migliavacca, and J. F. LaDisa. Computational replication of the patient-specific stenting procedure for coronary artery bifurcations: From OCT and CT imaging to structural and hemodynamics analyses. *J. Biomech.* 49:2102–2111, 2015.

20. Cho, H., M. Nango, Y. Sakai, E. Sohgawa, K. Kageyama, S. Hamamoto, T. Kitayama, A. Yamamoto, and Y. Miki. Neointimal hyperplasia after stent placement across size-discrepant vessels in an animal study. *Jpn. J. Radiol.* 32:340–6, 2014.

21. Choi, G., C. P. Cheng, N. M. Wilson, and C. a Taylor. Methods for quantifying three-dimensional deformation of arteries due to pulsatile and nonpulsatile forces: implications for the design of stents and stent grafts. *Ann. Biomed. Eng.* 37:14–33, 2009.

22. Conway, C., J. P. McGarry, and P. E. McHugh. Modelling of Atherosclerotic Plaque for Use in a Computational Test-Bed for Stent Angioplasty. *Ann. Biomed. Eng.* 42:2425–2439, 2014.

23. Conway, C., F. Sharif, J. P. McGarry, and P. E. McHugh. A Computational Test-Bed to Assess Coronary Stent Implantation Mechanics Using a Population-Specific Approach. *Cardiovasc. Eng. Technol.* 3:374–387, 2012.

24. Cunnane, E. M., H. E. Barrett, E. G. Kavanagh, R. Mongrain, and M. T. Walsh. The influence of composition and location on the toughness of human atherosclerotic femoral plaque tissue. *Acta Biomater.* 31:264–275, 2016.

25. Cunnane, E. M., J. J. Mulvihill, H. E. Barrett, D. A. Healy, E. G. Kavanagh, S. R. Walsh, and M. T. Walsh. Mechanical, biological and structural characterization of human atherosclerotic femoral plaque tissue. *Acta Biomater.* 11:295–303, 2015.

26. Cunnane, E. M., J. J. E. Mulvihill, H. E. Barrett, and M. T. Walsh. Simulation of human atherosclerotic femoral plaque tissue : the influence of plaque material model on numerical results. *Biomed. Eng. Online* 14:S7, 2015.

27. Dake, M. D., G. M. Ansel, M. R. Jaff, T. Ohki, R. R. Saxon, H. B. Smouse, S. a. Snyder, E. E. O’Leary, G. Tepe, D. Scheinert, and T. Zeller. Sustained safety and effectiveness of paclitaxel-eluting stents for femoropopliteal lesions: 2-year follow-up from the zilver PTX randomized and single-arm clinical studies. *J. Am. Coll. Cardiol.* 61:2417–2427, 2013.

28. Dake, M. D., D. Scheinert, G. Tepe, J. Tessarek, F. Fanelli, M. Bosiers, C. Ruhlmann, Z. Kavteladze, A. E. Lottes, A. O. Ragheb, and T. Zeller. Nitinol stents with polymer-free paclitaxel coating for lesions in the superficial femoral and popliteal arteries above the knee: twelve-month safety and effectiveness results from the Zilver PTX single-arm clinical study. *J. Endovasc. Ther.* 18:613–23, 2011.

29. Derksen, W. J. M., J. P. P. M. De Vries, A. Vink, E. Velema, J. A. Vos, D. De Kleijn, F. L. Moll, and G. Pasterkamp. Histologic atherosclerotic plaque characteristics are associated with restenosis rates after endarterectomy of the common and superficial femoral arteries. *J. Vasc. Surg.* 52:592–599, 2010.

30. Dick, P., H. Wallner, S. Sabeti, C. Loewe, W. Mlekusch, J. Lammer, R. Koppensteiner, E. Minar, and M. Schillinger. Balloon angioplasty versus stenting with nitinol stents in intermediate length superficial femoral artery lesions. *Catheter. Cardiovasc. Interv.* 74:1090–1095, 2009.

31. Diehm, N., S. Sin, H. Hoppe, I. Baumgartner, and P. Büchler. Computational biomechanics to simulate the femoropopliteal intersection during knee flexion: a preliminary study. *J. Endovasc. Ther.* 18:388–96, 2011.

32. Dordoni, E., A. Meoli, W. Wu, G. Dubini, F. Migliavacca, G. Pennati, and L. Petrini. Fatigue behaviour of Nitinol peripheral stents: The role of plaque shape studied with computational structural analyses. *Med. Eng. Phys.* 36:842–849, 2014.

33. Duda, S. H., M. Bosiers, J. Lammer, D. Scheinert, T. Zeller, V. Oliva, A. Tielbeek, J. Anderson, B. Wiesinger, G. Tepe, A. Lansky, M. R. Jaff, C. Mudde, H. Tielemans, and J.-P. Beregi. Drug-eluting and bare nitinol stents for the treatment of atherosclerotic lesions in the superficial femoral artery: long-term results from the SIROCCO trial. *J. Endovasc. Ther.* 13:701–710, 2006.

34. Dumoulin, C., and B. Cochelin. Mechanical behaviour modelling of balloon-expandable stents. *J. Biomech.* 33:1461–70, 2000.

35. Early, M., and D. J. Kelly. The role of vessel geometry and material properties on the mechanics of stenting in the coronary and peripheral arteries. *Proc. Inst. Mech. Eng. Part H, J. Eng. Med.* 224:465–476, 2010.

36. Early, M., and D. J. Kelly. The consequences of the mechanical environment of peripheral arteries for nitinol stenting. *Med. Biol. Eng. Comput.* 49:1279–88, 2011.

37. Early, M., C. Lally, P. J. Prendergast, and D. J. Kelly. Stresses in peripheral arteries following stent placement: a finite element analysis. *Comput. Methods Biomech. Biomed. Engin.* 12:25–33, 2009.

38. Elsheikh, A., C. Whitford, R. Hamarashid, W. Kassem, A. Joda, and P. Büchler. Stress free configuration of the human eye. *Med. Eng. Phys.* 35:211–216, 2013.

39. Fowkes, F. G. R., D. Rudan, I. Rudan, V. Aboyans, J. O. Denenberg, M. M. McDermott, P. E. Norman, U. K. a Sampson, L. J. Williams, G. a. Mensah, and M. H. Criqui. Comparison of global estimates of prevalence and risk factors for peripheral artery disease in 2000 and 2010: A systematic review and analysis. *Lancet* 382:1329–1340, 2013.

40. Ganguly, A., J. Simons, A. Schneider, B. Keck, N. R. Bennett, R. J. Herfkens, S. M. Coogan, and R. Fahrig. In-vivo imaging of femoral artery nitinol stents for deformation analysis. *J. Vasc. Interv. Radiol.* 22:244–249, 2011.

41. Garriboli, L., and a. M. Jannello. Fracture of a Popliteal Nitinol Stent: Case Report and Review of the Literature. *EJVES Extra* 25:e15–e17, 2013.

42. Gasser, T. C., R. W. Ogden, and G. a Holzapfel. Hyperelastic modelling of arterial layers with distributed collagen fibre orientations. *J. R. Soc. Interface* 3:15–35, 2006.

43. Gökgöl, C., N. Diehm, and P. Büchler. Numerical Models of Nitinol Stent Oversizing in Arteries with Clinically Relevant Levels of Peripheral Arterial Disease and Varying Degrees of Calcification. *Submitt. to Ann. Biomed. Eng.* , 2016.

44. Gökgöl, C., N. Diehm, L. Kara, and P. Büchler. Quantification of popliteal artery deformation during leg flexion in subjects with peripheral artery disease: a pilot study. *J. Endovasc. Ther.* 20:828–35, 2013.

45. Gökgöl, C., N. Diehm, F. R. Nezami, and P. Büchler. Nitinol Stent Oversizing in Patients Undergoing Popliteal Artery Revascularization: A Finite Element Study. *Ann. Biomed. Eng.* 43:2868–2880, 2015.

46. Gökgöl, C., S. Schumann, N. Diehm, G. Zheng, and P. Büchler. In-vivo Quantification of Femoro-popliteal Artery Deformations: Percutaneous Transluminal Angioplasty vs. Nitinol Stent Placement. *J. Endovasc. Ther.* , 2016.

47. Gornik, H. L., and J. a Beckman. Cardiology patient page. Peripheral arterial disease. *Circulation* 111:e169–72, 2005.

48. Grimm, J., S. Müller-Hülsbeck, T. Jahnke, C. Hilbert, J. Brossmann, and M. Heller. Randomized study to compare PTA alone versus PTA with Palmaz stent placement for femoropopliteal lesions. *J. Vasc. Interv. Radiol.* 12:935–942, 2001.

49. Harvey, S. M. Nitinol Stent Fatigue in a Peripheral Human Artery Subjected to Pulsatile and Articulation Loading. *J. Mater. Eng. Perform.* 20:697–705, 2011.

50. Herisson, F., M. F. Heymann, M. Chétiveaux, C. Charrier, S. Battaglia, P. Pilet, T. Rouillon, M. Krempf, P. Lemarchand, D. Heymann, and Y. Gouëffic. Carotid and femoral atherosclerotic plaques show different morphology. *Atherosclerosis* 216:348–354, 2011.

51. Hoffmann, R., G. S. Mintz, J. J. Popma, L. F. Satler, a D. Pichard, K. M. Kent, C. Walsh, P. Mackell, and M. B. Leon. Chronic arterial responses to stent implantation: a serial intravascular ultrasound analysis of Palmaz-Schatz stents in native coronary arteries. *J. Am. Coll. Cardiol.* 28:1134–9, 1996.

52. Holzapfel, G. a. Mechanics of Angioplasty: Wall, Balloon and Stent. *Casey J.,Bao G. Mech. Biol. ASME* , 2000.

53. Holzapfel, G. A., G. Sommer, and P. Regitnig. Anisotropic mechanical properties of tissue components in human atherosclerotic plaques. *J. Biomech. Eng.* 126:657–65, 2004.

54. Holzapfel, G. A., M. Stadler, and T. C. Gasser. Changes in the mechanical environment of stenotic arteries during interaction with stents: computational assessment of parametric stent designs. *J. Biomech. Eng.* 127:166–80, 2005.

55. Holzapfel, G. a., M. Stadler, and C. a. J. Schulze-Bauer. A Layer-Specific Three-Dimensional Model for the Simulation of Balloon Angioplasty using Magnetic Resonance Imaging and Mechanical Testing. *Ann. Biomed. Eng.* 30:753–767, 2002.

56. Huo, Y., T. Wischgoll, and G. S. Kassab. Flow patterns in three-dimensional porcine epicardial coronary arterial tree. *Am. J. Physiol. Heart Circ. Physiol.* 293:H2959–70, 2007.

57. Iida, O., S. Nanto, M. Uematsu, T. Morozumi, J. I. Kotani, M. Awata, T. Onishi, N. Ito, F. Sera, H. Minamiguchi, H. Akahori, and S. Nagata. Effect of Exercise on Frequency of Stent Fracture in the Superficial Femoral Artery. *Am. J. Cardiol.* 98:272–274, 2006.

58. Iida, O., M. Takahara, Y. Soga, M. Nakano, Y. Yamauchi, K. Zen, D. Kawasaki, S. Nanto, H. Yokoi, and M. Uematsu. 1-Year Results of the ZEPHYR Registry (Zilver PTX for the

Femoral Artery and Proximal Popliteal Artery). *JACC Cardiovasc. Interv.* 8:1105–1112, 2015.

59. Jørgensen, E., H. Kelbaek, S. Helqvist, G. V. H. Jensen, K. Saunamäki, J. Kastrup, J. K. Madsen, L. Kløvgaard, L. Thuesen, A. Villadsen, A. W. M. van Weert, and J. H. C. Reiber. Low restenosis rate of the NIR coronary stent: results of the Danish multicenter stent study (DANSTENT)--a randomized trial comparing a first-generation stent with a second-generation stent. *Am. Heart J.* 145:e5, 2003.

60. Katritsis, D. G., A. Theodorakakos, I. Pantos, M. Gavaises, N. Karcanias, and E. P. Efstathopoulos. Flow patterns at stented coronary bifurcations: computational fluid dynamics analysis. *Circ. Cardiovasc. Interv.* 5:530–9, 2012.

61. Kirsch, E. C., M. S. Khangure, P. Morling, T. J. York, and W. Mcauliffe. Oversizing of Self-Expanding Stents : Influence on the Development of Neointimal Hyperplasia of the Carotid Artery in a Canine Model. 121–127, 2002.

62. Klein, A. J., I. P. Casserly, J. C. Messenger, J. D. Carroll, and S.-Y. J. Chen. In vivo 3D modeling of the femoropopliteal artery in human subjects based on x-ray angiography: Methodology and validation. *Med. Phys.* 36:289, 2009.

63. Klein, A. J., S. J. Chen, J. C. Messenger, A. R. Hansgen, M. E. Plomondon, J. D. Carroll, and I. P. Casserly. Quantitative assessment of the conformational change in the femoropopliteal artery with leg movement. *Catheter. Cardiovasc. Interv.* 74:787–98, 2009.

64. Kleinstreuer, C., Z. Li, C. a Basciano, S. Seelecke, and M. a Farber. Computational mechanics of Nitinol stent grafts. *J. Biomech.* 41:2370–8, 2008.

65. Kröger, K., F. Santosa, and M. Goyen. Biomechanical incompatibility of popliteal stent placement. *J. Endovasc. Ther.* 11:686–94, 2004.

66. LaDisa, J. F., L. E. Olson, I. Guler, D. a Hettrick, J. R. Kersten, D. C. Warltier, and P. S. Pagel. Circumferential vascular deformation after stent implantation alters wall shear stress evaluated with time-dependent 3D computational fluid dynamics models. *J. Appl. Physiol.* 98:947–57, 2005.

67. Laird, J. R., B. T. Katzen, D. Scheinert, J. Lammer, J. Carpenter, M. Buchbinder, R. Dave, G. Ansel, A. Lansky, E. Cristea, T. J. Collins, J. Goldstein, A. Y. Cao, and M. R. Jaff. Nitinol Stent Implantation vs. Balloon Angioplasty for Lesions in the Superficial Femoral and Proximal Popliteal Arteries of Patients With Claudication: Three-Year Follow-up From the RESILIENT Randomized Trial. *J. Endovasc. Ther.* 19:1–9, 2012.

68. Laird, J. R., B. T. Katzen, D. Scheinert, J. Lammer, J. Carpenter, M. Buchbinder, R. Dave, G. Ansel, A. Lansky, E. Cristea, T. J. Collins, J. Goldstein, and M. R. Jaff. Nitinol stent implantation versus balloon angioplasty for lesions in the superficial femoral artery and proximal popliteal artery: twelve-month results from the RESILIENT randomized trial. *Circ. Cardiovasc. Interv.* 3:267–76, 2010.

69. Lally, C., F. Dolan, and P. J. Prendergast. Cardiovascular stent design and vessel stresses: a finite element analysis. *J. Biomech.* 38:1574–1581, 2005.

70. Li, F., M. M. McDermott, D. Li, T. J. Carroll, D. S. Hippe, C. M. Kramer, Z. Fan, X. Zhao, T. S. Hatsukami, B. Chu, J. Wang, and C. Yuan. The association of lesion eccentricity with plaque morphology and components in the superficial femoral artery: a high-spatial-resolution, multi-contrast weighted CMR study. *J. Cardiovasc. Magn. Reson.* 12:37, 2010.

71. Liao, R., D. Luc, Y. Sun, and K. Kirchberg. 3-D reconstruction of the coronary artery tree from multiple views of a rotational X-ray angiography. *Int. J. Cardiovasc. Imaging* 26:733–749, 2010.

72. Lichtenberg, M., O. Kolks, B. Hailer, W. Stahlhoff, C. Tiefenbacher, C. Nolte-Ernsting, J. Arjumand, and G. Wittenberg. PEACE I all-comers registry: patency evaluation after implantation of the 4-French Pulsar-18 self-expanding nitinol stent in femoropopliteal lesions. *J. Endovasc. Ther.* 21:373–80, 2014.

73. Loree, H. M., A. J. Grodzinsky, S. Y. Park, L. J. Gibson, and R. T. Lee. Static circumferential tangential modulus of human atherosclerotic tissue. *J. Biomech.* 27:195–204, 1994.

74. Lyden, S. P., and H. B. Smouse. TASC II and the endovascular management of infrainguinal disease. *J. Endovasc. Ther.* 16:II5–I18, 2009.

75. Meoli, A., E. Dordoni, L. Petrini, F. Migliavacca, G. Dubini, and G. Pennati. Computational Modelling of In Vitro Set-Ups for Peripheral Self-Expanding Nitinol Stents: The Importance of Stent-Wall Interaction in the Assessment of the Fatigue Resistance. *Cardiovasc. Eng. Technol.* 4:474–484, 2013.

76. Migliavacca, F., L. Petrini, P. Massarotti, S. Schievano, F. Auricchio, and G. Dubini. Stainless and shape memory alloy coronary stents: a computational study on the interaction with the vascular wall. *Biomech. Model. Mechanobiol.* 2:205–17, 2004.

77. Migliavacca, F., L. Petrini, V. Montanari, I. Quagliana, F. Auricchio, and G. Dubini. A predictive study of the mechanical behaviour of coronary stents by computer modelling. *Med. Eng. Phys.* 27:13–18, 2005.

78. Milnor, W. R. Hemodynamics. Baltimore: Willliams&Wilkins, 1989.

79. Mintz, G. S., K. M. Kent, A. D. Pichard, L. F. Satler, J. J. Popma, and M. B. Leon. Contribution of inadequate arterial remodeling to the development of focal coronary artery stenoses. An intravascular ultrasound study. *Circulation* 95:1791–8, 1997.

80. Moer, R., Y. Myreng, P. Mølstad, P. Albertsson, P. Gunnes, B. Lindvall, R. Wiseth, K. Ytre-Arne, J. Kjekshus, and S. Golf. Stenting in small coronary arteries (SISCA) trial. A randomized comparison between balloon angioplasty and the heparin-coated beStent. *J. Am. Coll. Cardiol.* 38:1598–603, 2001.

81. Mortier, P., G. a Holzapfel, M. De Beule, D. Van Loo, Y. Taeymans, P. Segers, P. Verdonck, and B. Verhegghe. A novel simulation strategy for stent insertion and deployment in curved coronary bifurcations: comparison of three drug-eluting stents. *Ann. Biomed. Eng.* 38:88–99, 2010.

82. Müller-Hülsbeck, S., P. J. Schäfer, N. Charalambous, H. Yagi, M. Heller, and T. Jahnke. Comparison of second-generation stents for application in the superficial femoral artery: an in vitro evaluation focusing on stent design. *J. Endovasc. Ther.* 17:767–76, 2010.

83. Mulvihill, J. J., E. M. Cunnane, S. M. McHugh, E. G. Kavanagh, S. R. Walsh, and M. T. Walsh. Mechanical, biological and structural characterization of in vitro ruptured human carotid plaque tissue. *Acta Biomater.* 9:9027–35, 2013.

84. Munir, M., J. Aliota, A. Ahmed, A. Mohammad, V. V. Lee, M. A. Elayda, and J. M. Wilson. Sirolimus-eluting Stents versus Bare-Metal Stents in Routine Clinical Use. *Texas Hear. Inst. J.* 38:508–515, 2011.

85. Ní Ghriallais, R., and M. Bruzzi. Effects of knee flexion on the femoropopliteal artery: A computational study. *Med. Eng. Phys.* 35:1620–1628, 2013.

86. Ní Ghriallais, R., and M. Bruzzi. A Computational Analysis of the Deformation of the Femoropopliteal Artery With Stenting. *J. Biomech. Eng.* 136:071003, 2014.

87. Nikanorov, A., M. Schillinger, H. Zhao, E. Minar, and L. B. Schwartz. Assessment of self-expanding nitinol stent deformation after chronic implantation into the femoropopliteal arteries. *EuroIntervention* 9:730–7, 2013.

88. Nikanorov, A., H. B. Smouse, K. Osman, M. Bialas, S. Shrivastava, and L. B. Schwartz. Fracture of self-expanding nitinol stents stressed in vitro under simulated intravascular conditions. *J. Vasc. Surg.* 48:435–440, 2008.

89. Norgren, L., W. R. Hiatt, J. a Dormandy, M. R. Nehler, K. a Harris, and F. G. R. Fowkes. Inter-Society Consensus for the Management of Peripheral Arterial Disease (TASC II). *J. Vasc. Surg.* 45 Suppl S:S5–67, 2007.

90. Pelton, A. R., V. Schroeder, M. R. Mitchell, X.-Y. Gong, M. Barney, and S. W. Robertson. Fatigue and durability of Nitinol stents. *J. Mech. Behav. Biomed. Mater.* 1:153–64, 2008.

91. Petrini, L., A. Trotta, E. Dordoni, F. Migliavacca, G. Dubini, P. V. Lawford, J. N. Gosai, D. M. Ryan, D. Testi, and G. Pennati. A Computational Approach for the Prediction of Fatigue Behaviour in Peripheral Stents: Application to a Clinical Case. *Ann. Biomed. Eng.* , 2015.doi:10.1007/s10439-015-1472-7

92. Petrini, L., W. Wu, E. Dordoni, A. Meoli, F. Migliavacca, and G. Pennati. Fatigue Behavior Characterization of Nitinol for Peripheral Stents. *Funct. Mater. Lett.* 05:1250012, 2012.

93. Piamsomboon, C., G. S. Roubin, M. W. Liu, S. S. Iyer, A. Mathur, L. S. Dean, C. R. Gomez, J. J. Vitek, N. Chattipakorn, and G. Yates. Relationship Between Oversizing of Self-

Expanding Stents and Late Loss Index in Carotid Stenting. *Cathet. Cardiovasc. Diagn.* 143:139–143, 1998.

94. Poon, E. K. W., P. Barlis, S. Moore, W.-H. Pan, Y. Liu, Y. Ye, Y. Xue, S. J. Zhu, and A. S. H. Ooi. Numerical investigations of the haemodynamic changes associated with stent malapposition in an idealised coronary artery. *J. Biomech.* 47:2843–2851, 2014.

95. Press, I. The Proof and Measurement of Association between Two Things Author (s): C . Spearman Source : The American Journal of Psychology , Vol . 15 , No . 1 (Jan ., 1904), pp . 72-101 Published by : University of Illinois Press Stable URL : http://www.jstor.o. 15:72–101, 2009.

96. Rebelo, N., R. Fu, and M. Lawrenchuk. Study of a Nitinol Stent Deployed into Anatomically Accurate Artery Geometry and Subjected to Realistic Service Loading. *J. Mater. Eng. Perform.* 18:655–663, 2009.

97. Rikhtegar, F., J. a Knight, U. Olgac, S. C. Saur, D. Poulikakos, W. Marshall, P. C. Cattin, H. Alkadhi, and V. Kurtcuoglu. Choosing the optimal wall shear parameter for the prediction of plaque location-A patient-specific computational study in human left coronary arteries. *Atherosclerosis* 221:432–7, 2012.

98. Rikhtegar, F., F. Pacheco, C. Wyss, K. S. Stok, H. Ge, R. J. Choo, A. Ferrari, D. Poulikakos, R. Müller, and V. Kurtcuoglu. Compound ex vivo and in silico method for hemodynamic analysis of stented arteries. *PLoS One* 8:e58147, 2013.

99. Rosenfield, K., M. R. Jaff, C. J. White, K. Rocha-Singh, C. Mena-Hurtado, D. C. Metzger, M. Brodmann, E. Pilger, T. Zeller, P. Krishnan, R. Gammon, S. Müller-Hülsbeck, M. R. Nehler, J. F. Benenati, and D. Scheinert. Trial of a Paclitaxel-Coated Balloon for Femoropopliteal Artery Disease. *N. Engl. J. Med.* 373:145–53, 2015.

100. Safar, M. E., P. Priollet, F. Luizy, J.-J. Mourad, P. Cacoub, H. Levesque, J. Benelbaz, P. Michon, M. Herrmann, and J. Blacher. Peripheral arterial disease and isolated systolic hypertension: the ATTEST study. *J. Hum. Hypertens.* 23:182–7, 2009.

101. Saguner, A. M., T. Traupe, L. Räber, N. Hess, Y. Banz, A. R. Saguner, N. Diehm, and O. M. Hess. Oversizing and restenosis with self-expanding stents in iliofemoral arteries. *Cardiovasc. Intervent. Radiol.* 35:906–13, 2012.

102. Sangiorgi, G., A. J. Taylor, A. Farb, A. J. Carter, W. D. Edwards, D. R. Holmes, R. S. Schwartz, and R. Virmani. Histopathology of postpercutaneous transluminal coronary angioplasty remodeling in human coronary arteries. *Am. Heart J.* 138:681–7, 1999.

103. Sarode, K., D. a. Spelber, D. L. Bhatt, A. Mohammad, A. Prasad, E. S. Brilakis, and S. Banerjee. Drug delivering technology for endovascular management of infrainguinal peripheral artery disease. *JACC Cardiovasc. Interv.* 7:827–839, 2014.

104. Scheinert, D., K. Katsanos, T. Zeller, R. Koppensteiner, P. Commeau, M. Bosiers, H. Krankenberg, I. Baumgartner, D. Siablis, J. Lammer, M. Van Ransbeeck, A. C. Qureshi, and H. P. Stoll. A prospective randomized multicenter comparison of balloon

angioplasty and infrapopliteal stenting with the sirolimus-eluting stent in patients with ischemic peripheral arterial disease: 1-year results from the achilles trial. *J. Am. Coll. Cardiol.* 60:2290–2295, 2012.

105. Scheinert, D., S. Scheinert, J. Sax, C. Piorkowski, S. Bräunlich, M. Ulrich, G. Biamino, and A. Schmidt. Prevalence and clinical impact of stent fractures after femoropopliteal stenting. *J. Am. Coll. Cardiol.* 45:312–5, 2005.

106. Schillinger, M., and E. Minar. Past, present and future of femoropopliteal stenting. *J. Endovasc. Ther.* 16 Suppl 1:I147–52, 2009.

107. Schillinger, M., S. Sabeti, P. Dick, J. Amighi, W. Mlekusch, O. Schlager, C. Loewe, M. Cejna, J. Lammer, and E. Minar. Sustained benefit at 2 years of primary femoropopliteal stenting compared with balloon angioplasty with optional stenting. *Circulation* 115:2745–9, 2007.

108. Schillinger, M., S. Sabeti, C. Loewe, P. Dick, J. Amighi, W. Mlekusch, O. Schlager, M. Cejna, J. Lammer, and E. Minar. Balloon angioplasty versus implantation of nitinol stents in the superficial femoral artery. *N. Engl. J. Med.* 354:1879–88, 2006.

109. Schlager, O., P. Dick, S. Sabeti, J. Amighi, W. Mlekusch, E. Minar, and M. Schillinger. Long-segment SFA stenting--the dark sides: in-stent restenosis, clinical deterioration, and stent fractures. *J. Endovasc. Ther.* 12:676–684, 2005.

110. Schulze-bauer, C. A. J., P. Regitnig, and G. A. Holzapfel. Mechanics of the human femoral adventitia including the high-pressure response. *Am J Physiol Hear. Circ Physiol* 282:2427–2440, 2002.

111. Schumann, S., X. Dong, M. Puls, L.-P. Nolte, and G. Zheng. Calibration of C-arm for orthopedic interventions via statistical model-based distortion correction and robust phantom detection. *2012 9th IEEE Int. Symp. Biomed. Imaging* 1204–1207, 2012.doi:10.1109/ISBI.2012.6235777

112. Schumann, S., C. Gökgöl, N. Diehm, P. Büchler, and G. Zheng. The Effects of Stent Implantation on the Deformations of the SFA and the Popliteal Artery: In-Vivo 3D Deformational Analysis from 2D Radiographs. *J. Vasc. Interv. Radiol.* , 2016.

113. Schwartz, R. S., E. J. Topol, P. W. Serruys, G. Sangiorgi, and D. R. Holmes. Artery size, neointima, and remodeling: time for some standards. *J. Am. Coll. Cardiol.* 32:2087–94, 1998.

114. Seo, T., L. G. Schachter, and A. I. Barakat. Computational study of fluid mechanical disturbance induced by endovascular stents. *Ann. Biomed. Eng.* 33:444–456, 2005.

115. Simpson, E. L., J. a. Michaels, S. M. Thomas, and a. J. Cantrell. Systematic review and meta-analysis of additional technologies to enhance angioplasty for infrainguinal peripheral arterial occlusive disease. *Br. J. Surg.* 100:1128–1137, 2013.

116. Smilde, T. J., F. W. van den Berkmortel, G. H. Boers, H. Wollersheim, T. de Boo, H. van Langen, and a F. Stalenhoef. Carotid and femoral artery wall thickness and stiffness in patients at risk for cardiovascular disease, with special emphasis on hyperhomocysteinemia. *Arterioscler. Thromb. Vasc. Biol.* 18:1958–1963, 1998.

117. Smouse, H., and A. Nikanorov. Biomechanical forces in the femoropopliteal arterial segment. *Endovasc. Today* , 2005.at <http://bmctoday.net/evtoday/2005/06/article.asp?f=EVT0605_F3_Smouse.html>

118. Solis, J., S. Allaqaband, and T. Bajwa. A case of popliteal stent fracture with pseudoaneurysm formation. *Catheter. Cardiovasc. Interv.* 67:319–22, 2006.

119. Stary, H. C., D. Blankenhorn, a B. Chandler, S. Glagov, W. Insull, M. Richardson, M. E. Rosenfeld, S. Schaffer, C. J. Schwartz, and W. D. Wagner. A Definition of the Intima of Human Arteries and of Its Atherosclerosis-Prone Regions. *Circulation* 85:391–405, 1992.

120. Stiegler, H., and R. Brandl. Importance of ultrasound for diagnosing periphereal arterial disease. *Ultraschall Med.* 30:334–74, 2009.

121. Stoeckel, D., A. Pelton, and T. Duerig. Self-expanding Nitinol stents: Material and design considerations. *Eur. Radiol.* 14:292–301, 2004.

122. Tai, N. R., a Giudiceandrea, H. J. Salacinski, a M. Seifalian, and G. Hamilton. In vivo femoropopliteal arterial wall compliance in subjects with and without lower limb vascular disease. *J. Vasc. Surg.* 30:936–45, 1999.

123. Takashima, K., T. Kitou, K. Mori, and K. Ikeuchi. Simulation and experimental observation of contact conditions between stents and artery models. *Med. Eng. Phys.* 29:326–35, 2007.

124. Tan, L. B., D. C. Webb, K. Kormi, and S. T. Al-Hassani. A method for investigating the mechanical properties of intracoronary stents using finite element numerical simulation. *Int. J. Cardiol.* 78:51–67, 2001.

125. Tepe, G., J. Laird, P. Schneider, M. Brodmann, P. Krishnan, A. Micari, C. Metzger, D. Scheinert, T. Zeller, D. J. Cohen, D. B. Snead, B. Alexander, M. Landini, and M. R. Jaff. Drug-coated balloon versus standard percutaneous transluminal angioplasty for the treatment of superficial femoral and popliteal peripheral artery disease 12-month results from the IN.PACT SFA randomized Trial. *Circulation* 131:495–502, 2015.

126. Thompson, R. B., and E. R. Mcveigh. Real-time volumetric flow measurements with complex-difference MRI. 50:1248–1255, 2008.

127. Tielliu, I. F. J., C. J. Zeebregts, G. Vourliotakis, F. Bekkema, J. J. a M. van den Dungen, T. R. Prins, and E. L. G. Verhoeven. Stent fractures in the Hemobahn/Viabahn stent graft after endovascular popliteal aneurysm repair. *J. Vasc. Surg.* 51:1413–1418, 2010.

128. Timmins, L. H., C. a Meyer, M. R. Moreno, and J. E. Moore. Effects of stent design and atherosclerotic plaque composition on arterial wall biomechanics. *J. Endovasc. Ther.* 15:643–654, 2008.

129. Timmins, L. H., M. W. Miller, F. J. Clubb, and J. E. Moore. Increased artery wall stress post-stenting leads to greater intimal thickening. *Lab. Invest.* 91:955–67, 2011.

130. Vorwerk, D., F. Redha, J. Neuerburg, C. Clerc, and R. W. Giinther. CardioVasct and Interventional Radiology Neointima Formation Following Arterial Placement of Self-Expanding Stents of Different Radial Force : Experimental Results i // I. 27–32, 1994.

131. Wang, W.-Q., D.-K. Liang, D.-Z. Yang, and M. Qi. Analysis of the transient expansion behavior and design optimization of coronary stents by finite element method. *J. Biomech.* 39:21–32, 2006.

132. Werk, M., S. Langner, B. Reinkensmeier, H. F. Boettcher, G. Tepe, U. Dietz, N. Hosten, B. Hamm, U. Speck, and J. Ricke. Inhibition of restenosis in femoropopliteal arteries. Paclitaxel-coated versus uncoated balloon: Femoral paclitaxel randomized pilot trial. *Circulation* 118:1358–1365, 2008.

133. Werner, B. Y. M. Factors Affecting Reduction in SFA Stent Fracture Rates. *Endovasc. Today* 13:93–95, 2014.

134. Windecker, S., A. Remondino, F. R. Eberli, P. Jüni, L. Räber, P. Wenaweser, M. Togni, M. Billinger, D. Tüller, C. Seiler, M. Roffi, R. Corti, G. Sütsch, W. Maier, T. Lüscher, O. M. Hess, M. Egger, and B. Meier. Sirolimus-Eluting and Paclitaxel-Eluting Stents for Coronary Revascularization. *N. Engl. J. Med.* 353:653–662, 2005.

135. Wu, W., W.-Q. Wang, D.-Z. Yang, and M. Qi. Stent expansion in curved vessel and their interactions: a finite element analysis. *J. Biomech.* 40:2580–5, 2007.

136. Zamora, C. A., K. Sugimoto, M. Yamaguchi, and K. Sugimura. Effect of stent oversizing on in-stent stenosis and lumen size in normal porcine veins. *J. Endovasc. Ther.* 12:495–502, 2005.

137. Zhao, H. Q., A. Nikanorov, R. Virmani, R. Jones, E. Pacheco, and L. B. Schwartz. Late stent expansion and neointimal proliferation of oversized Nitinol stents in peripheral arteries. *Cardiovasc. Intervent. Radiol.* 32:720–6, 2009.

138. Zhao, S., L. Gu, and S. R. Froemming. Finite Element Analysis of the Implantation of a Self-Expanding Stent: Impact of Lesion Calcification. *J. Med. Device.* 6:021001, 2012.

CAN GÖKGÖL

Address:

Home: Mühledorfstrasse 28/613
3018, Bern/Switzerland
Office: Stauffacherstrasse 78
3014, Bern/Switzerland
Contact: can.goekgoel@istb.unibe.ch, cgokgol@gmail.com
+41 78 891 03 27

RESEARCH INTERESTS:

- Stent Design & Implantation
- Balloon Angioplasty
- Arterial Biomechanics
- Finite Element Analysis
- Soft Tissue and Fracture Mechanics

EDUCATION:

2012 -	**University of Bern** **Inst. For Surgical Tech & Biomechanics** **Computational Biomechanics** ▪ PhD Candidate ▪ Advisor: Prof. Dr. Philippe Büchler ▪ Clinical Partner: Prof. Dr. Nicolas Diehm
2008 - 2011	**Koc University** **Faculty of Engineering** ▪ M. Sc. in Mechanical Engineering ▪ Advisor: Assoc. Prof. Cagatay Basdogan ▪ Co-Advisor: Asst. Prof. Demircan Canadinc
2004 - 2008	**Sabanci University** **Faculty of Engineering and Natural Sciences** ▪ B. Sc. in Mechatronics Engineering
2001 - 2004	**Ozel Sisli Terakki High School**

PROJECTS:

- **PhD Thesis, University of Bern (2012 – October 2016)**
  - Patient-Specific Characterization of the Mechanical Behavior of the Femoro-popliteal Arterial Tract: The Effects of Balloon Angioplasty, Stent Implantation, Stent Design and Nitinol Stent Oversizing

    - A 2 year collaboration with Biotronik AG (2012-2013)

- **M.Sc. Thesis, Koc University**
  - Estimation of Fracture Toughness of Liver Tissue: Experiments and Validation
  - Biomechanical and Finite Element Modeling of Needle Insertion into Soft Tissue with Applications to Medical Simulation and Robotics

- **Graduation Project, Sabanci University**
  - Design and Implementation of a Robotic Exoskeleton to Assist Hand Motions
    - Supervisor: Asst. Prof. **Volkan Patoglu**

- **Internship Project, Arcelik Inc.**
  - Research on the control mechanisms of clear and non-clear ice makers and design of a clear ice maker mechanism to the freezer of the side-by-side refrigerators

JOURNAL PUBLICATIONS:

- Gökgöl, C., N. Diehm, and P. Büchler. Numerical Modeling of Nitinol Stent Oversizing in Arteries with Clinically Relevant Levels of Peripheral Arterial Disease: The Influence of Plaque Type on the Outcomes of Endovascular Therapy. (**Submitted** to Annals of Biomedical Engineering, August, 2016)

- Gökgöl, C., S. Schumann, N. Diehm, G. Zheng, and P. Büchler. In-vivo Quantification of Femoro-popliteal Artery Deformations: Percutaneous Transluminal Angioplasty vs. Nitinol Stent Placement. (**Accepted** by Journal of Endovascular Therapy, August, 2016)

- Schumann, S., C. Gökgöl, N. Diehm, P. Büchler, and G. Zheng. The Effect of Stent Implantation on the Deformations of the SFA and the Popliteal Artery: In-Vivo 3D Deformational Analysis from 2D Radiographs. (**Accepted** by Journal of Vascular and Interventional Radiology, April, 2016).

- Gökgöl, C., N. Diehm, F. Rikhtegar, and P. Büchler. The Effects of Nitinol Stent Oversizing in Patients Undergoing Femoro-popliteal Artery Revascularization: A Geometrically Patient-specific Finite Element Study. (**Accepted** by Annals of Biomedical Engineering, June, 2015; **Published**: December, 2015).

- Gokgol, C., N. Diehm, L. Kara, and P. Büchler. Quantification of Popliteal Artery Deformation during Leg Flexion in Subjects with Peripheral Arterial Disease: A Pilot Study. (**Accepted** by Journal of Endovascular Therapy, July, 2013; **Published**: December, 2013)

- Gokgol, C., C. Basdogan, and D. Canadinc. Estimation of Fracture Toughness of Liver Tissue: Experiments and Validation. (**Accepted** by Medical Engineering & Physics, September, 2011; **Published**: September, 2012)

BOOK CHAPTERS

- Gökgöl C, Büchler P, Diehm N, 2015. The influence of arterial deformations and Nitinol stent oversizing in infrainguinal arteries. In: Chakfe N, Heim F, Meichelboeck W (eds), *9th European Symposium on Vascular Biomaterials (ESVB)*, Strasbourg, GEPROVAS, Strasbourg, pp 359-368.

CONFERENCE PROCEEDINGS

- C. Gokgol, N. Diehm, P. Büchler, 2016. The Effects of Primary Stent Implantation vs. Percutaneous Transluminal Angioplasty on the Femoro-popliteal Artery Deformations due to Leg Flexion. In *22nd Congress of the European Society of Biomechanics (ESB)*

- C. Gokgol, N. Diehm, P. Büchler, 2015. The Effects of Nitinol Stent Oversizing in Patients Undergoing Femoropopliteal Artery Revascularization: A Finite Element Study. In *9th European Symposium on Vascular Biomaterials (ESVB)*

- C. Gokgol, N. Diehm, P. Büchler, 2015. The Effects of Nitinol Stent Oversizing in Patients Undergoing Femoro-popliteal Artery Revascularization: A Geometrically Patient-Specific Finite Element Study. In *21st Congress of the European Society of Biomechanics (ESB)*

- C. Gokgol, N. Diehm, P. Büchler, 2014. Effects of Nitinol Stent Oversizing on Arterial Stresses based on Finite Element Analyses. In *12th International Symposium of Computer Methods in Biomechanics and Biomedical Engineering (CMBBE)*

- C. Gokgol, N. Diehm, P. Büchler, 2013. Quantification of Arterial Deformations during Leg Flexion in Subjects with Peripheral Arterial Disease. In *19th Congress of the European Society of Biomechanics (ESB)*.

WORK EXPERIENCE:

2012- **University of Bern, Bern/Switzerland**

- Teaching Assistant
  - Finite Element I (Spring 2012, 2013, 2014 & 2015)

2008 –2010 **Koc University, Istanbul/Turkey**

- Research Assistant under the Robotics and Mechatronics Laboratory

    - Research on “Estimation of Fracture Toughness of Liver Tissue: Experiments and Validation”

- Teaching Assistant
    - Dynamic Modeling and Control (Spring 2009)
    - Machine Design (Fall 2008-2009)
    - Introduction to Mechanical Engineering (Spring 2010)

July 2008 – September 2008 **MEKAR (Mechatronics Research), Istanbul Technical University, Istanbul/Turkey**

- Worked on an automotive control project on development of differential braking ESP, which was financed by TOFAS, for two months

June 2007 – September 2007 **Arcelik Inc., Istanbul/Turkey**

- Long-term internship for Arcelik’s Research and Technology Department Center (R&D), in Fluid Mechanics Department for three months

LANGUAGE and COMPUTER SKILLS and ACHIEVEMENTS:

English (Upper Advanced) - Toefl Score: 111/120 (February 2010)
German (Beginner)

Software Packages: ABAQUS, ANSYS, MATLAB, AMIRA, ITKsnap, SolidWorks, SolidCam, Unigraphics
Office Applications: MS Office, Open Office

- Full scholarship and stipend granted by Koc University
- Sabanci University “Faculty of Engineering and Natural Sciences”(FENS) Dean’s High Honor List, once, Fall 2007, and Honor List, three times, Fall 2004, Spring 2005 and Spring 2007

Declaration of Originality

Last name, first name: Gökgöl, Can

Matriculation number: 12-103-297

I hereby declare that this thesis represents my original work and that I have used no other sources except as noted by citations.
All data, tables, figures and text citations which have been reproduced from any other source, including the internet, have been explicitly acknowledged as such.
I am aware that in case of non-compliance, the Senate is entitled to withdraw the doctorate degree awarded to me on the basis of the present thesis, in accordance with the “Statut der Universität Bern (Universitätsstatut; UniSt)”, Art. 69, of 7 June 2011.

Place, date

Bern, 21.11.2016

Signature

Can Gökgöl

Digitally signed by Can Gökgöl
DN: cn=Can Gökgöl, o=University of Bern, ou=Institute for Surgical Technology & Biomechanics, email=can.goekgoel@istb.unibe.ch, c=CH
Date: 2016.11.21 11:33:17 +01'00'

Copyright © 2016 Can Gökgöl

”The copyright of this thesis rests with the author. No quotations from it should be published without the author’s prior written consent and information derived from it should be acknowledged”.